EISCAT
TECHNICAL
NOTE

NON-MAXWELLIAN ION VELOCITY DISTRIBUTION IN THE IONOSPHERIC F-REGION

by

Kari K. Suvanto

Physics Department
Imperial College
London SW7 2BZ

KIRUNA
Sweden

Non-Maxwellian ion velocity distributions in the ionospheric F-region

by

Kari K. Suvanto

Thesis submitted for the degree of Doctor of Philosophy of the University of London and for the Diploma of Membership of Imperial College

April 1989

Physics Department
Imperial College
London SW7 2BZ

EISCAT Scientific Association
Box 812, S-981 28 Kiruna, Sweden
September 1989
EISCAT Technical Note 89/51
Printed in Sweden
ISSN 0349-2710

To my Wife

ABSTRACT

Ionospheric consequences of distorted ion velocity distributions associated with supersonic plasma flows through the neutral gas in the high-latitude F-region are discussed. The theoretical incoherent scatter spectrum is compared with observations, and the role of ion cyclotron waves driven by non-Maxwellian ion distributions is investigated, with particular emphasis on weakly turbulent velocity space diffusion.

Analysis of incoherent scatter radar data shows that in the case of large ion flows, fits of much better quality than for the standard analysis are obtained if non-thermal effects are allowed for. Several aspects and difficulties associated with non-Maxwellian spectral analysis are discussed, along with the main ionospheric results obtained so far by this method.

The linearized Vlasov equation is used to study the threshold conditions for the ion cyclotron microinstability, allowing for electron Landau damping and a small deviation of the wave frequency from the ion gyrofrequency. The effect of the so called "non-resonant" terms in the ion contribution to the dielectric function is taken into account by an analytical approximation scheme. The threshold value of the drift parameter D^* ($\approx$1.3) is found to be insensitive to variations in the plasma temperatures and the ion composition, and the wavelengths of the unstable waves are typically of the order of a few meters. An expression for the instability growth rate is derived using the cold electron approximation.

By balancing wave-induced diffusion in velocity space and the effect of ion-neutral collisions, the shape of the ion velocity distribution is found to be affected by ion-wave interactions at very low fluctuation levels. The low-energy part of the ion velocity distribution, characterized by a pronounced positive slope in perpendicular velocity in non-turbulent theory, tends to become flatter, bringing the plasma closer to marginal stability.

PREFACE

This thesis is based on my work at Imperial College, the Rutherford Appleton Laboratory and the University of Helsinki during the academic years 1986–88. Its aim is to explore implications of non-Maxwellian ion velocity distributions in the presence of large DC electric fields in the auroral F-region and thereby demonstrate how fundamental principles of kinetic theory can be combined with knowledge of global ionospheric phenomena like high-latitude plasma flows driven by magnetospheric electric fields.

The importance of non-thermal ion velocity distributions on various ionospheric processes was first pointed out in the early seventies. However, the first observational evidence of their effect on the incoherent scatter spectrum was obtained in 1986 a few weeks before I started my studies as a research student at Imperial College. As a result, it was natural to start working in this area. Another reason for choosing this topic was the fact that the non-thermal nature of the ions invalidates many basic assumptions made so far in conventional ionospheric work, giving rise to "anomalous" phenomena, so to speak, which require investigation starting from first principles. These include modifications in the incoherent scatter spectrum and linear instabilities leading to weakly turbulent velocity space diffusion, which starts affecting the shape of the distribution function above the instability threshold. Knowledge of the shape of the ion velocity distribution is required to avoid misinterpretations in the routine analysis of satellite and incoherent scatter radar data.

First and foremost, I wish to thank Dr Mike Lockwood from the Rutherford Appleton Laboratory. His deep understanding of ionospheric phenomena and his infectious enthusiasm have led me to explore the subjects discussed in this thesis. I am grateful to Dr Lockwood and Professor Stan W.H. Cowley from Imperial College for their interest and helpful advice throughout this work. I thank them

for carefully reading and commenting on the draft manuscript, and all the members of the Space and Atmospheric Physics Group at Imperial College for providing a pleasant working atmosphere. I am also indebted to Dr David Willis and the staff of the EISCAT group at the Rutherford Appleton Laboratory.

It is a pleasure to thank Professor Jean-Pierre St.-Maurice on the other side of the ocean for a fruitful interaction in the form of correspondence and discussions, as well as my fellow research students at the University of Helsinki for their interest.

I am grateful to the Oskari Huttunen Foundation in Finland for funding this work. Financial support has also been provided by the British Council, the Finnish Academy, several Finnish foundations and the ORS award in the U.K.

Last, but certainly not least, I wish to thank my parents. Their continuous support and encouragement have made this work possible.

K. S.

REFEREED PUBLICATIONS

Most of the material presented in Chapters 2–5 of this thesis is based on the following research papers:

1. Suvanto, K., Auroral F-region ion velocity distributions in the presence of large flows and electrostatic waves, *Planet. Space Sci.* **35,** 1429, 1987.

2. Suvanto, K., Incoherent scattering of radar waves from non-thermal F-region plasma: analytical methods of spectral synthesis, *Radio Sci.* **23,** 989, 1988.

3. Suvanto, K., Ion cyclotron microinstability driven by non-thermal F-region plasma, *Planet. Space Sci.* **37,** 1, 1989a.

4. Suvanto, K., Microinstabilities driven by non-thermal plasma in the high-latitude F-region, *Adv. Space Res. (COSPAR Proceedings),* in press, 1989b.

5. Suvanto, K., M. Lockwood and T.J. Fuller-Rowell, The influence of anisotropic ion velocity distributions on ion upflows into the magnetosphere, *J. Geophys. Res.* **94,** 1347, 1989a.

6. Suvanto, K., M. Lockwood, K.J. Winser, A.D. Farmer and B.J.I. Bromage, Analysis of incoherent scatter spectra from non-thermal F-region plasma, submitted to *J. Atmos. Terr. Phys.,* 1989b.

7. Suvanto, K., M. Lockwood, K.J. Winser, A.D. Farmer and B.J.I. Bromage, Analysis of incoherent scatter spectra from non-Maxwellian plasma in the high-latitude F-region, *Adv. Space Res. (COSPAR Proceedings),* in press, 1989c.

8. Lockwood, M., K. Suvanto, J.-P. St.-Maurice, K. Kikuchi, B.J.I. Bromage, D.W. Willis, S.R. Crothers, H. Todd and S.W.H. Cowley, Scattered power from non-thermal F-region plasma observed by EISCAT – evidence for coherent echoes?, *J. Atmos. Terr. Phys.* **50,** 467, 1988.

9. Lockwood, M., K. Suvanto, K.J. Winser, S.W.H. Cowley and D.M. Willis, Incoherent scatter radar observations of non-Maxwellian ion velocity distributions in the auroral F-region, *Adv. Space Res. (COSPAR Proceedings),* in press, 1989a.

10. Lockwood, M., K. Suvanto, S.W.H. Cowley, R.B. Horne, T.J. Fuller-Rowell, B.J.I. Bromage, D.M. Willis and J.-P. St.-Maurice, Incoherent scatter observations of non-Maxwellian ion velocity distributions in the auroral F-region,

to be submitted, 1989b.

11. Farmer, A.D., M. Lockwood, T.J. Fuller-Rowell, K. Suvanto and U.P. Løvhaug, Model predictions of the occurrence of non-Maxwellian plasmas and analysis of their effect on EISCAT data, *J. Atmos. Terr. Phys.* **50**, 487, 1988.

12. Winser, K.J., M. Lockwood, G.O.L. Jones and K. Suvanto, Observations of non-thermal plasmas at different aspect angles, *J. Geophys. Res.* **94**, 1439, 1989a.

13. Winser, K.J., M. Lockwood, G.O.L. Jones and K. Suvanto, Radar observations of non-thermal plasmas at different aspect angles, *Adv. Space Res. (COSPAR Proceedings)*, in press, 1989b.

CONTENTS

LIST OF FIGURES AND TABLES

CHAPTER 1

INTRODUCTION

1.1. ORIGIN OF THE SUBJECT

Collisions between particles in a neutral gas or a plasma usually play an important role in establishing a thermal equilibrium. However, in the case of relative flows between particle populations, they can distort the species distribution functions significiantly from a Maxwellian and hence have the opposite effect. In particular, non-Maxwellian ion velocity distributions occur in the high-latitude ionosphere, where the ions are forced by magnetospheric electric fields to flow through the neutral atmosphere.

It is commonly believed that *magnetic reconnection* is the major agent driving magnetospheric convection, as first proposed by Dungey (1961). Other theories have been developed, but observations seem to favour reconnection as the most important coupling process between the solar wind and the magnetospheric plasma. The reconnection model for southward interplanetary magnetic field (IMF) is illustrated by Figure 1.1 [taken from Cowley (1983)]. In the magnetohydrodynamic approximation, the magnetic field and the plasma flow are "frozen together" if the field is sufficiently slowly varying in space, corresponding to large values of the magnetic Reynolds number. However, as the solar wind plasma and the associated magnetic flux approach the magnetosphere, short length scales become important in the boundary, giving rise to a localized break-down of the "perfect conductivity" approximation. Magnetic diffusion takes place, and geomagnetic field lines from the polar

regions become connected into the IMF. The resulting open field lines are carried anti-sunwards by the solar wind flow and form the geomagnetic tail. The oppositely-directed field lines drift together and reconnect. The newly-closed field lines return sunwards and complete the cycle, whereas the open field lines drift downstream together with the solar wind.

The magnetospheric plasma is effectively a perfect conductor (except for the boundary regions where diffusion can occur) so that the electric field in the drift frame is zero. This implies that an observer in the rest frame sees an electric field $\mathbf{E} = -\mathbf{v}\times\mathbf{B}$, where $\mathbf{v}$ is the plasma drift velocity and $\mathbf{B}$ the magnetic field. The resulting cross-magnetosphere voltage maps to ionospheric altitudes because the field-aligned voltage drops are small, and the ionospheric plasma is set into motion. The electron-neutral collision frequency is much less than the electron cyclotron frequency throughout the E- and F-regions so that the electrons drift in the $\mathbf{E}\times\mathbf{B}$ direction (Hall drift). The ions move in the Hall direction above about 160 km. The ion-neutral collision frequency becomes comparable to the ion cyclotron frequency at 130 km and, consequently, the ion motion is affected by the neutral gas: the drift velocity has a component in the direction of the electric field (Pedersen drift). Finally, at 100 km the ion drift is considerably reduced and almost parallel with the ambient electric field. Figure 1.2 [taken from Cowley (1983)] shows a typical twin-vortex flow pattern over the northern polar cap at F-region altitudes with anti-sunward flow over the polar cap and sunward flow in the auroral zone at lower latitudes.

Observations of non-thermal and highly anisotropic plasma tend to be made during transient increases in ion convection speed [Løvhaug and Flå (1986); Lockwood *et al.* (1987; 1988; 1989a,b); Winser *et al.* (1987); Farmer *et al.* (1988)]. As time passes, the neutral gas accelerates owing to the ion drag so that the relative bulk speed between ions and neutrals is reduced. The efficiency of this

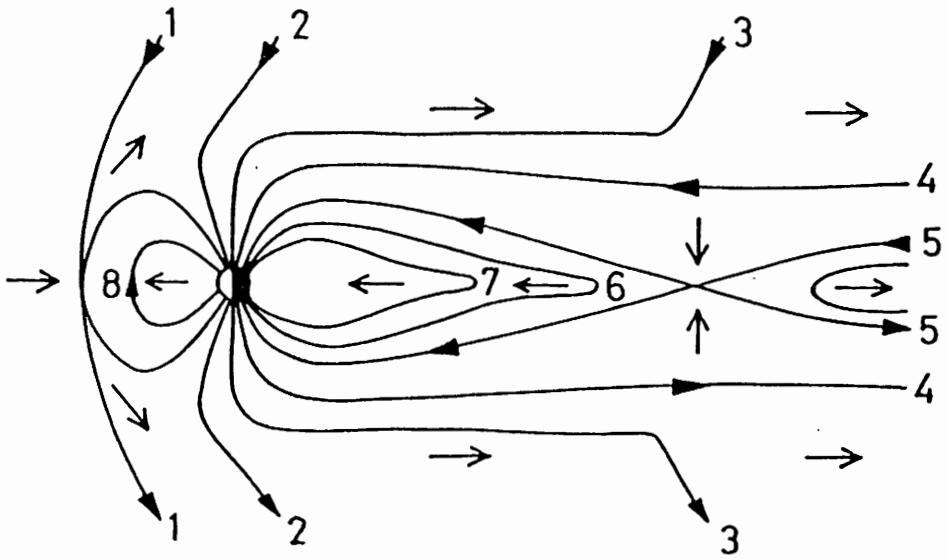

Figure 1.1. Reconnection for southward interplanetary magnetic field. [From Cowley (1983).]

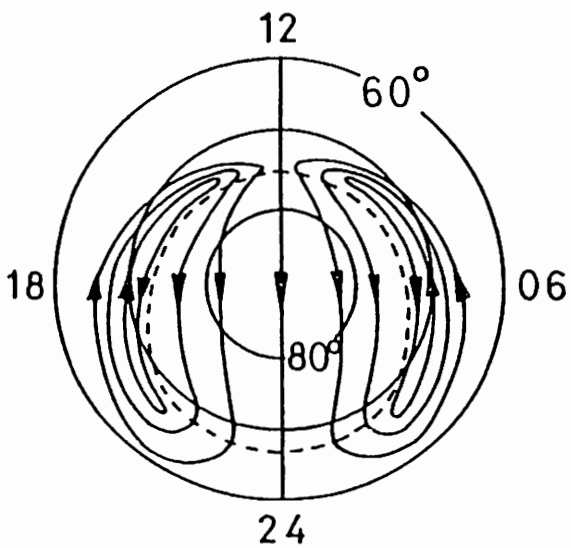

Figure 1.2. Schematic illustration of the typical ionospheric twin-vortex convection pattern with antisunward flow over the polar cap and sunward flow at lower latitudes. The coordinates are local time and magnetic latitude. [From Cowley (1983).]

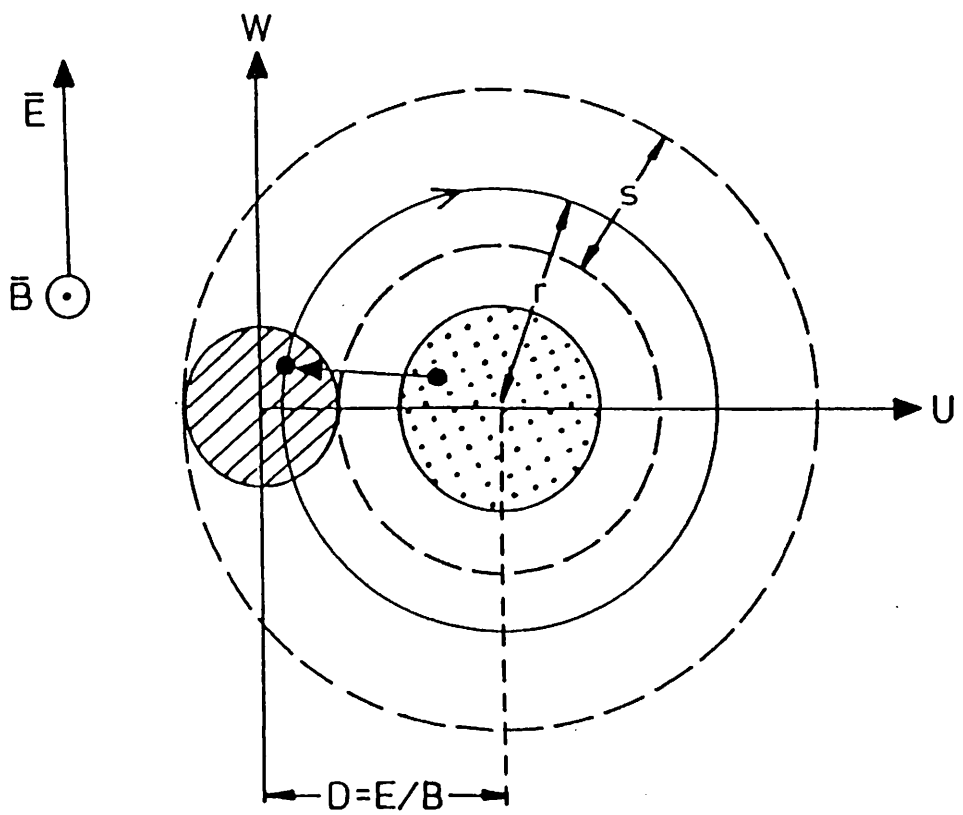

Figure 1.3. Velocity space diagram illustrating the ion-neutral collisional process, which drives the plasma into a non-thermal state. Here U and W are the velocity components perpendicular to the geomagnetic field. [From Lockwood *et al.* (1989b).]

process depends on the degree of ionization and the relaxation time for ion-neutral collisions, which is defined as the inverse of the appropriate collision frequency for momentum transfer and is of the order of a second at F-region altitudes. In fact, the time scale for the neutrals to be accelerated is roughly given by the product of these two quantities, its numerical value being about 20 minutes for 0.1% ionization and several hours for values of ionization less than 0.01%. Large ion drifts with respect to the neutrals thus occur, at least transiently. Lockwood and Fuller-Rowell (1987) used the coupled ionosphere–thermosphere model, developed by University College (London) and the University of Sheffield, to find out where the ionospheric convection pattern was likely to drive the plasma non-thermal. These authors showed that even for steady-state conditions and moderate magnetic activity, the merging gap of the convection pattern should contain non-thermal plasma continuously, and large relative drifts are also expected in the post-midnight auroral oval.

The fact that the ion velocity distribution is indeed driven non-Maxwellian when the drifting ions collide mostly with the background neutrals can be established using very simple physical arguments [St.-Maurice and Schunk (1979); Lockwood *et al.* (1989b)]. To do that, we take the ion-neutral collision frequency to be much less than the ion gyrofrequency and characterize the neutrals by a Maxwellian distribution with temperature T_n. The rest frame of the neutrals will be used for convenience. Now, if the ions are not drifting, collisions bring them into thermal equilibrium at the neutral temperature T_n, whatever the initial ion configuration was, because of the overwhelming majority of the neutral particles. In other words, the ions are driven towards a Maxwellian distribution with temperature T_n; they become concentrated around zero in velocity space and their velocity spread is given by $(2k_B T_n/m_i)^{1/2}$, where m_i is the ion mass and k_B the Boltzmann constant. Consider then the case where the ions have a field-perpendicular drift of magnitude $D=E/B$, where the electric field is measured in the

neutral rest frame. Figure 1.3, which is a velocity space diagram taken from Lockwood *et al.* (1989b), illustrates the collisional process in the plane perpendicular to the magnetic field. The cross-hatched area is the disk of radius $(2k_BT_n/m_i)^{1/2}$ into which most ions are scattered when they suffer a charge-exchange collision, as indicated by the arrow. If the ion and neutral masses are equal, this is the region occupied by most neutrals. After a collision, the ion gyrates in a circular orbit of radius r in velocity space and most ions form a ring of width $s = 2\ (2k_BT_n/m_i)^{1/2}$, as indicated by the dashed lines. If there were no ion-neutral collisions, the ion distribution would be thermalized by Coulomb interactions. Most ions could then be found inside the dotted area around the drift velocity D, where the perpendicular ion velocity distribution would have its maximum. The distortion from a Maxwellian due to ion-neutral interactions therefore becomes clear when the drift point is not located inside the hatched region into which most ions are scattered i.e. when $D > s/2 = (2k_BT_n/m_i)^{1/2}$. For typical ionospheric parameters, this requires relative ion-neutral drift speeds of the order of 1 kms^{-1} or more. According to our assumption, the ions gyrate many times about the magnetic field before they suffer a collision and, consequently, the distribution remains gyrotropic around the magnetic field in velocity space.

It should be noted that the above discussion is based on the simplification that the binary collisions can be described by a relaxation model (see Section 1.2.2). In reality, the degree of distortion depends on the details of the collisional process; the idea was just to point out the basic mechanism leading to non-thermal effects.

Considerable progress has been made in understanding the shape of the ion velocity distribution function in the presence of large ionospheric flows, and in this introductory chapter we will review some of the most important milestones related to that work. The other chapters are devoted to the consequences of the distribution shape. Before this review, however, it is necessary to introduce the

major theoretical tool to be used throughout this work, namely the kinetic equation along with various collision models and the concept of temperature.

1.2. KINETIC DESCRIPTION OF A PLASMA

Kinetic theory is the most comprehensive way of describing a plasma, as opposed to particle orbit theory and various fluid pictures like magnetohydrodynamics and warm plasma equations, which are, of course, all derivable from the kinetic equation by using various truncation schemes and other approximations. Although useful in the study of certain aspects of plasma behaviour, both orbit theory and the fluid description totally ignore various phenomena of potential interest. For example, single particle equations do not contain collective effects by definition. On the other hand, fluid theory can be used to study various wave modes of the plasma provided that wave-particle interactions are negligible.

The present work is devoted to the study of auroral F-region phenomena sensitive to the shape of the ion velocity distribution, namely the form of the incoherent scatter spectrum and the excitation of plasma instabilities. Both these effects involve considerations of the spectrum of collective density fluctuations. The actual fluctuation levels are intimately related to wave-particle interactions, so that a kinetic description is required. Although we are mainly interested in the applications of the kinetic equation, our study would be incomplete if we did not briefly discuss its origin and the limitations of its validity. Detailed mathematical derivations are well documented in the literature, and we will just point out the main features of interest here. The review presented in this section is based on Clemmow and Dougherty (1969; p. 392-446) and Sanderson (1981).

1.2.1. Kinetic equations for a plasma

The kinetic equation may be formally written as[1]

$$\frac{\partial f}{\partial t} + \mathbf{v} \cdot \frac{\partial f}{\partial \mathbf{r}} + \mathbf{a} \cdot \frac{\partial f}{\partial \mathbf{v}} = \left(\frac{\partial f}{\partial t}\right)_{\text{int}}, \tag{1.1}$$

where $f(\mathbf{r},\mathbf{v},t)$ is the distribution function of the ions (or, more generally, any species of interest) and $\mathbf{a}$ is the acceleration due to externally applied, macroscopic forces. The term on the right-hand side (RHS) accounts for all interactions between the particles, including other species, and is assumed to depend on f and possibly distribution functions of other species only.

Although the form of (1.1) looks obvious, it is not clear at all whether a differential equation of this form for the distribution function really exists. To cast some light into this problem, we note that the most complete description of a system of N identical point particles is given by the positions $\mathbf{r}_i$ and velocities $\mathbf{v}_i$ (i=1,...,N) of the particles[2] whose time development is governed by N one-particle equations of motion, once the initial state known. This corresponds to a point moving in the $6N$-dimensional space whose coordinates are the components of $\mathbf{r}_i$ and $\mathbf{v}_i$, often called the *phase space.* It is clear that equation (1.1) does not contain all these details of the system. If valid, (1.1) can be used to calculate f at any instant in the future

[1] In Chapters 2–4, subscripts i and e are used to denote physical quantities related to the ions and electrons respectively. In Chapters 1 and 5 we mainly consider the ion population, and the subscript i has been supressed to simplify the notation: we write f instead of f_i, T instead if T_i etc. In fact, many of the principles discussed in Chapter 1 like the concept of the self-consistent field and the various temperatures (Section 1.2.3) are not restricted to the ion gas but apply equally well to the electrons.

[2] The electrostatic approximation is made i.e. the transverse part of the electromagnetic field is ignored and, as a result, the positions and velocities of the particles form a complete set of variables. Also, our treatment is classical and non-relativistic.

provided it is known at some time. One can ask, however, whether the reduced information contained in f is really sufficient to predict its own future; in other words, the details of the system not included in f may be important in the time evolution of f even if they are not of primary interest in view of the particular problem at hand.

The usual procedure is to start from the *Liouville equation* for the quantity $\rho(\mathbf{r}_1,...,\mathbf{r}_N,\mathbf{v}_1,...,\mathbf{v}_N,t)$, which is called the *Liouville density* and used to quantify the probability that the system is in the phase space volume element around $(\mathbf{r}_1,...,\mathbf{r}_N,\mathbf{v}_1,...,\mathbf{v}_N)$ at time t. The Liouville equation is based on the conservation of particles in the phase space of N particles and the assumption that the velocity-dependent part of the force acting on a particle is of the form $\mathbf{v}_i \mathrm{x} \mathbf{B}$. Instead of dealing with the *exact* n-particle distribution function which contains all the information of the system except the identity of the particles, one uses a statistical description and finds that the *average* n-particle distribution function (=the ensemble average of the exact distribution) is essentially the Liouville density integrated over the variables $\mathbf{r},\mathbf{v}$ of $N-n$ particles. Integrating the Liouville equation $N-1$, $N-2$,..., 1 times yields a set of differential equations for the average n-particle distribution functions, which is often called the *BBGKY chain* after Bogolyubov, Born, Green, Kirkwood and Yvon, who developed this theory.

The basic problem with the system is that the equation for the n-particle distribution function always contains the $(n+1)$-particle distribution function so that wherever the chain is truncated, there will always be one more unknown than there are equations. Solving these equations simultaneously would thus be as difficult as finding the solution for the original equations of motion: some physical approximation is needed to close the chain, making the set tractable. By "physical approximation" we mean that the resulting reduced information should determine its own future to an acceptable degree of accuracy. We note in passing that one is actually faced with similar problems when deriving the fluid equations by taking velocity moments of the kinetic equation (1.1).

In particular, the kinetic equation given by (1.1) is formally obtained as the first equation of the chain described above. The interaction term on the RHS depends on the two-particle distribution function, however. It is convenient to write the two-particle distribution function as a sum of the product of two one-particle distributions and the function P [in the notation of Sanderson (1981)], which is called the *correlation function*: if $P=0$, any two particles are uncorrelated. Accordingly, the interaction term in (1.1) is split into two terms. The first one describes the interaction between a test particle and the rest of the charged particles which are regarded as a continuous fluid. This is known as the *self-consistent field* interaction. The second term, which includes the correlation function P, is called the *collision integral.* As far as long-range Coulomb interactions between charged particles are concerned, regarding the particles as uncorrelated corresponds to zeroth order accuracy in the small parameter $(n_e\lambda_D^3)^{-1}$, where n_e is the electron number density and $\lambda_D=(\varepsilon_0 k_B T_e/n_e e^2)^{1/2}$ the *Debye length,* which characterizes the effective range of the Coulomb force due to a test particle in a plasma. Here ε_0 is the vacuum permittivity, k_B the Boltzmann constant, e the electron charge and T_e the electron temperature. The smallness of the parameter $(n_e\lambda_D^3)^{-1}$ means that there is a large number of particles in the *Debye sphere,* a sphere in physical space with radius λ_D, so that a test particle sees the rest of the plasma as a fluid and is not correlated to the individual motions of a single particle of the background plasma. In fact, the condition $(n_e\lambda_D^3)^{-1} \ll 1$ states that the thermal energy is much less than the typical electrostatic energy between the particles. This indicates that "close encounters" are rare, which is another physical argument for the replacement of microscopic Coulomb interactions between the particles by an averaged electric field. The kinetic equation for a plasma in which all particle interactions are described by the self-consistent electric field, is called the *Vlasov equation.* Several collective phenomena

particularly typical of plasmas, like the existence and collisionless damping of plasma oscillations, can be explained by this theory.

The actual collision term, which is due to correlations between the particles, can also be important if Coulomb interactions are to be described more accurately than by the self-consistent field. In the case of a partly ionized plasma, this term must also account for collisions between charged and neutral particles. However, the collision term depends on P, the correlation function, whose determination without further approximations presents a "formidable mathematical problem" (Sanderson, 1981). Two ways to overcome this problem have been suggested. First, one can work in the spirit of *Bogolyubov's hypothesis* and assume that the time scale related to variations in P is much shorter than that for the temporal evolution of the one-particle distribution function so that the asymptotic, time-independent form of P can be used in the collision term. Alternatively, one can avoid complex mathematics by totally ignoring the form of the collision term obtained from the BBGKY chain and use some model for the collisions instead, writing the collision term as a function of f, and thereby arrive at an equation of the form (1.1). This is, of course, unsatisfactory from the theoretical point of view because the model is not part of the original theory but has to be supplied in a somewhat arbitrary way.

In our region of interest, close ion-ion and ion-electron interactions are assumed to be negligible compared with ion-neutral collisions so that Coulomb interactions are to be described in the Vlasov approximation, the actual collision term accounting for ion-neutral collisions only. The particle interaction term in (1.1) can be written as

$$\left(\frac{\partial f}{\partial t}\right)_{\text{int}} = -q\,\mathbf{E}\cdot\frac{\partial f}{\partial \mathbf{v}} + \left(\frac{\partial f}{\partial t}\right)_{\text{C}}, \tag{1.2}$$

where q is the ion charge. The two terms on the RHS are related to the self-consistent field (due to plasma density fluctuations) and ion-

neutral collisions respectively. In what follows, we will review the two collision models used in the study of non-thermal plasma in the high-latitude ionosphere.

1.2.2. Collision models

The simplest model for collisions between the ions and the neutrals which conserves particles locally is the *relaxation model* (e.g. St.-Maurice and Schunk, 1973),

$$\left(\frac{\partial f}{\partial t}\right)_C = -\nu\ (f - f_n)\,, \tag{1.3}$$

where f_n is a Maxwellian velocity distribution in the neutral rest frame at the neutral temperature; f and f_n are normalized such that their velocity integrals are equal.[1] The effect of this collision term is to drive the ion distribution function towards a Maxwellian at the characteristic rate given by the phenomenological "collision frequency" ν. The details of the collisions such as particle orbits during the interaction are omitted, as well as the fact that the velocity of a particle after a collision is correlated to that before; also, collisions are regarded as instantaneous and local in physical space. The relaxation model is often used as a rough guide in order-of-magnitude estimates and cases where collisions give rise to a small modification of some process but are not the "zeroth-order effect" themselves. Incoherent scattering of radar waves from the upper E-region or the F-region serves as an example.

One of the most widely-used collision models is the *Boltzmann collision integral* [e.g. equation 1 of Schunk and Walker (1972)],

[1] In Chapter 5, small-amplitude plasma waves are considered and the distribution function is taken to be a sum of a "zeroth order" distribution and a rapidly oscillating part. In that study, f_n is normalized such that its velocity integral is equal to the *average* ion density. The factor n/n_0 in equation (5.1) then ensures local particle conservation. This form of the collisional operator has been discussed e.g. by Dougherty (1963).

which describes short-range binary collisions. Clemmow and Dougherty point out that this expression can actually be derived from the collision term in the first equation of the BBGKY chain by iteration, the small expansion parameter being $n_e r_0^3$, where r_0 is the range of the molecular force field. It is thus valid only if the gas is sufficiently dilute, so that simultaneous interactions of more than two particles are rare. A model for the interaction between the particles has to be specified in order to evaluate the collision term. It should be noted that the Boltzmann collision integral treats the collisions as instantaneous and local but the correlation of particle velocities before and after a collision can be controlled by varying the law of the force between the interacting particles.

In the case where the masses of the colliding particles are equal, it turns out that the relaxation model is a special case of the Boltzmann collision integral (St.-Maurice and Schunk, 1979). For a pure backscattering process in the center-of-mass frame of reference of the colliding particles, the differential cross section being of the form

$$\sigma(g,\chi) = \frac{\nu}{2\pi C} \frac{\delta(\cos\chi + 1)}{g}, \tag{1.4}$$

the Boltzmann collision integral reduces to the expression (1.3). In (1.4), g is the relative velocity between the colliding particles, χ is the center-of-mass scattering angle, δ the Dirac delta function and C is the constant to which the velocity integrals of f and f_n are normalized.

The fact that the relaxation collision model can be regarded as a backscattering model for binary collisions makes it more suitable for the qualitative description of resonant charge exchange interactions (between O^+ and O in the F-region, say) in which the velocity of a particle is changed substantially in a collision, than for polarization interactions, which give rise to more isotropic scattering.

1.2.3. Kinetic temperatures

When the velocity distribution of a species is not a Maxwellian i.e. the plasma is not in thermal equilibrium, temperature in the usual thermodynamic sense does not exist. It is useful, however, to consider "kinetic temperatures", which are related to random particle motions in different directions. We start by defining the three-dimensional (3-D) temperature T in terms of the second random velocity moment of the distribution function,

$$\frac{3}{2}k_B T = \frac{1}{2}m \int d^3\mathbf{v}\, \mathbf{c}^2 f(\mathbf{v}) = \frac{1}{2}m \left\langle \mathbf{c}^2 \right\rangle, \tag{1.5}$$

where the angular brackets are defined to denote the average value, the velocity integral of f is normalized to unity and $\mathbf{c}$ is the random part of the particle velocity,

$$\mathbf{c} = \mathbf{v} - \langle \mathbf{v} \rangle . \tag{1.6}$$

In general, kinetic temperatures associated with particle motions in various directions are not equal. The temperature in the direction of the unit vector $\mathbf{u}$ may be defined as

$$\frac{1}{2}k_B T_{\mathbf{u}} = \frac{1}{2}m \left\langle (\mathbf{u}\cdot\mathbf{c})^2 \right\rangle . \tag{1.7}$$

In particular, we can consider the temperatures T_x, T_y and T_z corresponding to the directions of x, y and z in a rectangular coordinate system (x,y,z). Choosing the coordinate system such that

$$\langle c_x c_y \rangle = \langle c_y c_z \rangle = \langle c_z c_x \rangle = 0 , \tag{1.8}$$

we find that an arbitrary 1-dimensional (1-D) temperature can be

conveniently expressed in terms of T_x, T_y and T_z:

$$T_u = T_{\xi,\phi} = (T_x \cos^2\xi + T_y \sin^2\xi) \sin^2\phi + T_z \cos^2\phi . \qquad (1.9)$$

Here ϕ and ξ are the polar and azimuthal angle in the spherical coordinate system whose polar axis is in the z direction; ξ is measured with respect to the x axis. On the other hand, the 3-D temperature in terms of T_x, T_y and T_z is

$$T = \frac{T_x + T_y + T_z}{3} . \qquad (1.10)$$

It is interesting to note that $T_{\xi,\phi}$ is equal to the 3-D ion temperature if $\cos^2\phi = 1/3$ and $\cos^2\xi = 1/2$ (Raman, 1980). However, this is not to say that T could be always deduced from a single 1-D measurement without any *a priori* knowledge of the distribution function. The point is that the coordinate system has to be such that the conditions (1.8) are satisfied i.e. the pressure tensor is in a diagonal form. In order to make this choice, one has to have some information of the velocity distribution; otherwise the "magic direction" remains unknown. If the velocity distribution is gyrotropic about the z axis (say), then $T_x = T_y$ and (1.9) takes the simple form

$$T_\phi = T_\perp \sin^2\phi + T_{||} \cos^2\phi , \qquad (1.11)$$

where we have renamed the 1-D temperatures perpendicular and parallel to the z axis for future reference. In this case, $T_\phi = T$ if ϕ equals 54.7°, which can be used to test the validity of 3-D models of gyrotropic velocity distributions. This topic will be further discussed in Chapter 3.

1.3. AURORAL ION VELOCITY DISTRIBUTIONS

1.3.1. Solutions of the kinetic equation

There are various approaches to obtaining an approximate expression for the velocity distribution of a given species. In the method discussed by Grad (1958), the distribution function is expanded as an orthogonal polynomial series about a Maxwellian. Stress, heat flow and all higher-order velocity moments are neglected in the lowest-order (5-moment) approximation and only taken into account via the polynomial terms of the series. Schunk (1977) has pointed out that an expansion of this kind is ideal for gases with enough collisions to maintain approximate thermal equilibrium but is not likely to be convergent if there are large relative drifts between the species or if the gas is collisionless, two well-known examples being ionospheric flows and the solar wind respectively. The reason is obvious: large departures of the distribution function from the Maxwellian shape and the increasing importance of the higher-order moments, for example the fact that temperature may be highly anisotropic, cannot be accounted for just by introducing a few correction terms. The temperature anisotropy for the solar wind protons is typically between 2 and 4, whereas in the terrestrial polar wind the anisotropy can be as large as 20 for H^+ at the distance of 8 earth radii (Holzer *et al.*, 1971). It is clear that these particle populations are far from thermal equilibrium and that a Maxwellian is not a reasonable lowest-order approximation for their distribution functions.

The effect of ion-neutral collisions on the ionospheric ion velocity distribution in the auroral zone was first investigated by Schunk and Walker (1972) who used the Grad method. The fact that the zeroth-order distribution function was a Maxwellian and only a few terms in the expansion were considered restricted these authors to small ambient electric fields or large ion-neutral collision frequencies.

However, they were able to predict that non-Maxwellian signatures become appreciable for field strengths above about 10 mV m^{-1} and that temperature is anisotropic in these cases: $T_\perp > T_{||}$.

St.-Maurice and Schunk (1973; 1974; 1976; 1977; 1979) published a remarkable series of papers in which various approaches to the solution of the kinetic equation were used. Their basic point was that in order to make quantitative predictions of the distribution shape for large electric fields, one has to choose the weighting function in the spirit of the problem at hand and not employ the usual Maxwellian, as this is the only way to avoid the labour associated with the computation of high-order polynomial terms describing the deviation from thermal equilibrium. The zeroth-order distribution function may be found by making an educated guess of the form of the distribution function, or it can be a solution of a simplified but related problem. The method of solution where the distribution function is expanded in a generalized orthogonal series about an arbitrary weight function has been discussed by Mintzer (1965). Grad's expansion is a special case of this method, the weight function being a Maxwellian.

In order to allow for large deviations of the velocity distribution from a Maxwellian, St.-Maurice and Schunk (1973) used the simple relaxation model (1.3) to simulate ion-neutral collisions and were able to obtain a closed-form solution for the Boltzmann equation. They found that non-Maxwellian features become important if, roughly speaking, the ion drift velocity is comparable to the thermal speed of the neutral gas. In the case of a large drift, the distribution in velocity space is bean-shaped if the collision frequency is comparable to the ion gyrofrequency but takes the form of a torus in the limit where the plasma is strongly magnetized i.e. the collision frequency is much smaller than the ion gyrofrequency. St.-Maurice and Schunk (1973) actually considered the full time-dependent Boltzmann equation and solved it by integration along the unperturbed orbits (or by the method of characteristics, as a mathematician would say). The transient part of the solution related

to the initial distribution was shown to die out in a time scale given by the inverse of the ion-neutral collision frequency. This time scale is typically of the order of a second in our region of interest. As a result, it is sufficient for most applications to consider solutions of the steady-state Boltzmann equation, as pointed out by St.-Maurice and Schunk (1979).

In the limit $\nu/\Omega<<1$, the simplicity of the relaxation model makes the analytical solution of the Boltzmann equation possible (St.-Maurice and Schunk, 1973). Assuming that the typical time scale for variations in the macroscopic quantities affecting the shape of the distribution, e.g. the ambient electric field, is much longer than the inverse of the collision frequency and the length scales associated with spatial inhomogeneities are much larger than the mean free path of the ions (~ thermal speed/collision frequency ~ 1km), the first two terms on the left-hand side (LHS) of (1.1) can be dropped, i.e. the plasma is regarded as time-independent and spatially homogeneous [e.g. Suvanto *et al.* (1989a)]. Furthermore, in the **ExB** drift frame the steady electric field is zero and only the magnetic part of the Lorentz force enters the acceleration **a** in the third term. Now, using (1.3), equation (1.1) becomes

$$\Omega \frac{\partial f}{\partial \theta} = -\nu \, (f - f_n) \, , \tag{1.12}$$

where θ is the gyrophase angle around the magnetic field in velocity space. Our notation is similar to that used by Ott and Farley (1975). The solution of (1.12), correct to zeroth order in the small parameter ν/Ω, is

$$f(\mathbf{v}) = \pi^{-3/2} \nu_n^{-3} I_0\left(2D' \frac{\nu_\perp}{\nu_n}\right) \exp\left(-D'^2 - \frac{\nu_\perp^2 + \nu_\parallel^2}{\nu_n^2}\right), \tag{1.13}$$

where I_0 denotes the modified Bessel function of zeroth order

(Abramowitz and Stegun, 1972) and the parameter D' is the ratio of the relative ion-neutral drift speed, which is assumed to be perpendicular to the magnetic field, to the thermal speed v_n of hypothetical particles at the neutral temperature whose mass is equal to the ion mass. It is customary to speak of "the neutral thermal speed" in the definition of D', as the relaxation model is usually applied to charge exchange reactions between O and O^+, in which case the ion and neutral masses are equal. The shape of the 1-D distribution function related to a particular angle ϕ with respect to the geomagnetic field, obtained by integrating the distribution function over the velocity components perpendicular to the line-of-sight, depends on ϕ and the parameter D' such that increasing D' tends to flatten the usual Gaussian shape until for D' large enough, the actual number depending on ϕ, a minimum develops at the origin (corresponding to the **ExB** drift point), and the distribution becomes double-humped. On the other hand, as ϕ varies from 0° to 90°, the distribution shape evolves from a Maxwellian to a double-humped shape provided D' is larger than about 1.3. The non-Maxwellian features are thus predicted to be most important in the field-perpendicular direction and are non-existent in the parallel direction according to this simple model.

St.-Maurice and Schunk compared their results with the calculations by Schunk and Walker (1972), who had used the Boltzmann collision integral and the Grad method, and showed that the relaxation model describes the momentum and energy moments of the distribution function correctly but overestimates the field-perpendicular components of the higher-order pressure and heat flow tensors and thereby exaggerates the temperature anisotropy. These shortcomings are due to the simplicity of the relaxation model, especially the fact that collisions are regarded as a pure backscattering process, as can be seen from the expression (1.4) for the differential cross section. Non-Maxwellian features are thus likely to be overestimated in the field-perpendicular direction but are

not allowed for in the parallel direction.

St.-Maurice and Schunk (1977) used the generalized orthogonal polynomial method to investigate the effect of polarization interactions between the ions and neutrals on the distribution function. The important conclusion of this work was that a bi-Maxwellian with different temperatures parallel and perpendicular to the geomagnetic field is a more appropriate lowest-order approximation for the ion velocity distribution than the usual (one-temperature) Maxwellian. This was in agreement with earlier calculations by Schunk and Walker (1972). It was found, however, that for relative ion-neutral drifts of the order of the neutral thermal speed, deviations from the bi-Maxwellian form become important. This confirmed the prediction based on the simple relaxation collision model.

At this stage, it is necessary to summarize all the approximations and simplifications made in the investigations discussed so far. In addition to the limitations inherent in the collision models, which were discussed in Section 1.2.2, the spatial and temporal variations have been assumed to be so slow that quasi-steady plasma conditions and spatial homogeneity can be assumed. Ott and Farley (1975) have discussed the assumptions related to the timescales for ion gyration, ion-neutral collisions and Coulomb collisions. They point out that the assumption $\nu/\Omega<<1$, which is a necessary condition for the analytical expression (1.13) to be valid, holds above about 130–140 km because the neutral density decreases exponentially with altitude. The requirement that Coulomb collisions should be less important than ion-neutral collisions is found to be more restrictive. Using the expressions by Spitzer (1956; p. 78) and Banks (1966) for the collision frequencies, Ott and Farley came to the conclusion that the above ordering of the timescales is valid above 130–140 km and well below 250 km, above which Coulomb collisions become important due to the increasing degree of ionization.

1.3.2. Empirical extension of theory

The first quantitative comparison between observed distribution functions and theoretical expectations was presented by St.-Maurice *et al.* (1976) who studied retarding potential analyzer (RPA) data from the Atmospheric Explorer C satellite. This work led to the re-interpretation of the theoretical distribution function predicted by the relaxation collision model and has provided the basis for a number of applications, e.g. calculations of the theoretical incoherent scatter spectrum and studies of plasma instabilities.

An RPA measures the current produced by ions whose kinetic energy is sufficient to overcome the applied potential at the gate of the instrument. As a result, one thus obtains the current as a function of the applied voltage. The analysis of about 50 volt-ampere characteristics revealed the fact that the 1-D distribution functions, which were measured in the field-perpendicular direction only, could be fit within noise level using theoretical 1-D distributions obtained from equation (1.13) provided the "neutral thermal speed" parameter was replaced by an adjustable parameter, which characterizes the ion speed after a collision. Motivated by this work, Raman (1980) and Raman *et al.* (1981) later used a distribution function of the form

$$f(\mathbf{v}) = \pi^{-3/2} v^{*-2} v_p^{-1} I_0\left(2D^* \frac{v_\perp}{v^*}\right) \exp\left(-D^{*2} - \frac{v_\perp^2}{v^{*2}} - \frac{v_\parallel^2}{v_p^2}\right) \qquad (1.14)$$

in their study of the incoherent scatter spectrum. The functional form of the perpendicular part of the distribution is the same as that of (1.13) but D' and v_n have been replaced by semi-empirical parameters D^* and v^*, and a Maxwellian description with thermal speed v_p is used in the magnetic field direction. For the relaxation model $D^*=D'$ (and $v^*=v_p=v_n$) but in a real situation we expect to

have $D^*<D'$ for the best fit to the real distribution function because the simple relaxation model tends to overestimate the degree of distortion from the Maxwellian shape. The introduction of the empirical parameter D^* has been further justified by Monte Carlo simulations (Barakat *et al.*, 1983) which showed that highly non-Maxwellian distributions which are qualitatively of the type (1.13) can be formed but this occurs for considerably higher electric fields than indicated by the simple relaxation model. The parameter D^* has also been employed by Hubert (1984) in his method of solution based on an analytical truncation scheme. Raman *et al.* used $v_p=v^*$ in their simulations of the incoherent scatter spectrum. It has been pointed out by Kikuchi *et al.* (1988) that this choice could have been improved by using kinetic theory arguments to fix the temperature anisotropy factor $T_\perp/T_{||}$. Furthermore, their simulations indicate deviations from the Maxwellian shape also in the field-parallel direction. In this thesis, we take $v_p=v^*$. It should be noted, however, that most of the results presented in this thesis are not sensitive to the assumption of a Maxwellian distribution in the field-parallel direction. For example, in fitting incoherent scatter spectra (Chapters 2–3), all that is required is a model of the 1-D line-of-sight distribution function. We will concentrate on large aspect angles, for which theoretical one-dimensional distributions derived from (1.14) are expected to be good approximations, in view of the observations by St.-Maurice *et al.* (1976). Furthermore, in our study of the ion cyclotron instability (Chapters 4 and 5), it will be shown that the growth rates only depend on the perpendicular distribution. These points will be discussed later in more detail.

It is useful to define a temperature T^* corresponding to the velocity parameter v^* (Raman *et al.*),

$$k_B T^* = \frac{1}{2} m v^{*2} . \tag{1.15}$$

The ion temperature related to the distribution function (1.14) with

$v_p=v^*$ can now be written as

$$T = T^*\left(1+\frac{2}{3}D^{*2}\right). \tag{1.16}$$

Examples of 1-D distribution functions for various values of D^* are presented in Figure 1.4. Here ϕ=73.5° is representative of the aspect angles used by the EISCAT UK Special Programme POLAR, which will be discussed in Chapter 3. As the non-Maxwellian parameter D^* is increased, the width of the velocity distribution increases with enhanced ion-neutral frictional heating; the distribution becomes flatter and a local minimum finally develops at the origin as a result of the ion-neutral scattering process. The plots may be compared with the discussion of Section 1.1 and Figure 1.3.

Figure 1.5, which is taken from St.-Maurice *et al.* (1976), shows deduced values of D^* as a function of perpendicular ion temperature, based on fits to 1-D velocity distributions perpendicular to the geomagnetic field. The theoretical curves A and B are based on the pure relaxation model. It is seen that the O^+ velocity distribution is closer to the shape predicted by the relaxation model than the molecular distributions. This is what one would expect because resonant charge exchange between O and O^+ is more efficient in producing a highly non-Maxwellian distribution than polarization interactions between molecular ions and neutrals. The slopes of the experimental curves behave according to theory for D^* less than about unity, but as the ion temperature is increased beyond 3000–4000K or so, the observed D^* values are less than those obtained by extrapolating from the small D^* data points. In fact, curve (D) indicates that the values of D^* may saturate at D^*~1.4, as pointedout by St.-Maurice *et al.* (1976). More observational evidence is clearly needed for this suggested saturation. However, the value 1.4 is close to the predicted instability threshold to be discussed in Chapter 4, so that the behaviour of D^* may be a reflection of the wave-induced diffusion process discussed in Chapter 5.

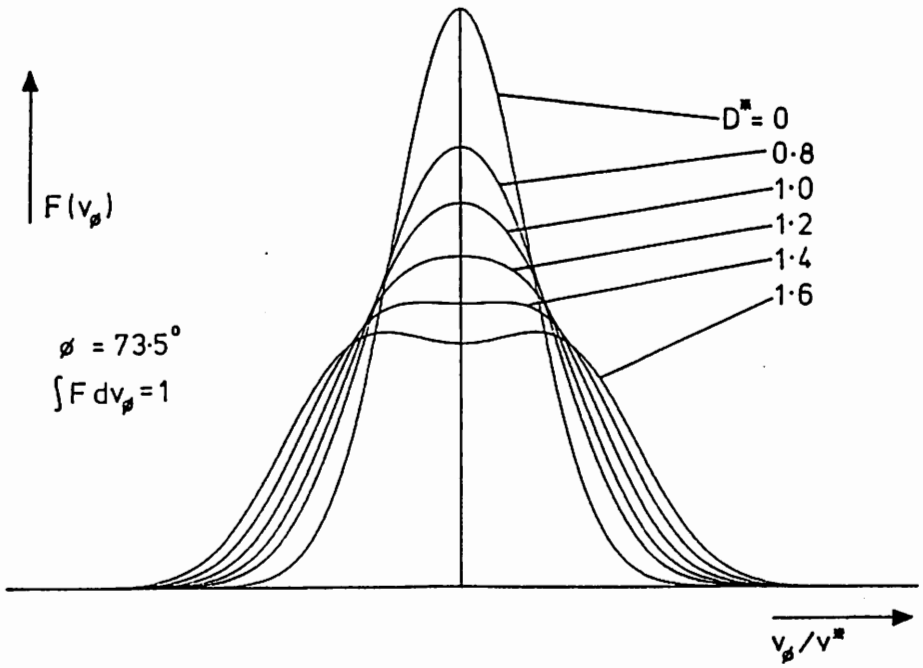

Figure 1.4. 1-D ion velocity distributions based on the empirical extension of the relaxation collision model for the aspect angle of 73.5°. Here v_ϕ denotes the line-of-sight speed.

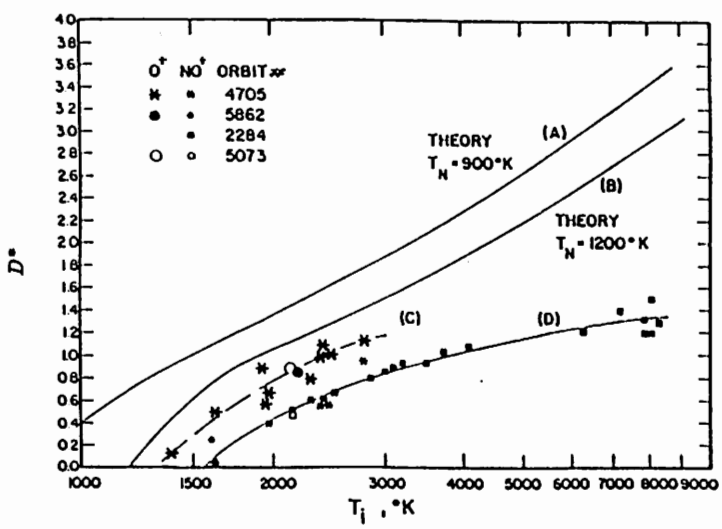

Figure 1.5. The parameter D^* as a function of ion temperature, as determined by fitting RPA data from the AE-C satellite to perpendicular 1-D distributions obtained from (1.14). The theoretical curves A and B are based on the pure relaxation collision model [equation (1.3)], while C and D indicate the measured shapes of the O^+ and NO^+ distributions, respectively. [From St.-Maurice *et al.* (1976).]

Alternatively, the nature of ion-neutral collisions may become different for very large drifts (Hubert, 1984).

As mentioned above, the RPA only measured the distribution function in the direction perpendicular to the magnetic field. Recently, incoherent scatter observations have revealed the effect of non-thermal ions on the scatter spectrum. The advantage of this method is that the plasma can be observed at various angles to the field. Also, studies of the temporal evolution of non-Maxwellian velocity distributions have been possible. Chapters 2 and 3 are devoted to this topic.

CHAPTER 2

INCOHERENT SCATTER FROM NON-MAXWELLIAN PLASMA

2.1. INTRODUCTION

In the late fifties, Gordon (1958) pointed out that Thomson scattering of electromagnetic waves by free electrons could be used to probe the upper atmosphere by radar, and soon the first incoherent scatter signals from the ionosphere were indeed recorded by Bowles (1958). It became clear, however, that the observations could not be explained by the simple concept of individual electrons doing the scattering with the ions being unimportant. Incoherent scatter only became a very powerful tool for studying the upper atmosphere when it was realized that for the radar frequencies commonly used, the exact shape of the spectrum is actually a reflection of collective density fluctuations maintained at the thermal level within the plasma and depends on a number of ionospheric parameters. A correct interpretation of the data could thus yield much information on the ionosphere. Several approaches to obtain the theoretical scatter spectrum were used in a series of papers [Dougherty and Farley (1960); Fejer (1960); Salpeter (1960); Hagfors (1961)], all of which led to the same result and showed remarkable agreement with observations. They formed the basis for later incoherent scatter experiments, which "afford a pleasing contact between real plasmas, which are so often badly behaved, and kinetic theory, which is often so abstruse", as summarized by Clemmow and Dougherty (1969).

Theoretical work on ion velocity distributions in the high-latitude ionosphere showed that significiant distortions from the Maxwellian shape are possible in the case of a supersonic ion flow through the neutral gas. However, one limitation to the incoherent scatter theory in its original form was the assumption of a Maxwellian ion gas. Raman (1980) performed a parametric study of the spectral shape using the ion velocity distribution based on the relaxation model for ion-neutral collisions and retarding potential analyzer studies (St.-Maurice *et al.*, 1976), and showed that the assumption of Maxwelian plasma in incoherent scatter data analysis can lead to relative errors of possibly more than 50% in the determination of electron and ion temperatures, even if the ion composition is assumed to be known. After conclusive evidence of non-Maxwellian spectral signatures had been obtained (Lockwood *et al.*, 1987), a need became apparent to develop an analysis procedure which takes into account the non-thermal nature of the ions, not only to study non-Maxwellian velocity distributions in their own right but also to avoid misinterpretations in general ionospheric research; although the details of the velocity distribution may not be the main interest for most ionospheric physicists studying global phenomena, they have to be considered in order to avoid errors in the quantities of interest such as the ion and electron temperatures.

In this chapter, the basic idea of incoherent scatter is reviewed, followed by a discussion of the scatter spectrum based on the semi-empirical ion velocity distribution (1.14), which was also employed by Raman (1980) and Raman *et al.* (1981). A semi-analytical method of computing the spectral density function is described, following Suvanto (1988). Finally, we describe the data analysis procedure to be used in Chapter 3.

2.2. BASIC PRINCIPLE OF INCOHERENT SCATTER

In an incoherent scatter experiment, the radar detects plasma structures with the scale length $2\pi/k$, where $k = |\mathbf{k}|$, $\mathbf{k}$ being fixed

by the radar geometry such that

$$\mathbf{k} = \mathbf{k}_S - \mathbf{k}_I . \tag{2.1}$$

Here $\mathbf{k}_S$ and $\mathbf{k}_I$ are the scattered and incident wave vectors respectively. The nature of the scattering process depends on the relative magnitudes of $\mathbf{k}$, associated with the experimental set-up, and the Debye length λ_D, which is a length scale characterizing the target itself. As discussed in Chapter 1, λ_D is the effective range of the Coulomb force due to a test particle in a plasma and can be regarded as the transition length between collective phenomena, typical of a plasma, and processes related to single particle properties. Defining the parameter α such that

$$\alpha = k \lambda_D , \tag{2.2}$$

we note that for $\alpha >> 1$, which corresponds to small radar wavelengths, the probing signal can "penetrate" into the Debye sphere, so to speak, and "see" single particles, the scattering thus being classical Thomson scatter from individual electrons, while in the long wavelength limit $\alpha << 1$ the scattering is controlled by collective density fluctuations within the plasma. As a result, the dielectric properties of both the ions and the electrons must be considered in a theoretical scheme. Furthermore, the fluctuation levels are closely related to the appropriate damping rates governed by interactions between waves and particles and, referring to Section 1.2, a kinetic description is thus required. The shape of the scatter spectrum, i.e. the normalized scattered power as a function of the Doppler shift from the incident frequency, thus depends on the distribution functions of all the charged particle species so that in the long wavelength limit, the scattered signal contains information of physical parameters related to both the ion and electron populations, at least in principle.

For $\alpha<<1$, the scatter spectrum splits into two parts often referred to as the ion and electron components. The ionic part is concentrated around the radar operating frequency, and its width is typically orders of magnitude less than the radar frequency. It is this part of the spectrum which is usually analysed and yields most information of the ionosphere, the reason being that it contains most of the scattered power. The double-humped shape of the ionic part of the spectrum in the case of a Maxwellian ion velocity distribution, which can be seen from Figures 2.1 (the plot with $D^*=0$) and 2.2 (the plots with small α), is often interpreted as being due to scattering from two ion-acoustic waves propagating towards and away from the radar along the **k** vector. The electron part of the spectrum, related to scattering from electrostatic plasma oscillations, consists of two lines, one of which is above and one below the incident frequency. These are, however, beyond the scope of this work, which is devoted to non-Maxwellian ion distribution functions, and will not be discussed any further.

Finally, we note that as far as Maxwellian plasma is concerned, agreement between observations and theory is very good. Farley (1979) has pointed out that in some cases, the experimental results differ from theoretical predictions by less than 1%. Furthermore, incoherent scatter provides an experimental verification of the effect of Landau damping of plasma density fluctuations. This phenomenon was predicted theoretically by Landau (1946) but was not generally accepted in the early days of incoherent scatter experiments, until "Landau damped" theories proved to better in explaining the observations than approaches where this effect was neglected. Incoherent scatter thus provides a fruitful link between geophysical research and fundamental concepts of plasma physics.

2.3. SPECTRAL DENSITY FUNCTION

Adopting the notation used by Raman *et al.*, we write the spectral density function, which is the normalized scattered power per unit

frequency, as

$$S(\mathbf{k},\omega) = 2\left|\frac{H_e}{\varepsilon}\right|^2 M_i + 2\left|1-\frac{H_e}{\varepsilon}\right|^2 M_e, \tag{2.3}$$

where

$$\varepsilon = 1 + H_e + H_i \tag{2.4}$$

is the plasma dielectric function; H_e and H_i are the contributions due the electrons and the ions respectively.[1] The quantities affected by the non-thermal nature of the ions,

$$H_i = \frac{1}{2\alpha^2}\frac{T_e}{T^*}\left[\int_P dp\,\frac{dg/dp}{y-p} + i\pi\left(\frac{dg}{dp}\right)_{p=y}\right] \tag{2.5}$$

and

$$M_i = \frac{\pi}{kv^*}g(y), \tag{2.6}$$

are of primary interest here. The corresponding electron functions, H_e and M_e, are given by Raman (1980) and Raman *et al.* (1981) for the cases $\mathbf{B}=0$ and $\mathbf{B}\neq 0$ respectively. Except for a brief comment on the role of the magnetic field, these well-known functions will not be discussed here as they do not contain non-Maxwellian effects.

In (2.5), P denotes the Cauchy principal value and the second term on the RHS is the contribution from the pole which is by-passed

[1] These correspond to ε_e and ε_i to be introduced in Chapter 4. The sign convention in the periodicity factor $\exp[-i(\mathbf{k}\cdot\mathbf{r}-\omega t)]$ used by Raman to derive them is different from that adopted in Chapter 4, however, so that different symbols are used here to avoid confusion. Also, the ions are considered here as unmagnetized, whereas the effect of the magnetic field is taken into account in the instability calculations.

according to the Landau prescription [compare with equation (5.21)]. Also, y is the normalized Doppler shift from the incident frequency and g is the 1-D ion velocity distribution along **k**:

$$y = \frac{\omega}{k\, v^*} \tag{2.7}$$

$$g(p) = \frac{1}{\pi^{3/2}} \int_{-\infty}^{\infty} \int_{-\infty}^{\infty} dq\, dr\, I_0\left(2D^* \sqrt{r^2 + (p \sin\phi - q \cos\phi)^2} \right) \times$$

$$\times \exp\left\{ -D^{*2} - \left[r^2 + (p \cos\phi + q \sin\phi)^2 + (p \sin\phi - q \cos\phi)^2 \right] \right\}. \tag{2.8}$$

In (2.8), the specific form (1.14) of the ion velocity distribution function has been used, ϕ is the angle between **k** and the geomagnetic field (the aspect angle), I_0 is the modified Bessel function of zeroth order, and the integration is over the normalized velocity components perpendicular to **k**.

We note in passing that in many existing incoherent scatter analysis programs, it is customary to ignore the effect of the magnetic field, i.e. both the ion and electron functions are written for the case **B**=0. While this approach can be used for the ions (as discussed e.g. by Raman), it is not the appropriate lowest-order approximation for the electrons, which are strongly magnetized in the scattering process because of their large gyrofrequency and small Larmor radius. In fact, the magnetization is so strong that the electrons are essentially constrained to move one-dimensionally along the field line. It has been pointed out [e.g. Vallinkoski (1987)], however, that the unmagnetized expressions yield practically the same spectrum for the ion line as the magnetized approach for the geometrical configurations of most radar experiments. The reason is that the parts of the electron functions which are affected by letting $\mathbf{B} \to 0$ happen to be negligible anyway for sufficiently small frequencies.

Referring to the expressions given by Raman and Raman *et al.*, the function H_e is essentially constant ($\approx\alpha^2$) for the ion line, and the choice between **B**=0 and **B**≠0 only specifies the form of a quantity of the order of $\omega/k_{||}v_e<<1$, where $v_e=(2k_BT_e/m_e)^{1/2}$ is the electron thermal speed. The approximation $H_e\approx\alpha^2$ can therefore be used instead of the more complicated unmagnetized electron expressions, which give rise to irrelevant (though luckily negligible) extra terms, to obtain essentially the same spectrum but by using the physically reasonable approach and less CPU time in spectral computations. This approximation fails if $\omega/k_{||}v_e$ is of the order of unity or larger, corresponding to roughly 1^0 or less off perpendicularity. Similar arguments can be used for the estimation of M_e. In this work, however, the "unmagnetized" expressions were used to enable direct comparison between the results by Raman *et al.* and the computational method used here.

We now turn to the calculation of the line-of-sight ion distribution function, equation (2.8). Changing the integration variables,

$$\begin{aligned} x &= r \\ y &= -p\sin\phi + q\cos\phi \end{aligned} \qquad (\cos\phi \neq 0), \tag{2.9}$$

equation (2.8) can be written as

$$g(p) = \frac{\exp(-D^{*2}-p^2)}{\pi^{3/2}|\cos\phi|} \times$$

$$\times \int_{-\infty}^{\infty}\int_{-\infty}^{\infty} dx\,dy\; I_0\left(2D^*\sqrt{x^2+y^2}\right)\exp\left[-x^2-\left(\frac{y+p\sin\phi}{\cos\phi}\right)^2\right]. \tag{2.10}$$

Introducing the series expansion of I_0 , equation (A.10), in (2.10), the double integral becomes

$$\sum_{k=0}^{\infty} \frac{D^{*2k}}{k!^2} \int_{-\infty}^{\infty} \int_{-\infty}^{\infty} dx\, dy\, \left(x^2+y^2\right)^k \exp\left[-x^2-\left(\frac{y+p\sin\phi}{\cos\phi}\right)^2\right]$$

$$= \sum_{k=0}^{\infty} \frac{(-1)^k D^{*2k}}{k!^2} \times$$

$$\times \left\{ \frac{\partial^k}{\partial \alpha^k} \int_{-\infty}^{\infty} \int_{-\infty}^{\infty} dx\, dy\, \exp\left[-\alpha\,(x^2+y^2)+y^2-\left(\frac{y+p\sin\phi}{\cos\phi}\right)^2\right] \right\}_{\alpha=1} . \tag{2.11}$$

The elementary integrations over x and y give the result

$$g(p) = \frac{\exp(-p^2)}{\pi^{1/2}} \sum_{k=0}^{\infty} A_k(p)\, D^{*2k}, \tag{2.12}$$

where

$$A_k(p) = \frac{(-1)^k}{k!^2} \frac{\exp(-D^{*2} - p^2\tan^2\phi)}{|\cos\phi|} \times$$

$$\times \left\{ \frac{\partial^k}{\partial \alpha^k} \frac{\exp\left[\dfrac{p^2\tan^2\phi}{\cos^2\phi\,(\alpha+\tan^2\phi)}\right]}{\left[\alpha\,(\alpha+\tan^2\phi)\right]^{1/2}} \right\}_{\alpha=1} . \tag{2.13}$$

An expression for the slope of the distribution, which is also needed in the derivation of the spectral density function, is obtained simply by taking the derivative of (2.12); it includes dA_k/dp as well as A_k. Note that for $D^*=0$ only the $k=0$ term in (2.12) is nonzero and we recover the usual Maxwellian distribution.

The Cauchy principal value integral in (2.5) was performed numerically by Raman, who applied the Gauss-Hermite quadrature

procedure to the singular integrand directly. As pointed out by Raman himself, the method works provided that none of the points where the integrand is computed is too close to the singular point. Also, a large number of integration points are needed in the neighbourhood of the pole, and they should be located symmetrically about $p=y$ because no explicit information about the principal value character of the integral is included in the numerical integration procedure itself. As a result, the integration points should be taken to be functions of the singular point, which depends on frequency ω. This would make the computations very lengthy, however. Furthermore, the polynomial approximation of the integrand, which is the basis of the Gauss-Hermite quadrature method (Abramowitz and Stegun, 1972), fails in the case of a singular integrand. Raman checked his calculations graphically, but the question still remains whether a set of parameters exists for which this method leads to erroneous results. The problem can be removed by noting that

$$\int_P dp \frac{dg/dp}{y-p} = g_1(y) \int_P dp \frac{\exp(-p^2)}{y-p} - \int_{-\infty}^{\infty} dp \exp(-p^2) g_2(p) \quad (2.14)$$

with the notations

$$g_1(p) = \exp(p^2) \frac{dg}{dp} \quad (2.15)$$

$$g_2(p) = \frac{g_1(p) - g_1(y)}{p-y}. \quad (2.16)$$

The first term on the RHS of (2.14) is equal to $-\pi^{1/2} g_1(y) Z_R(y)$, where Z_R is the real part of the plasma dispersion function (see Appendix A.1). The function g_2 in the second term is analytic so that the Gauss-Hermite integration method can be rigorously

applied. We have thus expressed the integral of a singular integrand in terms of the well-known plasma dispersion function and an integral of an analytic function.

2.4. SPECTRAL SHAPES

Raman presented a detailed parametric study of the spectrum, so that we will only review a few main features of physical interest here. First of all, we have checked that the results of our procedure are in agreement with his predictions in the special case ϕ=54.7°.

Examples of non-Maxwellian spectra are shown in Figure 2.1. The associated ion distribution functions were presented in Figure 1.4. Referring to equation (2.3), local maxima of the spectral density function occur when, roughly speaking, the dielectric function ε is "small". It is clear that ε is always nonzero; ε=0, ω being real, would correspond to marginally unstable waves along the line-of-sight, which is beyond the region of validity of the scatter theory used here. (In fact, growth of linear waves is restricted to directions almost perpendicular to **B**.) If, however, some particular wave mode is only weakly damped, ε can become small, resulting in a peak in the spectrum. Increasing D^* makes the slope of the velocity distribution more positive for small values of velocity, which tends to cancel the electron Landau damping. The nett result is reduced damping of the fluctuations for small phase velocities, hence the central peak of the spectrum. Also, the peaks due to scattering from ion-acoustic waves at larger phase velocities, as they are traditionally explained, are depressed because the distribution function falls off to zero more rapidly than the Maxwellian distribution and, consequently, Landau damping is increased, as pointed out by Raman *et al.*

Figures 2.2 and 2.3 show the finite Debye length effect on the spectrum for the well-known Maxwellian case [the plots are identical to those presented by Evans (1969)] and for non-thermal

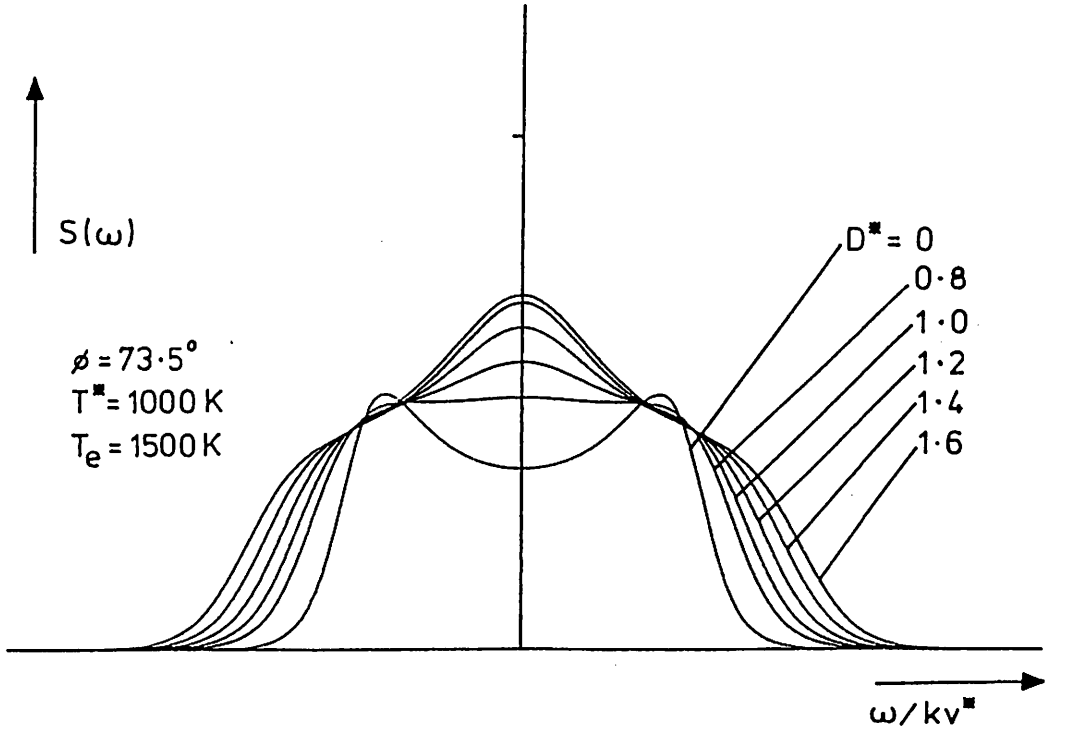

Figure 2.1. Incoherent scatter spectra for various values of D^*. The aspect angle is 73.5°. The associated line-of-sight ion velocity distributions are shown in Figure 1.4.

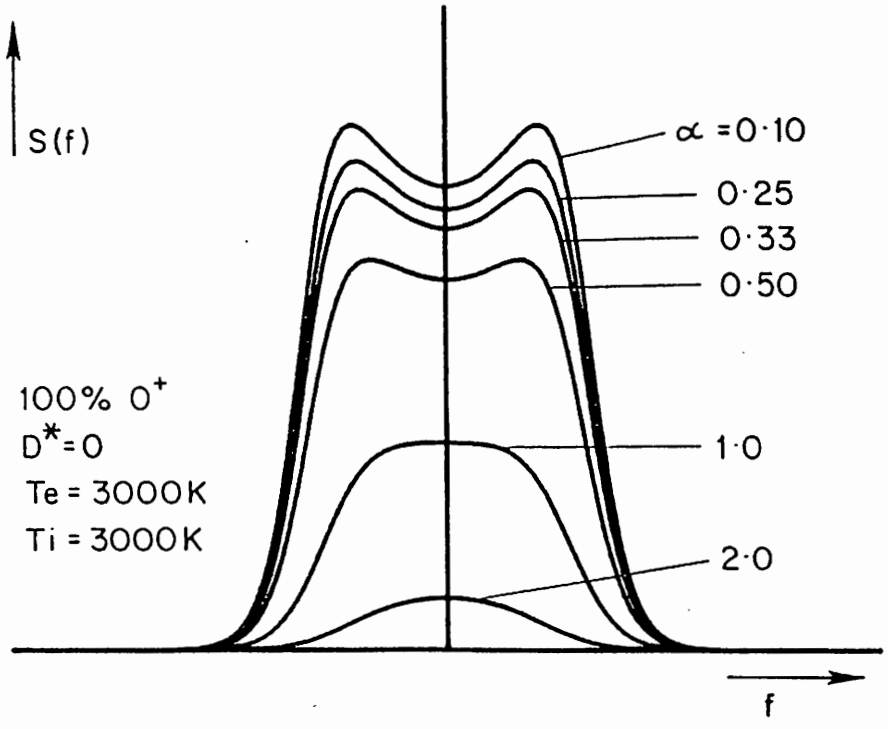

Figure 2.2. Finite Debye length effect on the scatter spectrum in the case of a Maxwellian ion velocity distribution i.e. for $D^*=0$. The spectra are shown for various values of α.

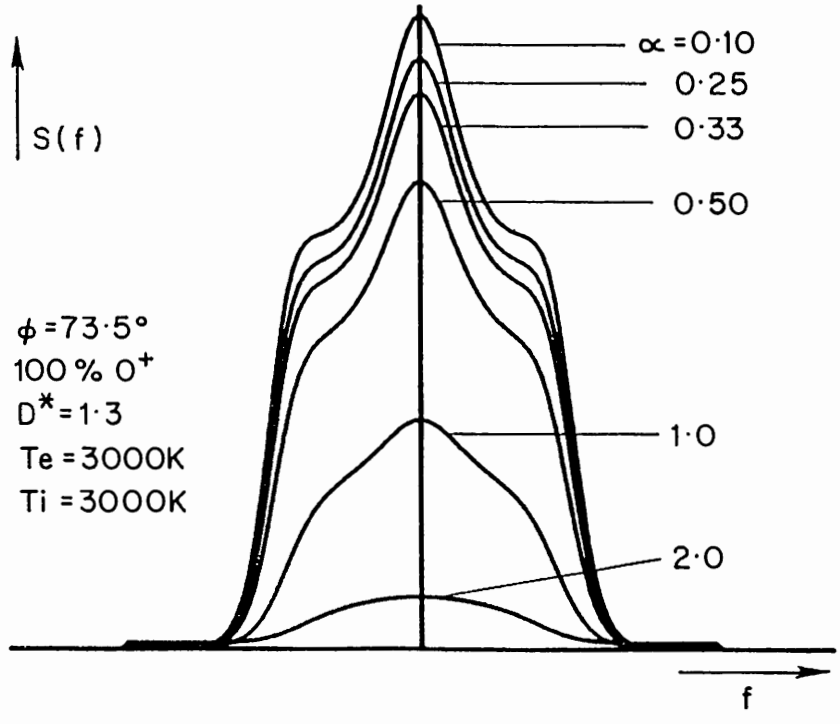

Figure 2.3. Same as Figure 2.2, but for a highly non-Maxwellian ion velocity distribution ($D^*=1.3$) viewed at the aspect angle of 73.5°.

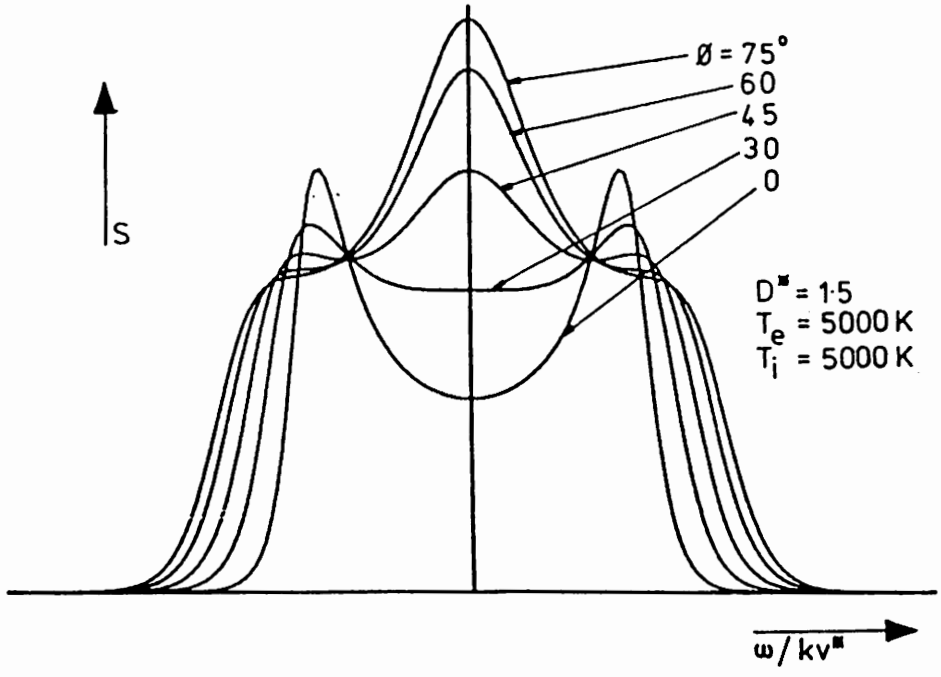

Figure 2.4. The aspect angle dependence of a non-Maxwellian spectrum.

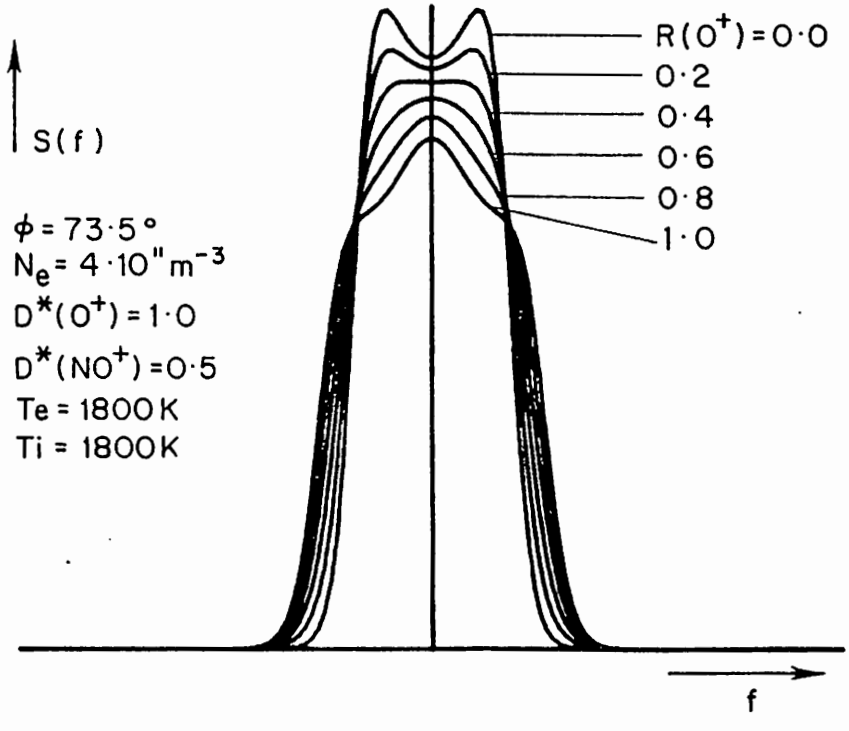

Figure 2.5. The effect of ion composition on the scatter spectrum for a mixture of highly non-Maxwellian O^+ ions and slightly non-thermal NO^+ ions. Here $R(O^+)$ denotes the fractional O^+ concentration.

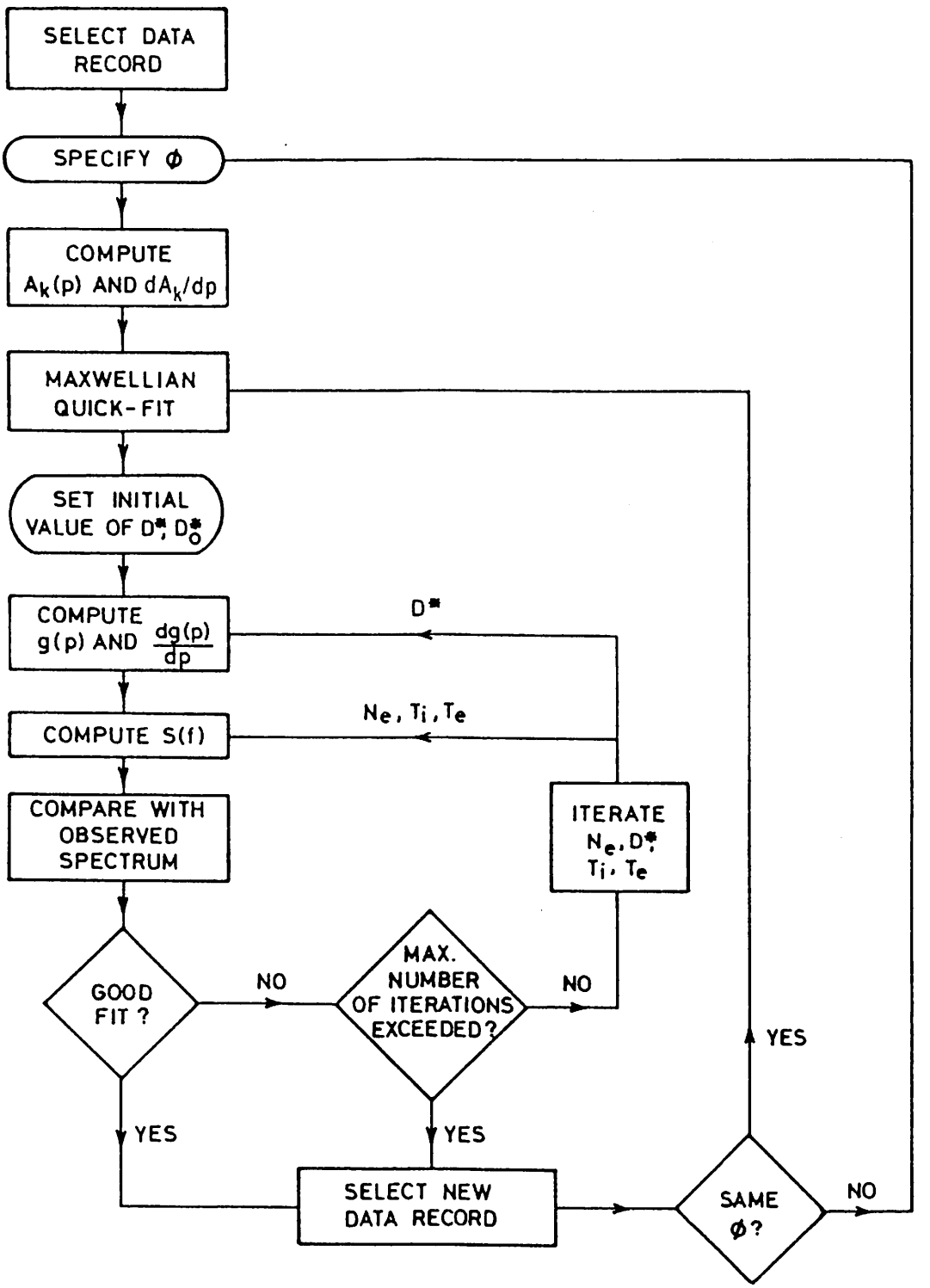

Figure 2.6. Flow chart illustrating the non-Maxwellian data analysis procedure. See the last paragraph of Section 2.4.

plasma, respectively. Note that for the largest value of α, the spectra are very similar to each other, owing to the fact that the scattering in this case is Thomson scatter from individual electrons rather than due to collective density fluctuations within the plasma and, consequently, the form of the ion velocity distribution is not important in this limit. In the transition region corresponding to $\alpha \sim 1$, the features which are characteristic of non-thermal plasma appear, and non-Maxwellian spectra can be identified by the central peak, as opposed to the double-humped shape, typical of thermal plasma.

The aspect angle dependence of the spectral shape is illustrated in Figure 2.4. Increasing the aspect angle for fixed D^* has qualitatively the same effect as increasing D^* for fixed ϕ. For $\phi=0$, the empirical extension of the relaxation model, on which our calculations are based, allows for no deviations from the Maxwellian spectral shape.

The expressions for the spectral density function given above were generalized to allow for two ion species, and tested against previously published spectra for a mixture of O^+ and He^+ thermal ions (e.g. Moorcroft, 1964) and for O^+ and NO^+ non-thermal ions (Raman, 1980). Other tests have been carried out in the Maxwellian limit, by making comparisons with the results of the spectral synthesis routines in the standard EISCAT analysis programme (Lejeune, 1979). In all tests, the routines gave identical spectra, to within computational rounding errors. An example of how the ion composition affects the spectrum is shown in Figure 2.5. The O^+ velocity distribution has been chosen to be more distorted from a Maxwellian than the NO^+ distribution, as observed by St.-Maurice *et al.* (1976) and discussed by St.-Maurice and Schunk (1979). We note that although NO^+ is considered, our results apply to cases where the molecular ion is N_2^+ or O_2^+ because the masses of the all three ions are close to each other and, as a result, the corresponding spectra are practically identical. It is seen that as the fractional

concentration of O^+, $R(O^+)$, increases and the average ion mass thus decreases the spectrum becomes wider, as in the case of mixed-species thermal plasma. However, when the plasma is pure NO^+ [$R(O^+)$=0] the spectrum appears to be very similar to that for Maxwellian plasma, on account of the low $D^*(NO^+)$ value. When the plasma is pure O^+ [$R(O^+)$=1], the spectrum is of the single-peaked form shown in Figure 2.1. At intermediate $R(O^+)$, the spectra evolve smoothly between these two limits, with a flat-topped spectrum at $R(O^+)$=0.4 and a "bullet" shape (very similar to that for high-temperature Maxwellian ions) for $R(O^+)$=0.6.

The non-Maxwellian analysis procedure, illustrated by Figure 2.6 for the single species case (the multiple species case is a simple extension of this algorithm), can be divided into two parts. The first part includes the calculation of the coefficients A_k and dA_k/dp needed in the evaluation of the theoretical line-of-sight velocity distribution and its slope. These computations are very time-consuming but do not need to be repeated until data for a different aspect angle are selected. The actual fitting procedure then follows. The initial value of D^*, D^*_0, is arbitrarily specified and the initial values of N_e, T_e and T_i are taken from an approximate Maxwellian "quick fit" to the data. The model spectrum is then computed for various sets of values for the plasma parameters which are iterated until an agreement with the observed spectrum is obtained. The fitting is actually carried out in the time domain i.e. on the autocorrelation function, which is essentially the Fourier transform of the spectral density function.

2.5. DISCUSSION

A procedure has been discussed for analysing incoherent scatter spectra from non-thermal plasma. An analytic series representation for the line-of-sight ion velocity distribution function was derived; the advantage of this approach is that the coefficients of the expansion need only be computed once for a given aspect angle. We also

discussed a simple way of avoiding the singular integrand in the ion part of the dielectric function.

For $\alpha >> 1$, individual electrons do the scattering, and the shape of the ion velocity distribution function is unimportant in this limit. For incoherent scatter radar work one typically has $\alpha << 1$ i.e. the scattering is from collective plasma density fluctuations, which are also controlled by the ion velocity distribution function, among other factors. It was shown that the distinction between spectra associated with thermal and non-thermal plasma is nonexistent for large α but becomes evident as soon as α becomes comparable to unity. The fact that non-thermal signatures are visible in the transition region between "truly incoherent" i.e. Thomson scatter and "quasi-coherent" scattering is of some importance because $\alpha \sim 1$ may occur for realistic (though not typical) sets of values of ionospheric parameters.

In Chapter 3, the analysis procedure will be applied to data from the EISCAT Special Programme POLAR and Common Programmes CP-4 and CP-3-E. Before concluding the present chapter, however, we would like to make a comment on the relevance of the use of the Raman *et al.* ion velocity distribution function, in the light of recent Monte Carlo calculations by Kikuchi *et al.* (1988). It should be noted that although the 3-D distribution given by (1.14) implies a 1-D distribution of the form (2.12) for a particular value of ϕ, the reverse is not true; the latter is more general as it does not contain any information of 3-D properties of the ion velocity distribution for a single value of ϕ. This information is lost in the integration over the velocity components perpendicular to the line-of-sight, of course. Line-of-sight distribution functions (2.12) were actually used by Kikuchi *et al.* to approximate the simulation outputs. However, the simulations show that one should not rely too heavily on the 3-D distribution function (1.14) itself. In other words, a *single* function given by (1.14) cannot be used to produce the 1-D distribution functions for *all* aspect angles simply by varying ϕ and keeping the other parameters fixed. Instead, fitting of (2.12) to observed line-of-

sight distributions at different aspect angles would probably yield a variety of values for D^* and T^*, and one is motivated to consider two approaches to data analysis. First, it can be assumed that (1.14) *is* a good approximation of the 3-D distribution. In this case, the line-of-sight ion temperature as well as the average ion temperature can be determined (although the reliability of the latter quantity should be questioned) by viewing the plasma at only one aspect angle. Secondly, one can completely ignore the 3-D structure of (1.14), using (2.12) as the starting point and a convenient analytic approximation to the line-of-sight distribution function and determine only the line-of-sight temperature by fitting (2.12) with the data. As a result, less information is obtained, but the approach is more general. Kikuchi *et al.* (1988) used the field-perpendicular Raman *et al.* distribution function to approximate results of their Monte Carlo simulations for all aspect angles. In other words, they simply set ϕ=90° in (2.8) and let D^* alone account for non-Maxwellian effects in (2.12), including the aspect angle dependence. In Chapter 3, we will use the correct aspect angle in each case and, in addition to the determination of the line-of-sight ion temperature, we also have the option to deduce the average ion temperature T_i and the ion temperature anisotropy related to the semi-empirical distribution function (1.14). If the validity of (1.14) is not assumed, T_i given by (1.16) is regarded just a mathematical quantity without any physical meaning and only the line-of-sight temperature is considered. We stress that the fitting procedure itself does not require the complete validity of the 3-D distribution function (1.14).

CHAPTER 3

INCOHERENT SCATTER OBSERVATIONS

3.1. INTRODUCTION

Although the series of theoretical papers about non-Maxwellian ion velocity distributions in the auroral ionosphere appeared in the seventies, observations of non-thermal effects remained few for a long time. Swift (1975) interpreted asymmetric incoherent scatter spectra from the Chatanika radar as indications of non-equilibrium E-region plasma. However, the spread of velocities within the scattering volume could give the same asymmetry by smearing the spectrum, as pointed out by Lockwood *et al.* (1987). The ion velocity distribution function based on the relaxation collision model was found to be in qualitative agreement with retarding potential analyzer data from the Atmospheric Explorer C satellite (St.-Maurice *et al.*, 1976); it should be noted, however, that information was only obtained in the field-perpendicular direction and studies of the temporal evolution of non-thermal plasma were not possible. These measurements remained the only clear evidence for non-thermal plasma for over a decade.

In 1980 Raman predicted the effect of non-Maxwellian plasma on the incoherent scatter spectrum in his Ph.D. thesis; about a year later, the European Incoherent SCATter (EISCAT) radar started its operation. Perraut *et al.* (1984) described tristatic EISCAT observations showing evidence for bi-Maxwellian ion velocity distributions in the auroral oval, and temperature anisotropies deduced by Løvhaug and Flå (1986) were, on occasion, larger than

those predicted for realistic collisional models. This meant that either the standard ion-neutral frictional heating theory was invalid at times or that the assumption of a Maxwellian line-of-sight ion velocity distribution made in the analysis was erroneous. However, the observed field-parallel temperatures could be explained by conventional arguments. We note that this conclusion is in agreement with the theoretical prediction that the deviation of the ion velocity distribution function from a Maxwellian is small in the field-parallel direction and, consequently, the standard Maxwellian analysis is likely to yield the correct line-of-sight temperature in this case.

The first ground-based observations providing conclusive evidence of non-Maxwellian plasma were presented by Lockwood *et al.* (1987), who used the UK Special Programme POLAR, for which the aspect angle remained large (~70°) and fixed. These authors studied the shape of the incoherent scatter spectrum during rapid, transient poleward flows at high latitudes in the dayside ionosphere (Todd *et al.*,1986). Owing to the burst-like nature of these events, the neutral atmosphere does not have time to respond (see Section 1.1), so that a large relative drift between the ions and the neutrals must occur. Also, it is possible to unambiguously relate variations in the ion drift velocity to changes in the spectral width and shape. In cases where the line-of-sight ion drift velocity became comparable to or larger than the estimated neutral thermal speed, Lockwood *et al.* (1987) were able to identify non-Maxwellian spectral signatures predicted by Raman (1980) and Raman *et al.* (1981) and showed that these features could exist for at least the lifetimes of the flow burst events, i.e. several minutes. It was also pointed out that performing the standard analysis of the data assuming a Maxwellian ion distribution function leads to "anti-correlation" of the deduced ion and electron temperatures: the apparent electron temperature was deduced to decrease at the same time as excessively high apparent ion temperatures were observed [Lockwood *et al.* (1987); Winser *et al.* (1987); Lockwood *et al.* (1988); Moorcroft and Schlegel (1988)].

This phenomenon seemed to lack any reasonable physical explanation, but was expected to result from the invalidity of the analysis procedure. Raman *et al.* had found the anti-correlation to be a feature of performing a Maxwellian analysis in the case of non-thermal ions, and the presence of this effect was regarded as one evidence for non-Maxwellian plasma. Winser *et al.* (1987) used data from EISCAT Common Program CP-3-E to show that the aspect angle dependence of the spectral shape was qualitatively similar to that predicted by Raman *et al.* for periods when the apparent ion temperature anisotropy, deduced assuming a bi-Maxwellian velocity distribution, exceeded the values computed using realistic collisional models. It was also found that spectra indicating the presence of non-thermal ions could exist in a quasi-steady state for periods up to one hour. Further evidence for non-Maxwellian plasma was presented by Moorcroft and Schlegel (1988) who made the first attempts to fit incoherent scatter data (from the Common Program CP-3-C) to the Raman *et al.* model. Significiant non-thermal effects were detected, although the spectra did not visually appear non-Maxwellian, unlike those reported by Lockwood *et al.* (1987). However, there were some discrepancies in the analysis, and the authors pointed out that the theory should be improved by allowing for the presence of molecular ions and instabilities, for example.

As discussed in Chapter 1, Lockwood and Fuller-Rowell (1987) have employed the Sheffield University–UCL coupled ionosphere–thermosphere model to show that large ion drifts relative to the neutral gas and hence non-Maxwellian ion velocity distributions are expected to occur in certain magnetic local time sectors of the auroral oval even for steady-state conditions and only moderate magnetic activity. Farmer *et al.* (1988) have made similar predictions for their effects on the analysis of EISCAT data.

In this chapter, we consider some results of fitting EISCAT data taking the non-thermal nature of the plasma into account. Examples have been chosen to illustrate various features and problems of this

kind of fit. We do not attempt to survey the occurrence of non-thermal plasma. However, it should be noted that appreciably non-Maxwellian ion velocity distributions ($D^*>0.5$) are found whenever the drift is large and that these effects are quite common in the auroral zone. We concentrate on a limited number of spectra to illustrate technical aspects of non-Maxwellian spectral analysis (Suvanto *et al.,* 1989b,c); finally, some ionospheric results are discussed which have been obtained in collaboration with the EISCAT group at the Rutherford Appleton Laboratory using the analysis procedure outlined in Chapter 2.

As discussed in detail at the end of Chapter 2, two approaches are possible when using the line-of-sight ion velocity distribution given by (2.12). One can regard (2.12) as an analytical approximation to some more rigorous theoretical 1-D distribution function, limiting the investigation to line-of-sight effects only or, alternatively, assume the general validity of the 3-D distribution function (1.14) which implies that the parameter T_i given by equation (1.16) has a physical interpretation and is the 3-D ion temperature. It is stressed that our fitting procedure is valid for both of these approaches, which will be referred to as the 1-D and 3-D interpretation respectively, because the choice between the two is only made after the actual fitting when the results are interpreted. If a good fit cannot be obtained when the aspect angle ϕ is small, one should, however, perform the 1-D analysis using the distribution function (2.12) with ϕ sufficiently larger than its correct value to check whether there are considerable distortions from the Maxwellian shape in the field-parallel direction; these are not allowed for by the relaxation model as the distribution function is insensitive to changes in D^* when ϕ is small. For example, the value ϕ=90° could be used for all aspect angles so that D^* alone accounts for the spectral shape distortion (Kikuchi *et al.,* 1988). Features of fitting for small ϕ will be discussed in Section 3.3. Before that, we concentrate on some results for large aspect angles for which non-Maxwellian signatures have been predicted to be clearest.

3.2. RESULTS OF FITTING FOR LARGE ASPECT ANGLES

The EISCAT UK Special Programme experiment UK-POLAR has been discussed by van Eyken *et al.* (1984) and Willis *et al.* (1986). In this experiment, signals are transmitted from Tromsø alternately along two look-directions with azimuthal angles (measured east of geographic north) of 332° and 356° and received at Tromsø, Kiruna and Sodankylä. However, POLAR is essentially monostatic because the viewing geometries for the three stations are similar. The elevation of the antenna is 21.5°. The experiment employs 12 signal range gates, each being 75 km long, and the nearest (gate 1) being centred on a range of 525 km. An autocorrelation function is recorded every 15 seconds, and the antenna is moved between the two azimuths in a fixed cycle.

The mountains near Tromsø make observations perpendicular to the geomagnetic field (or nearly so) impossible. In fact, this site was chosen for the radar in order to avoid coherent echo contamination related to such directions. For the low elevation used by POLAR, the aspect angles for gates 1–6 are larger than about 70°. As a result, non-Maxwellian signatures in the scatter spectrum should be clearly visible.

3.2.1. Results for 15-second integrated data

Spectra from POLAR were fitted for the electron density, the plasma temperatures and the non-Maxwellian parameter (N_e,T_e,T_i,D^*), initially assuming a pure oxygen plasma. An example of an observed spectrum, which is from range gate 4 (centred on a range of 750 km from Tromsø and a height of 311 km) and integrated over the time period 06:35:45–06:36:00 UT on 27 October, 1984, is shown in Figure 3.1 together with the best Maxwellian and non-Maxwellian fits. At this time, the peak velocity (~ 1.5 kms^{-1}) of a poleward flowburst was observed, as discussed by Todd *et al.* (1986). The

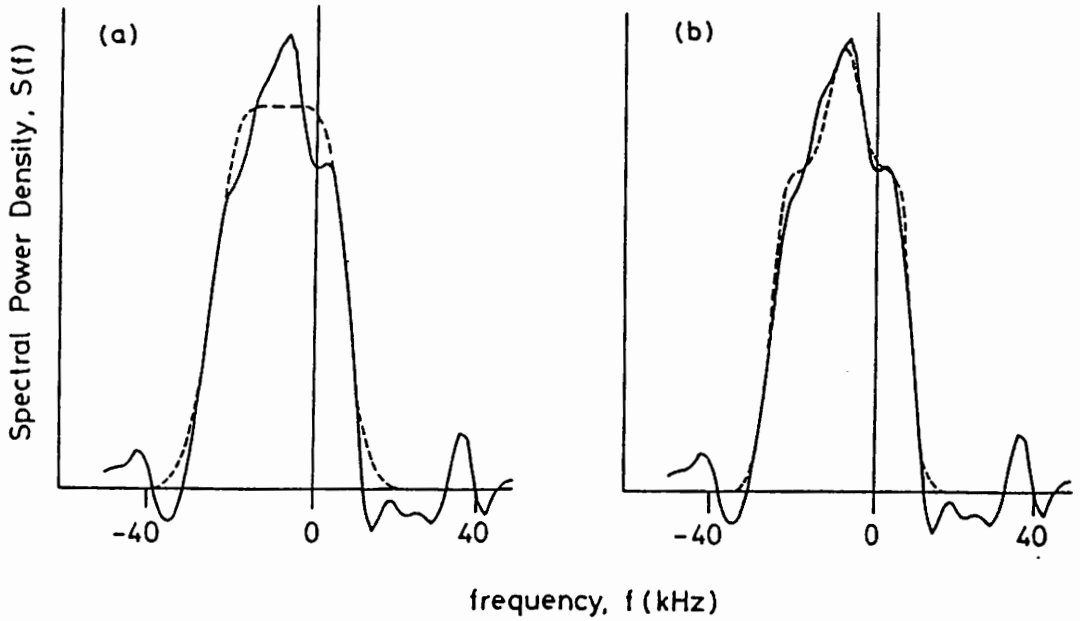

Figure 3.1. A spectrum observed by the U.K. Special Program POLAR from range gate 4 and the time period 06:35:45–06:36:00 UT on 27 October, 1984 (solid lines). The best Maxwellian and non-Maxwellian fits (broken lines) are shown in parts (a) and (b) respectively.

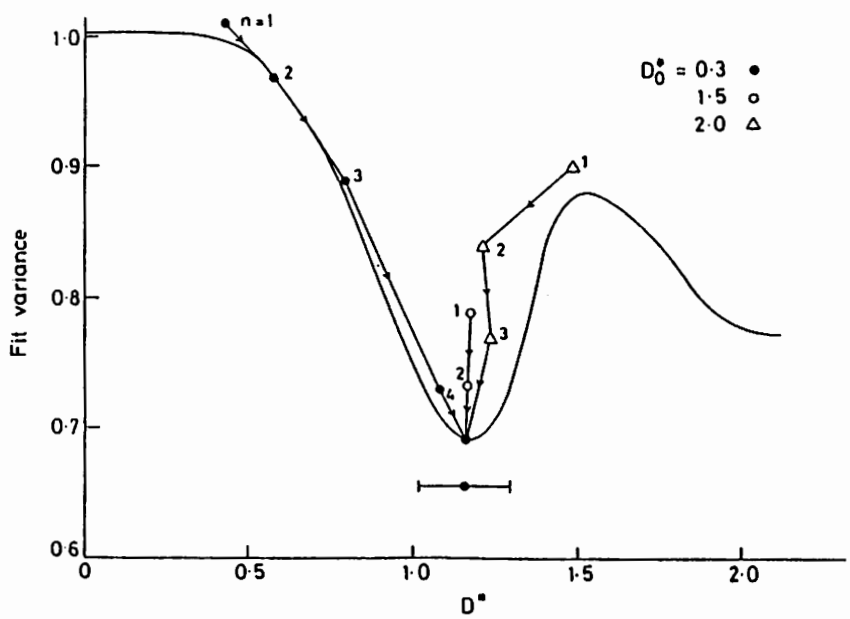

Figure 3.2. Fit variance (arbitrary units) as a function of D^* for three-parameter (n_e, T_e, T_i) fits for the observed spectrum shown in Figure 3.1. The sequences of straight lines show three iteration paths for the given D^*_0 values for four-parameter (n_e, T_e, T_i, D^*) fits. Here n numbers the iteration steps taken to reach each point. The error bar shows the computed error in D^* for the four-parameter fit.

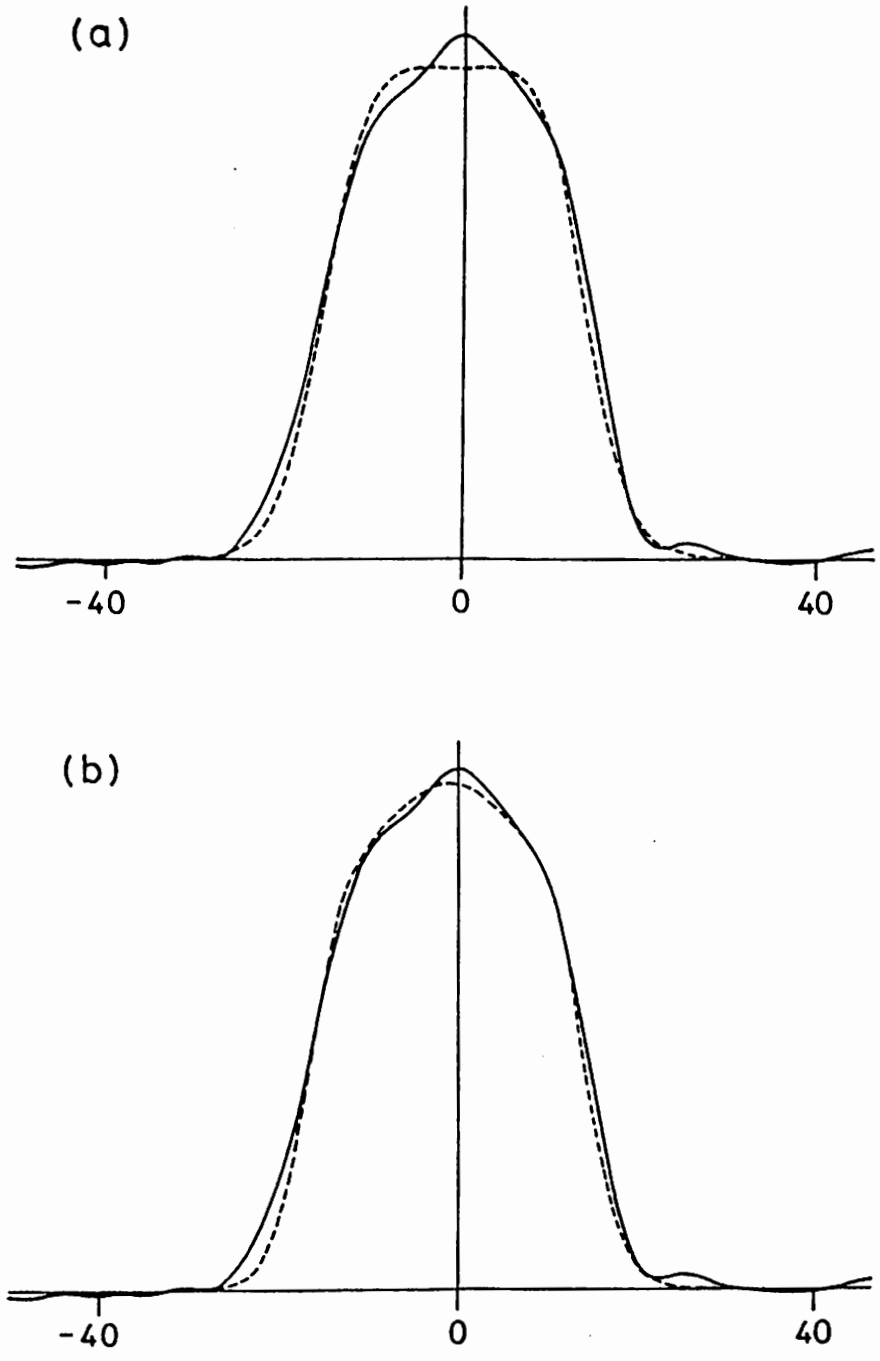

Figure 3.3. Same as Figure 3.1 but for a spectrum observed by the Common Programme CP-4 and post-integrated over a period of one minute (10:45:50–10:46:50 UT on 12 January, 1988).

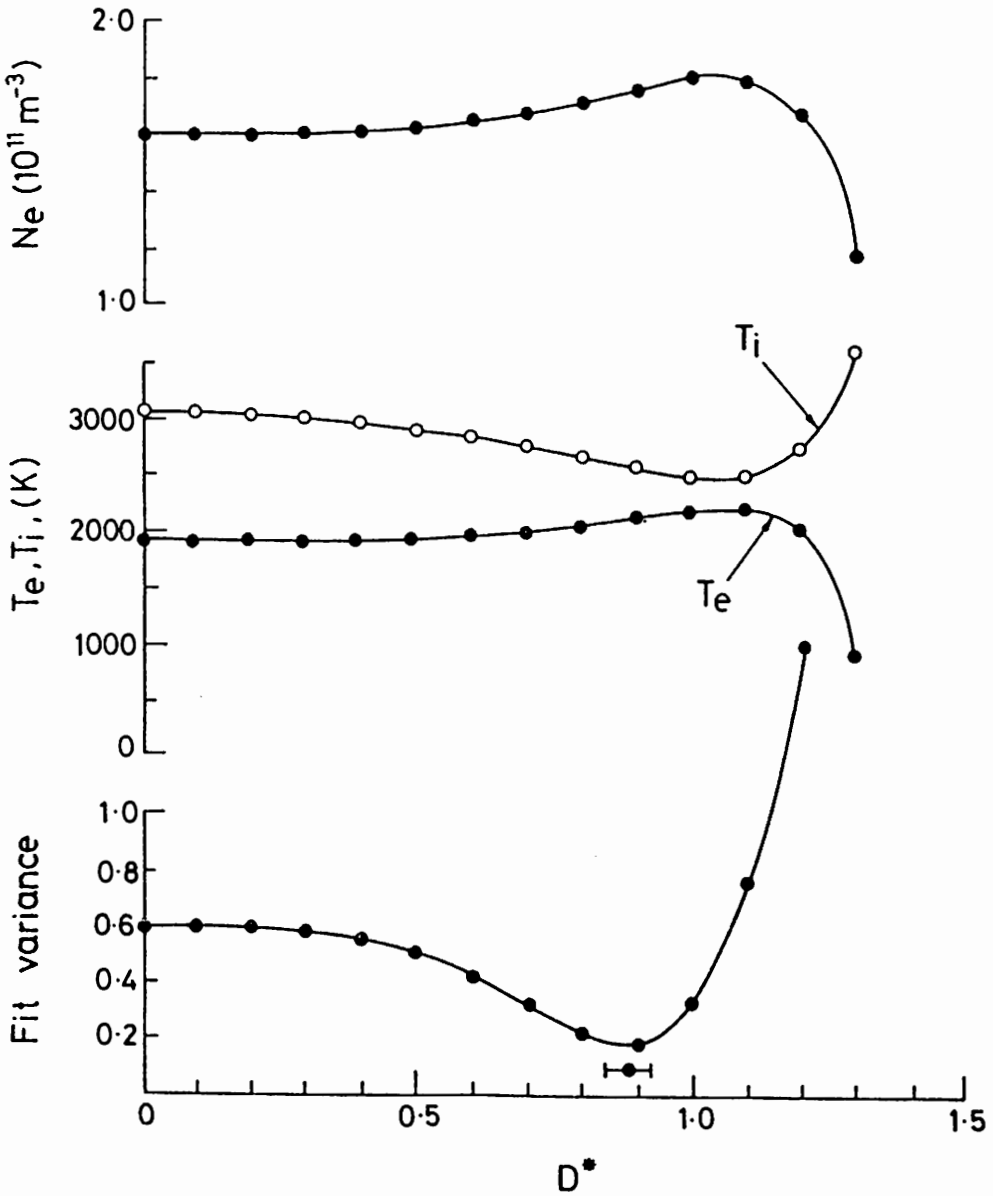

Figure 3.4. Deduced electron density, ion and electron temperatures and fit variance as a function of D^* for three-parameter fits to the observed spectrum shown in Figure 3.3. The error bar shows the computed error in D^*.

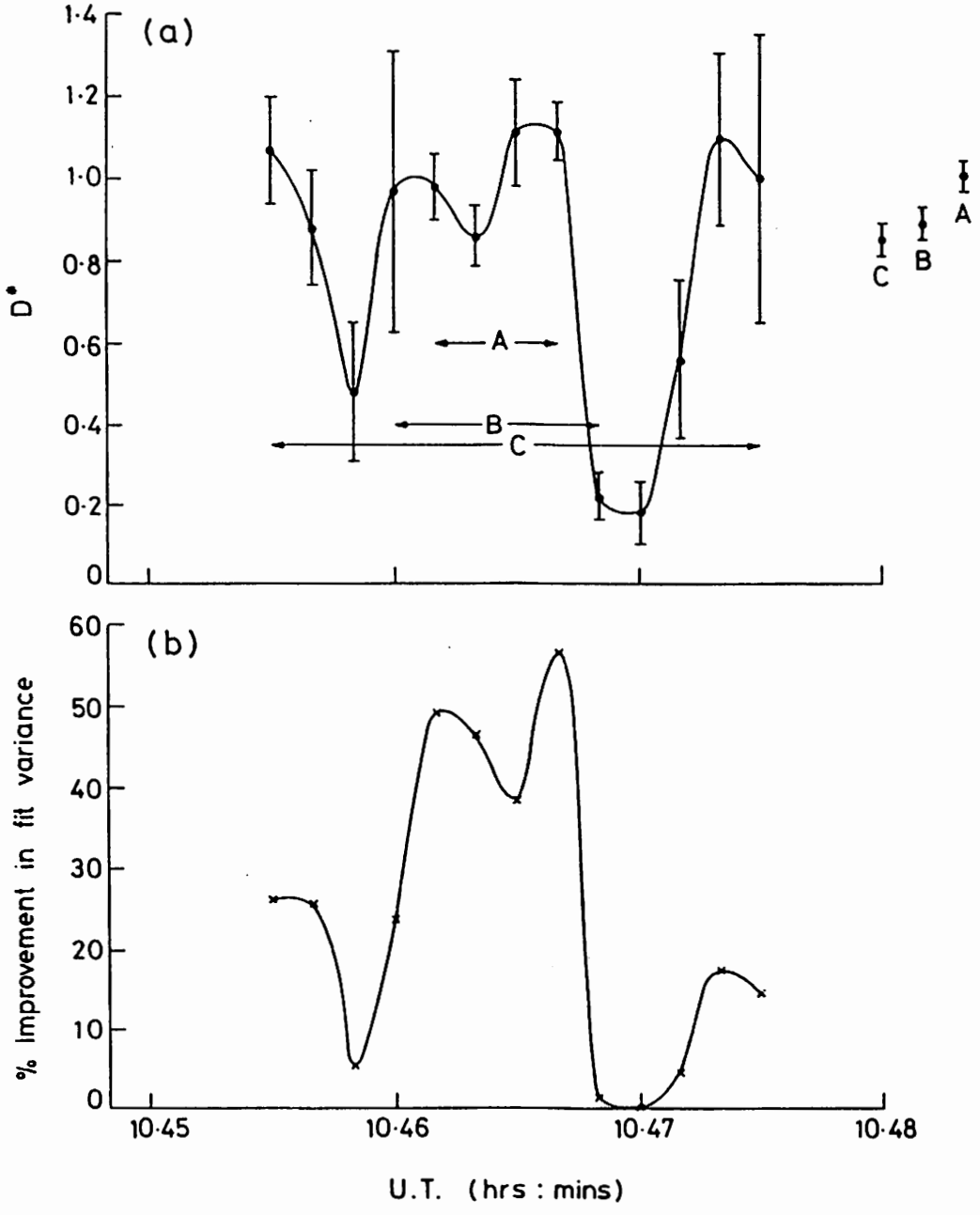

Figure 3.5. (a) Values of D^* from fits to 10-second pre-integrated data for the antenna dwell period 10:45:25–10:47:35 on 12 January 1988. The D^* values corresponding to the periods (A), (B) and (C) are shown on the right. Here (B) is the period studied in Figures 3.3, 3.4 and 3.6. (b) The relative improvement (decrease) in fit variance due to the allowance for non-thermal effects, as compared to a Maxwellian fit.

spectrum is actually one of those used by Lockwood *et al.* (1987) to present the first conclusive evidence of non-thermal effects on incoherent scatter spectra. The relation between the parameter D^* and the ion drift Mach number D' has been discussed by Lockwood *et al.* (1989a,b).

In order to quantify the improvement to the fit due to the allowance for non-Maxwellian ions, we have also carried out three-parameter (N_e,T_e,T_i) fits for various assumed values of D^*. The results are shown by the smooth curve in Figure 3.2, which plots the fit variance in arbitrary units as a function of the D^* value. It can be seen that the best fit corresponds to a clear minimum in variance, which is reduced to about 70 % of its value for thermal ions. Also shown are three iteration paths associated with four-parameter fits for different values of D^*_0 (the initial value for D^*), the integer number n beside each point numbering the iteration steps taken to reach that point. In all three cases, the fits converge to the same point, which is the minimum of the three-parameter fit curve. The only effect of choosing an initial value for D^* which is far from the "correct" value is to slightly increase the number of iterations taken to reach the fit and, provided the maximum number of iterations allowed is not set to be too small, there is no need for some form of "quick fit" for D^*, as used for the other parameters. It should be noted that the fit variance begins to decrease again for very large D^*, as also noted by Moorcroft and Schlegel (1988). However, no D^*_0 value used gave a four-parameter fit corresponding to this region of parameter space, and having $D^*>2$ seems unlikely because of the excitation of plasma instabilities (see Chapters 4 and 5).

3.2.2. Effects of post-integrating the data

The solid lines in parts (a) and (b) of Figure 3.3 show a spectrum from the EISCAT experiment CP-4, which is identical to the POLAR experiment except that data are recorded at 10 s integration rather

than 15 s. These data, which were chosen because they have signatures typical of non-thermal plasma, have been post-integrated over a period of one minute (10:45:50–10:46:50 UT on 12 January, 1988). This period is again within a burst of plasma flow, which is this time rather longer lived (~10 minutes) than that presented by Todd *et al.* (1986). This is long enough to allow the beam-swinging technique to define the plasma velocity to be roughly 3 kms^{-1} (Lockwood *et al.*, 1989c). The best Maxwellian and non-Maxwellian fits to the data are shown as dashed lines in parts (a) and (b) respectively. The fit appears to be considerably more satisfactory in (b). To quantify this visual impression, we have plotted the best-fit variance for a three-parameter fit as a function of the fixed D^* value in Figure 3.4. The variance has a clear minimum at $D^*=0.89$, and is reduced to about 30 % of its value for $D^*=0$. If it is assumed that the 3-D ion velocity distribution (1.14) is valid and, consequently, the parameter T_i given by (1.16) is interpreted as the average ion temperature, we find from Figure 3.4 that the ion temperature is overestimated (by about 20 %) by the Maxwellian analysis, as discussed by Raman *et al.*; furthermore, the electron temperature and the electron density are underestimated by roughly 10 %.

Post-integration can alter the deduced values of D^* because information about rapid variations in the plasma parameters is lost in the temporal averaging process. Figure 3.5 (a) shows D^* values up to more than unity deduced from fits to 10-second pre-integrated data for the antenna dwell period 10:45:25–10:47:35 UT. Two sudden and deep minima are apparent at 10:45:50 and 10:47:00 when the spectra return to double-peaked forms. On the right of the figure are plotted the deduced D^* values corresponding to the post-integration periods A, B and C; here B is the period associated with Figures 3.3, 3.4 and 3.6. The behaviour of D^* may reflect rapid variations in the relative ion-neutral drift velocity. It should be noted, however, that the theoretical ion velocity distribution function used in the fitting procedure was originally derived assuming a steady state (St.-Maurice and Schunk, 1979). This approach can be justified if the

typical time scale for variations in the physical quantities related to the ion velocity distribution, such as the ambient electric field, is much larger than the relaxation time associated with ion-neutral collisions which drive the non-thermal distribution. If this condition is satisfied, the time evolution of the ion population is characterized by a succession of equilibrium states i.e. the plasma is in a quasi-steady state. In the case of very rapid changes in the drift, temporal effects could possibly be important. Also, the length scale associated with spatial gradients must be much longer than the mean free path of the ions for the spatial homogeneity assumption to be satisfied, as discussed in Chapter 1.

The D^* values for fitting post-integrated data are very close to the averages of the results of fits to data which have not been post-integrated, but the error bars are much smaller in the former case as the effect of stochastic noise is reduced. As a result, the smallest D^* which can be resolved as being non-zero is decreased by post-integration. Part (b) of Figure 3.5 shows the percentage improvement in fit variance achieved by non-Maxwellian four-parameter fits to the 10-second data compared with that for a Maxwellian three-parameter fit. It is clear, of course, that the fit is improved in each case because of the addition of an extra degree of freedom.

3.2.3. Fits allowing for mixed ion composition

In the case of two ion species, we have as many as seven free parameters, namely the electron density and the electron temperature, the ion composition, two ion temperatures and two D^* parameters for each of the ion species. Obtaining a "unique" fit is thus very much more difficult than in the single species case. At least two approaches to overcome this problem are possible. First, theory can be invoked to provide some functional relation between the parameters and hence reduce their number. Secondly, one can fit for a fixed value of one of the parameters, for example ion composition, then vary the parameter and fit again, searching for a minimum in

variance.

Figure 3.6 illustrates an attempt to determine the ion composition for the spectrum shown in Figure 3.3, with the assumption that the 3-D temperatures are equal for the two ion species. The results of five-parameter $[n_e, T_e, T_i, D^*(O^+), D^*(NO^+)]$ fits with various values of ion composition are shown. The molecular ion species was chosen to be NO^+, but it should be noted that the spectrum will remain virtually unaffected if NO^+ is replaced by O_2^+, N_2^+ or a mixture of the three. Although the fit variance is practically constant and the composition thus remains unknown, we are left with an important conclusion: performing the spectral analysis under the assumption of 100% O^+ yields a lower limit of $D^*(O^+)$ in this case. In other words, allowing for a molecular component acts to increase the D^* estimate for O^+. In the example given in Figure 3.3, the deduced value of $D^*(O^+)$ is always > 0.89, and the non-thermal nature of the plasma is thus confirmed, although the ion composition remains ambiguous. It should be remembered that the analysis was carried out assuming that the ion temperatures were equal for the two species. However, it seems natural to assume that our conclusion is more general: the allowance for a molecular ion component which is less non-thermal than O^+ in the analysis must be effectively cancelled by a rise in $D^*(O^+)$ to obtain the same degree of distortion in the spectrum as in the case of pure O^+. This idea is supported by the results of similar analysis for other, fixed values of the ion temperature ratio.

3.3. RESULTS OF FITTING FOR A RANGE OF ASPECT ANGLES

One shortcoming of the theoretical ion velocity distribution function (1.14) based on the relaxation collision model is that no deviations from the Maxwellian shape are allowed for in the field-parallel direction, although recent Monte Carlo simulations by Kikuchi *et al.* (1988) indicate that such distortions exist. Adopting this model

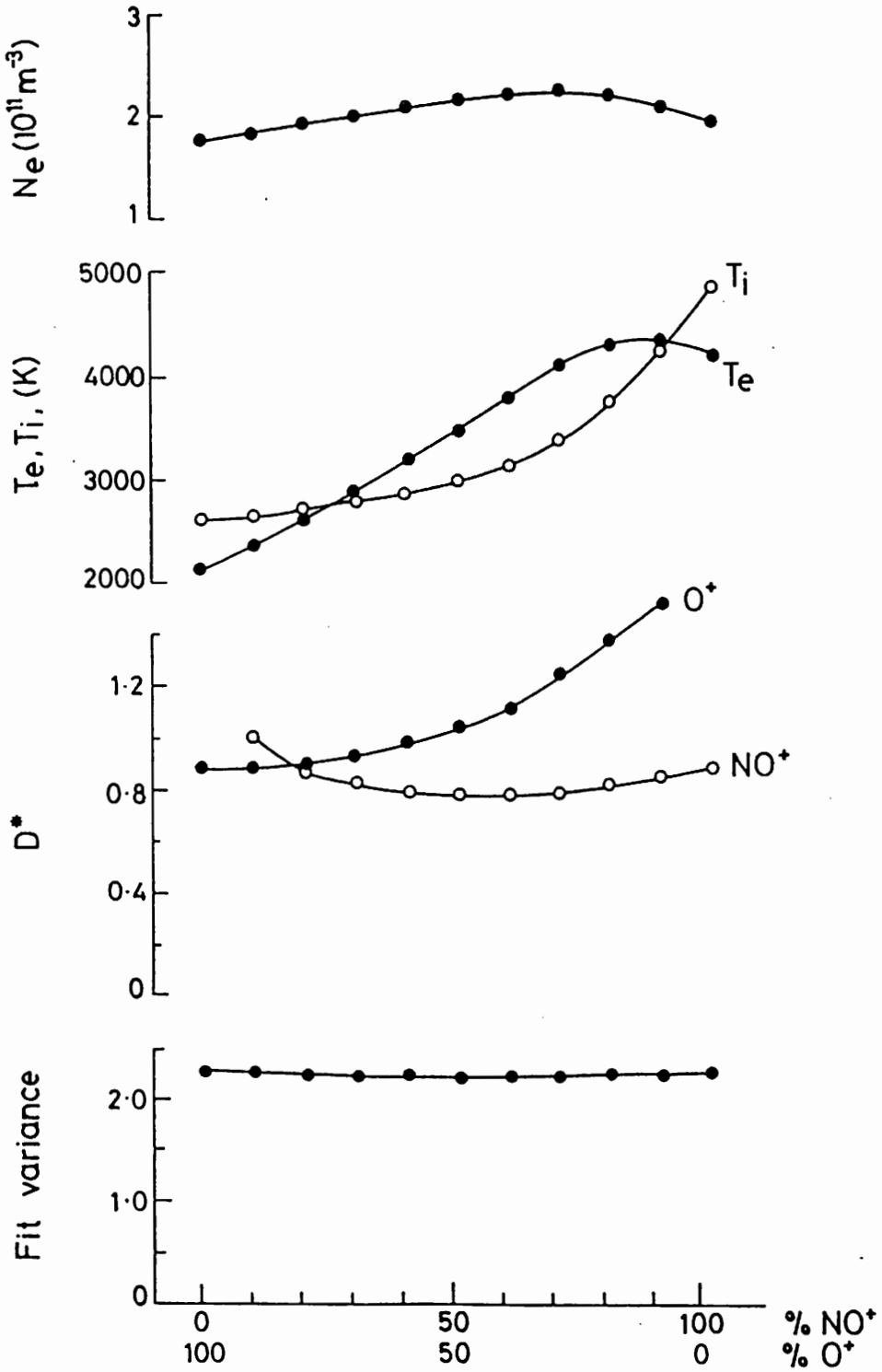

Figure 3.6. Deduced electron density, ion and electron temperatures, non-Maxwellian parameters and fit variance as a function of ion composition for five-parameter [n_e,T_e,T_i,$D^*(O^+)$,$D^*(NO^+)$] fits to the observed spectrum shown in Figure 3.3, assuming that the plasma consists of O^+ and NO^+ ions only.

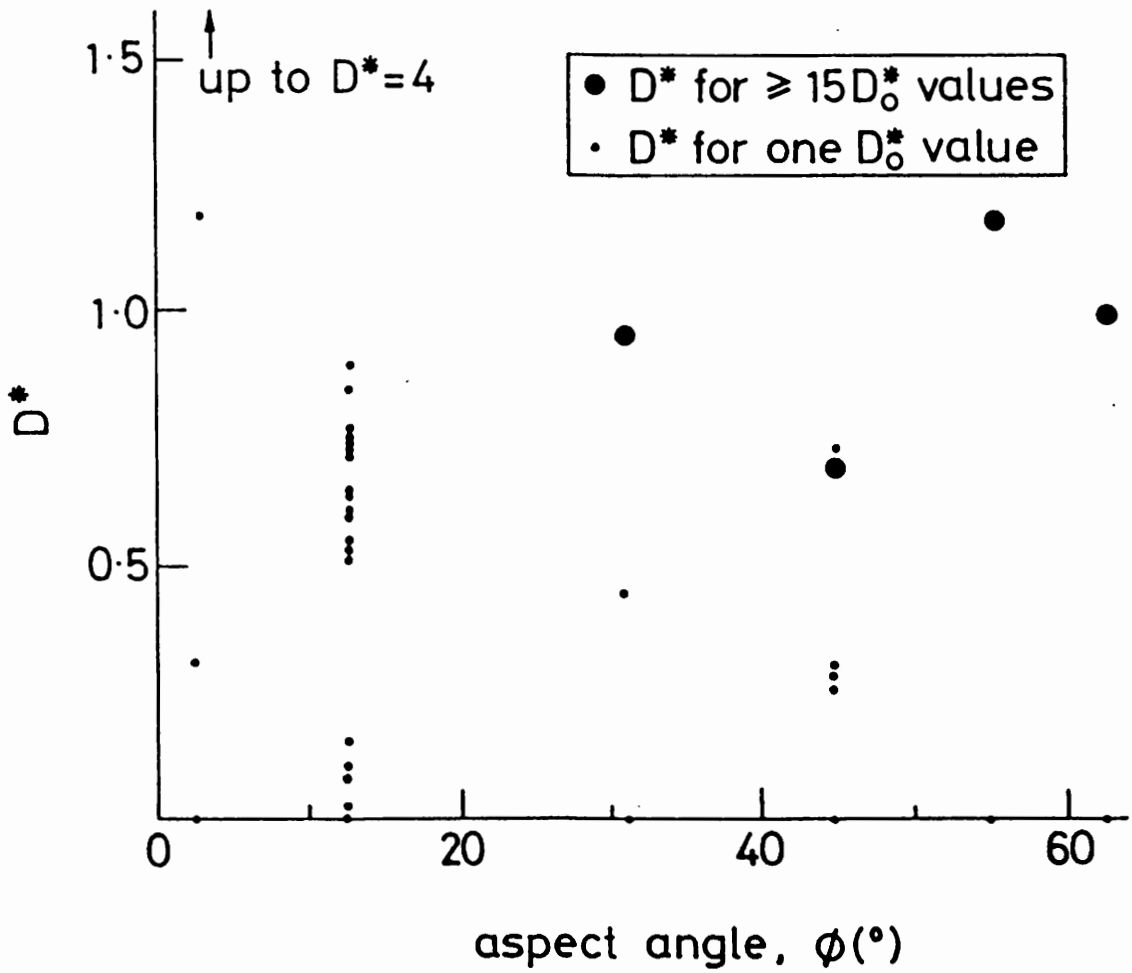

Figure 3.7. Values of D^* from 21 four-parameter fits corresponding to 21 different values of D^*_0 between 0 and 2 for various aspect angles. The data are from the Common Programme CP-3-E and were recorded in the latitude scan between 1300 and 1330 UT on 27 August, 1986.

sets limitations to the data analysis procedure: technically speaking, if we let the aspect angle tend to zero, the functional dependence of the line-of-sight distribution (2.12) on D^* disappears so that no information on D^* can be obtained by studying the plasma in the field-parallel direction only. This implies that the 3-D ion temperature and the temperature anisotropy remain unknown as well. In practice, the problem is present for sufficiently small, nonzero aspect angles. We stress, however, that this is a feature of the naive relaxation collision model rather than a reflection of real plasma behaviour, although spectral noise may well result in this being the case for more rigorous models of the 3-D distribution function if non-Maxwellian spectral signatures are small in the magnetic field direction, as expected.

To illustrate this point, data for each of the aspect angles used in the EISCAT CP-3-E experiment [Winser *et al.* (1987; 1989a,b)] were fitted for n_e, T_e, T_i and D^* assuming 100% O^+. CP-3-E is a latitude-scanning program, and data are collected from 17 positions corresponding to aspect angles between about 0° and 73° and invariant latitudes from 61° to 72.5°. The fact that the beams of the remote receiving stations at Kiruna and Sodankylä intersect the beam of the transmitter/receiver antenna, located at Tromsø, at 275 km for all the positions enables the deduction of the ion drift velocity and hence the ambient electric field without the assumptions of a steady state and spatial homogeneity inherent in the beam-swinging technique. Figure 3.7 shows the results of 21 fits corresponding to 21 values of D^*_0 between 0 and 2 for each scan position. For the aspect angle of 2.5° the deduced values of D^* are scattered between 0 and a highly unrealistic value of about 4 so that no conclusions about the "correct" value can be drawn. Around 20°, the determination of D^* becomes possible within the set maximum number of iterations (20). However, the choice of D^*_0 still plays a minor role for aspect angles up to about 50°: if D^*_0 is too far away from D^*, the analysis program cannot reach the "correct" answer within 20 iterations. Finally, for aspect angles larger than about 50°, the "correct" value of D^* is

always obtained, regardless of D^*_0. The range of aspect angles over which fits can be obtained can be increased by increasing the maximum allowed number of iterations. At aspect angles close to zero, the dependence of the spectral shape on D^* becomes weak, and the non-thermal features are masked by spectral noise. The minimum aspect angle thus depends on the level of stochastic noise and the maximum number of iterations: the value quoted above is probably quite low as these are unusually "clean" spectra.

A small value of the aspect angle does not prevent the determination of the line-of-sight ion temperature, for which the analysis always yields the same value, but using a variety of combinations of D^* and T_i values to obtain exactly the same quality fit in each case. This is a matter of importance since it is the average (or 3-D) temperature which characterizes the ions in any energy balance considerations. We stress that even if the spectrum is the familiar double-humped one, typical of thermal plasma, for a small aspect angle, the ion temperature deduced by the Maxwellian interpretation should not be used e.g. in the standard frictional heating equation if limits to the effects of non-thermal plasma cannot be set by other means. Also, any results of non-Maxwellian analysis at low aspect angles must be assessed very critically because the shape of the spectrum is insensitive to variations in D^* in this case, as discussed above.

The calculations by Raman *et al.* based on the relaxation model not only predict a distortion of the spectrum from the usual double-humped shape but also indicate a considerable dependence of the degree of this distortion on the aspect angle, as shown in Figure 2.4. Winser *et al.* (1987) observed ionospheric flows as large as 2.5 kms^{-1} over five degrees of latitude, and presented experimental evidence of this kind of behaviour. For large flows, non-Maxwellian signatures were found to be pronounced only for large enough aspect angles: in cases where the plasma was viewed almost parallel to the geomagnetic field the spectrum remained double-humped even for

large drift velocities.

Assuming that the neutral temperature was equal to the ion temperature when the ambient electric field was small, Winser *et al.* (1989a) were able to estimate the neutral thermal speed. Neglecting the effect of the neutral drift velocity, the approximate Mach number D' associated with the flows was found, and it was related to the degree of distortion of the spectrum (i.e. D^*). Figure 3.8, taken from Winser *et al.*, shows that D^* increases with the ion drift velocity, as expected theoretically. A similar dependence was found by Lockwood *et al.* (1989a). These results are particularly encouraging and, happily, act as a consistency check: they strongly indicate that the physical mechanism causing the spectral shape distortion is indeed the one the whole spectral analysis routine is based on.

3.4. COMPOSITION EFFECTS: THE POSSIBILITY OF N_2^+

Winser *et al.* (1989a) pointed out that although there was a qualitative agreement between the observations and theory, the well defined "shoulders" in some of the experimental spectra could not be reproduced by the spectral synthesis routine under the assumption of a pure oxygen plasma. The analysis was therefore repeated, allowing for two ion species. The species were characterized by two distinct values of D^* but the ion temperatures were assumed to be equal. The results of the analysis for one particular spectrum are presented in Figure 3.9, also taken from the paper by Winser *et al.* (1989a), which shows a clear minimum in fit variance corresponding to 75 % O^+, in contrast to the ambiguity in ion composition in Figure 3.6. Winser *et al.* have discussed the possibilities of fitting for ion composition in detail. Surprisingly, $D^*(NO^+)$ is larger than $D^*(O^+)$ for the best fit although resonant charge exchange between O and O^+ should be more efficient in producing a highly non-thermal distribution than polarization interactions between NO^+ and the neutral molecules. Similar results

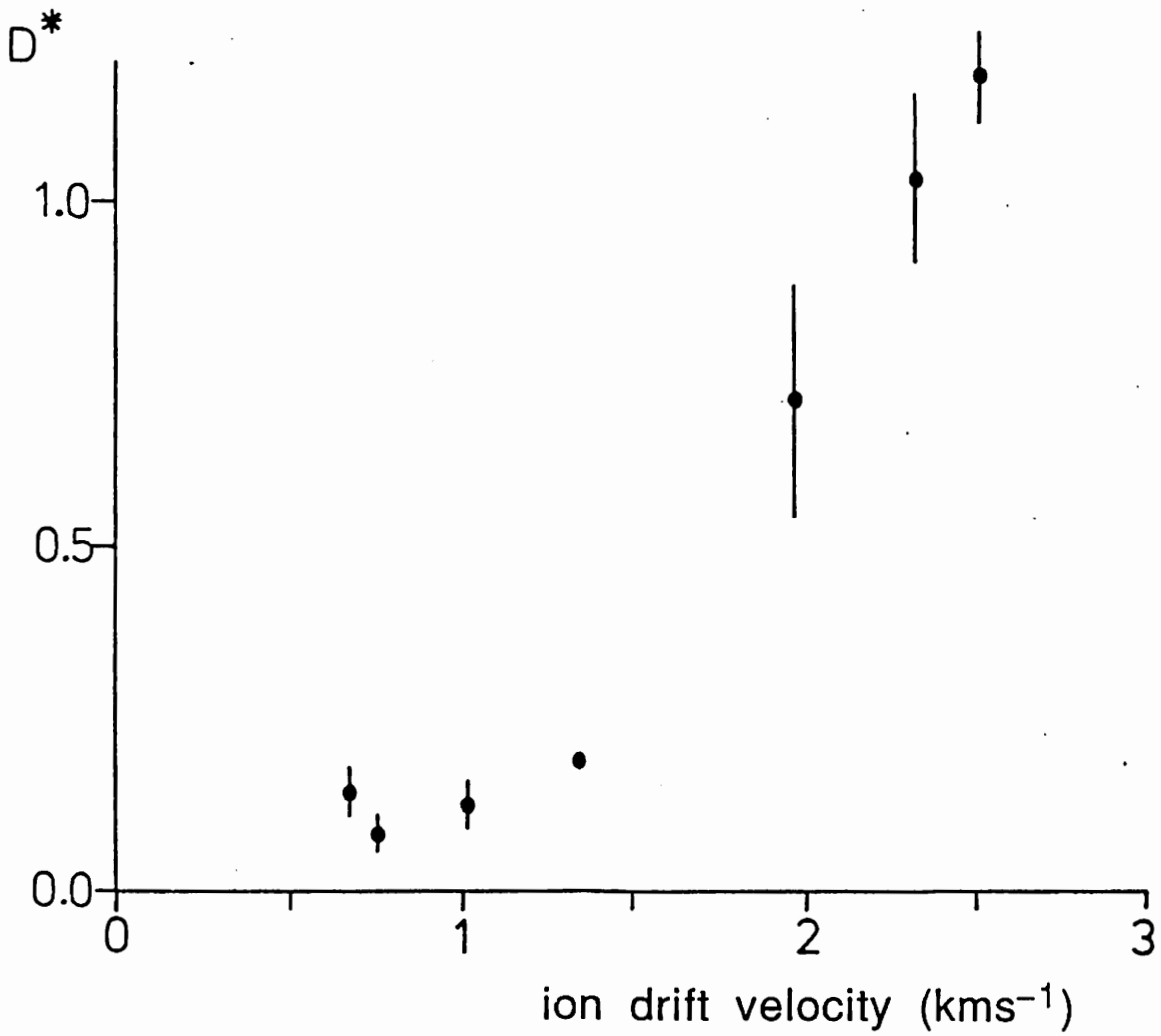

Figure 3.8. Deduced D^* values as a function of the ion drift velocity obtained using data from the Common Programme CP-3-E and from the time period between 13:00 and 13:15 UT on 27 August, 1986. Only points corresponding to aspect angles larger than 30° are included. [From Winser *et al.* (1989a)].

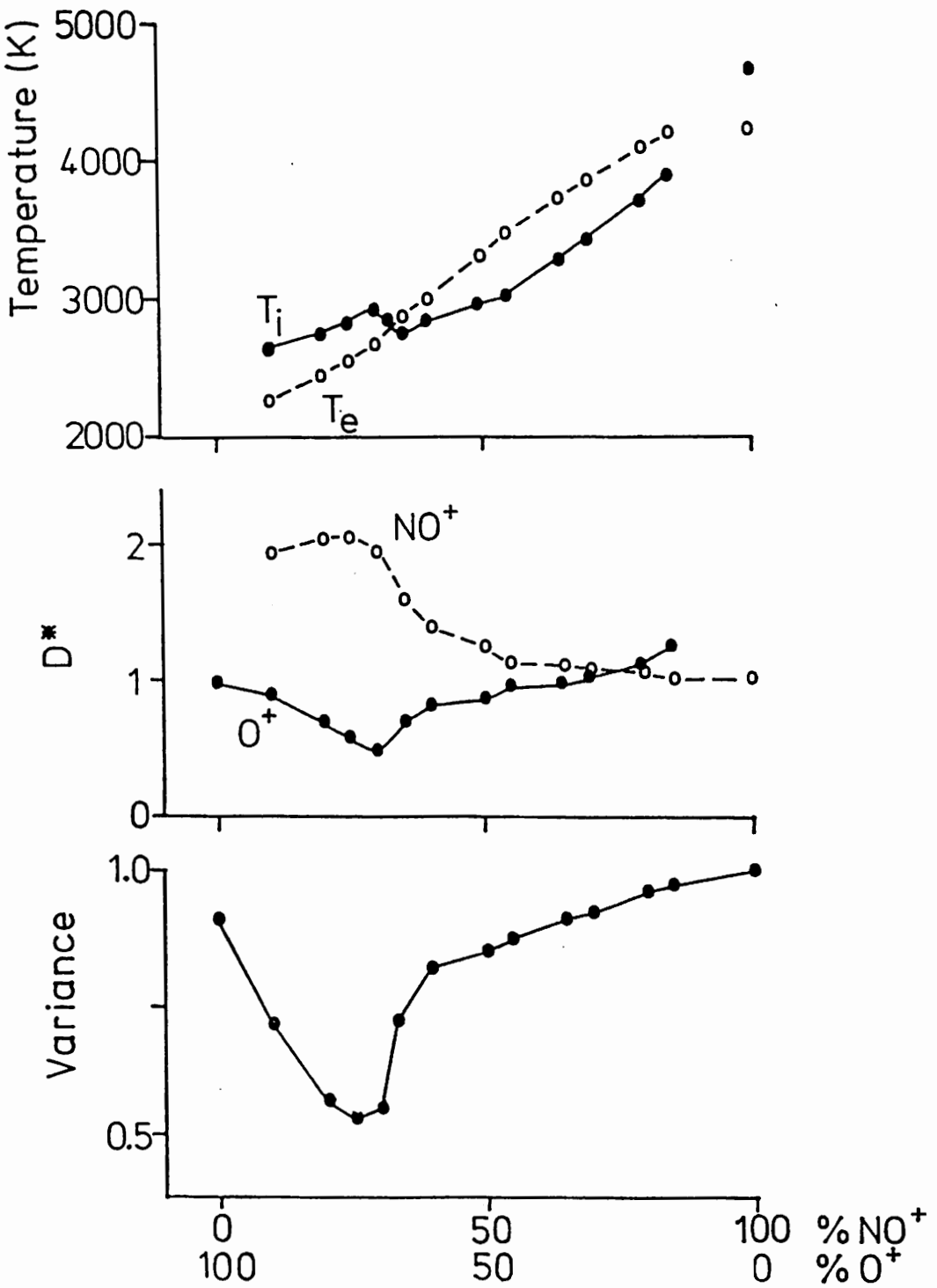

Figure 3.9. Deduced ion and electron temperatures, D^* values for the two ion species and fit variance (in arbitrary units) as a function of ion composition for a spectrum obtained at 295 km in scan position 5 of the CP-3-E experiment on 27 August, 1986. The integration period was 110 s and the aspect angle 62.7°. [From Winser *et al.* (1989a).]

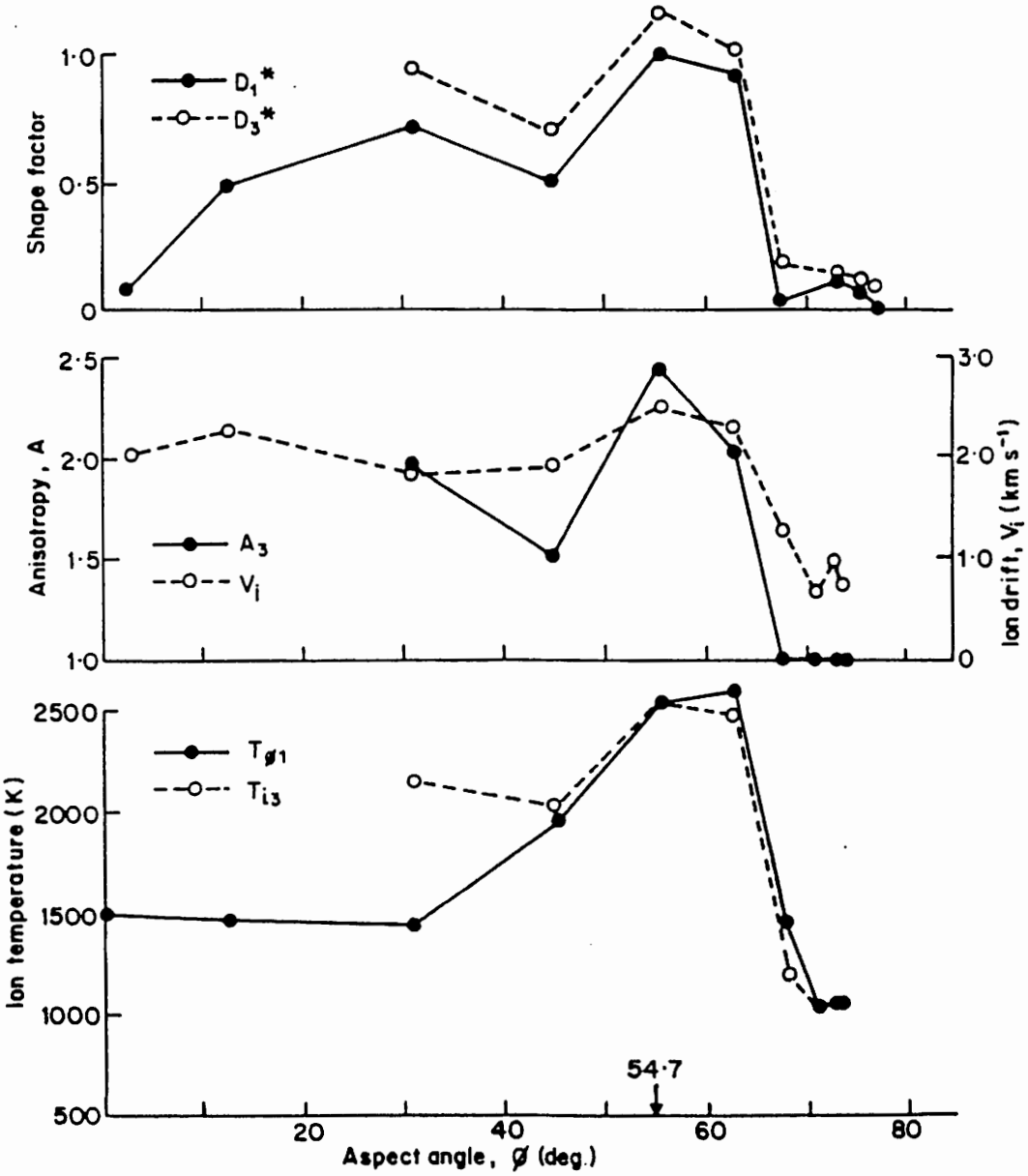

Figure 3.10. Non-Maxwellian shape deformation factors, ion temperature anisotropy and ion line-of-sight and average temperatures deduced by 1-D analysis (denoted by the subscript 1) and the 3-D model (denoted by 3). Here v_i is the observed ion convection speed. The data are from the CP-3-E experiment and were recorded in the latitude scan between 1300 and 1330 UT on 27 August, 1986. [From Lockwood and Winser (1989).]

were obtained for two other gates, and the authors came to the conclusion that at altitudes greater than about 260 km, the molecular ion velocity distribution is more distorted than the O^+ distribution and suggested that the molecular species was N_2^+ instead of NO^+, or a mixture of the two. They argued that the chemical lifetime of N_2^+, which is produced by charge exchange or photoionization, is more than two orders of magnitude longer than the appropriate gyroperiod so that the N_2^+ population is gyrotropic. In fact, N_2^+ produced by photoionization should provide the best example of the relaxation model -based distribution function one can think of: the velocity of a newly-born ion has the same velocity as the neutral molecule had before the reaction if recoil effects are neglected. This could explain why D^* values for the molecular species are even larger than for O^+, which suffers predominantly charge exchange reactions.

It should be noted that this is the only example of a successful non-Maxwellian, mixed-species fit. The fits are usually ambiguous to ion composition, as in Figure 3.6. A situation of this kind is expected if the distribution function of the molecular species is less distorted than the O^+ distribution, as would be true for NO^+ ions, because the spectral shape is then insensitive to variations in composition.

3.5. TESTING THE 3-D MODEL OF THE DISTRIBUTION FUNCTION

The data investigated by Winser *et al.* (1989a,b) showed that the aspect angle dependence of the spectral shape is qualitatively as discussed by Raman *et al.* (1981). However, it would be of great interest to test quantitatively the validity of the theoretical 3-D distribution function given by (1.14). As discussed earlier, this model predicts that the deviation of the line-of-sight distribution function from the Maxwellian form becomes small as the aspect angle is decreased, and the ions look Maxwellian when viewed along the magnetic field line. Lockwood and Winser (1989) performed a 1-D re-

analysis of the CP-3-E data discussed in Sections 3.3 and 3.4 using ϕ=75° in (2.13) whatever the *actual* aspect angle was, and simply varied D^* to fit the observed shape. They thus allowed for non-thermal signatures in the near-parallel direction rather than forced the analysis program to fit with a Maxwellian as $\phi \rightarrow 0$. The actual analysis procedure employed was the one discussed in Chapter 2. The results are presented in Figure 3.10 taken from Lockwood and Winser (1989); here the subscripts 1 and 3 denote quantities deduced by 1-D and 3-D analysis respectively. The top panel shows that for all aspect angles (< 75°) $D^*_1 < D^*_3$, as expected from the behaviour of the Raman *et al.* line-of-sight distribution function as a function of ϕ. It is also evident that $D^*_1 \approx 0$ for very small ϕ i.e. no non-thermal effects are detected, even though the ion drift is of order 1 kms^{-1} (middle panel, dashed line), which is consistent with the Raman *et al.* predictions.

The solid line of the middle panel of Figure 3.10 shows that the temperature anisotropy factor deduced by 3-D analysis takes values around 2 for ion drift speeds of ~ 2 kms^{-1} and the plasma becomes almost isotropic as the drift speed drops to ~ 1 kms^{-1}. In the bottom panel, the line-of-sight ion temperature deduced by 1-D analysis and the average ion temperature from 3-D analysis are compared. When the drift is high, the line-of-sight temperature exceeds the average ion temperature at large ϕ, and vice versa at small ϕ. The two are the same for ϕ=54.7° because the distribution function employed is gyrotropic, as discussed in Section 1.2.3.

Suppose that the 1-D spectral analysis has been performed using two distinct values of the aspect angle, ϕ and ϕ', the deduced line-of-sight temperatures being T_ϕ and $T_{\phi'}$ respectively. For any gyrotropic velocity distribution, two such line-of-sight temperature measurements are enough to determine the general behaviour of the line-of-sight temperature as a function of the aspect angle. In particular, the perpendicular and parallel temperatures and thereby the ansisotropy factor $A = T_\perp / T_{||}$ can be determined without

assuming a particular form for the 3-D distribution function. Measurements of this kind can thus be used to test any 3-D model of the velocity distribution. The above statement is easily verified by noting that

$$T_{\perp} = \frac{(1+\delta)T_{\phi} - (1+\delta')T_{\phi'}}{\delta - \delta'} \tag{3.1}$$

$$T_{\parallel} = \frac{\delta'(1+\delta)T_{\phi} - \delta(1+\delta')T_{\phi'}}{\delta' - \delta} \tag{3.2}$$

by equation (1.11). Here $\delta = \tan^2\phi$ and $\delta' = \tan^2\phi'$. The general behaviour of the line-of-sight temperature is now given by (1.11), $T_{\perp}$ and $T_{\parallel}$ being known. Furthermore,

$$A = \frac{1 - \dfrac{1+\delta'}{1+\delta}\dfrac{T_{\phi'}}{T_{\phi}}}{\delta\dfrac{1+\delta'}{1+\delta}\dfrac{T_{\phi'}}{T_{\phi}} - \delta'} \; . \tag{3.3}$$

Lockwood and Winser examined cases where the average ion temperature and the anisotropy could be determined from two 1-D fits and compared these results with the values obtained by 3-D analysis. Such tests could be carried out where the drift speed was very similar at the scan positions giving aspect angles ϕ and ϕ'. Within this limitation, it was found that the 3-D fit values were reasonably accurate and hence that the 3-D model distribution function was a good "zeroth-order" approximation.

3.6. SUMMARY

Theoretical predictions by Raman *et al.* and the computational method described in Chapter 2 have been used to analyse incoherent

scatter data obtained during the presence of very large ambient electric fields in the high-latitude F-region, circumstances in which the standard Maxwellian analysis would yield highly erroneous values of the plasma parameters. The fit variance was found to be typically around 30%–70% of the "Maxwellian" fit variance (indicating the improvement in fit quality due to allowance for a non-thermal ion population) in cases where the ion drift velocity became comparable to or exceeded the estimated neutral thermal speed. The associated scatter spectra were characterized by a pronounced central peak, and standard analysis programs, which assume a Maxwellian ion velocity distribution, can only reproduce this feature by increasing T_i/T_e, which leads to "anti-correlation" of the apparent ion and electron temperatures, as pointed out by Raman *et al.* Spectra of the kind discussed here can also be produced by spatial/temporal variations within the scattering volume/integration period. However, Lockwood *et al.* (1989a) have shown that this would require a set of highly improbable ionospheric conditions. In fact, there is no reason to *try* to explain the spectra using "thermal" arguments. Why would the velocity distribution of a minor gas flowing supersonically through a major background constituent remain Maxwellian?

Two approaches to the non-thermal analysis of incoherent scatter data can be taken. First, the analysis can be restricted to line-of-sight effects without the specification of the complete 3-D structure of the ion velocity distribution. Secondly, assumed forms of the 3-D distribution function can be used to estimate 3-D features from a single measurement. The former procedure can only yield information about the line-of-sight temperature but is more general. Comparisons between 1-D fits with the results of 3-D analysis indicates that the Raman *et al.* distribution function could be used to characterize the ion population to lowest order in 3-D velocity space (Lockwood and Winser, 1989). More observations are clearly required to further test this model, ideally with the same volume of plasma viewed at two widely-separated aspect angles. However, motivated by

the initial results, we will use this model in Chapters 4 and 5 to study the ion cyclotron instability.

CHAPTER 4

LINEAR ION CYCLOTRON INSTABILITY THEORY

4.1. INTRODUCTION

The work of the previous chapters is based on the implicit assumption that as far as the shape of the ion velocity distribution is concerned, the effect of the self-consistent electric field associated with plasma density fluctuations is negligible compared with ion-neutral collisions and the applied magnetic field. Fluctuations at the thermal level give rise to observable phenomena like the characteristic form of the incoherent scatter spectrum but cannot change the macroscopic properties of the gas. If, however, there is a source of free energy available from which energy can be continuously fed to the fluctuations, the plasma is said to be unstable. Waves grow to a large amplitude, a turbulent state is reached and wave-induced processes become important. The energy source can be due to the geometrical configuration of the plasma in physical space, in which case it is possible to study the instability using fluid equations. A second class of instabilities, the one of interest here, arises from velocity space considerations. Kinetic theory is required in this case because the averaging over velocity space leading to fluid theory removes the details of the particle velocity distribution and hence all information about the resonant particles interacting with the waves.

It was pointed out by Harris (1959) that anisotropic velocity distributions can give rise to high-frequency electrostatic instabilities

in a plasma. Rosenbluth and Post (1965) and Post and Rosenbluth (1966) discussed velocity distributions characterized by a loss-cone; they found that unstable waves can be driven by an ion velocity distribution which is peaked around a nonzero energy in the rest frame of the plasma. As a result, researchers were motivated to look for instabilities related to the auroral ion velocity distribution function (1.14) because both temperature anisotropy and a positive slope in perpendicular velocity are associated with it. Ott and Farley (1975) studied the instability threshold conditions, using the criterion of Sagdeev and Galeev (1969), and the relaxation model for ion-neutral collisions, to predict that short-wavelength irregularities could be produced if the ion drift Mach number exceeds a critical value of 1.27. We note that in their paper, the quoted value is actually 1.8 instead of 1.27 because of a different definition of the neutral thermal speed. The presence of a second ion species (in addition to highly non-thermal O^+, say) which is only slightly non-thermal can raise the instability threshold considerably because of the Landau damping of the waves by this ion population (St.-Maurice, 1978). Electron Landau damping becomes important if the ion temperature is less than about twice the electron temperature. Finally, the wavelengths of the unstable waves have been found to be of the order of 0.5 m.

The above theoretical studies concerned waves with growth rates (γ) and frequencies much larger than the ion gyrofrequency so that the ions could be considered as unmagnetized because the instability has time to grow before ion gyration becomes important. Furthermore, the various instability parameters were found to depend on the field-perpendicular velocity distribution only. This was an advantage because the perpendicular distribution already had some experimental verification at that time (St.-Maurice *et al.*, 1976) but the field-parallel one had not been measured. It should be noted that there is, at least in principle, a contradiction in the determination of the instability threshold using the unmagnetized

ion approximation. The reason is simply that threshold conditions correspond to $\gamma \rightarrow 0$, which certainly violates the requirement $\gamma >> \Omega_i$. The sensitivity of the results depends on the typical frequency scale in which the dielectric function varies. This scale is presumably of the same order as the typical growth rate, which is, in turn, much larger than the ion gyrofrequency: as a result, the error associated with the unmagnetized ion approximation should not completely undermine the results.

After the linear theory of high-frequency Post-Rosenbluth waves had been investigated in detail, attention was turned on the other extreme, namely instabilities which arise from the resonance between the density fluctuations and the ion gyromotion. Lakhina and Bhatia (1984) came to the conclusion that the threshold for the ion cyclotron instability was about the same as the Post-Rosenbluth threshold, at least in the limit of cold electrons.

While the threshold conditions for the Post-Rosenbluth instability are already known for realistic values of ionospheric parameters (ion composition, plasma temperatures, electron density), we wish here to generalize the linear ion cyclotron instability theory to allow for the effect of electron Landau damping (Suvanto, 1989a). In the presence of large ion drifts relative to the neutral atmosphere, frictional heating has an effect on ion chemistry, which results in increased molecular ion concentrations. Allowance for two ion species must therefore be made. We present an analytical method which is used to calculate the ion contribution to the plasma dielectric function more accurately than in the previous studies of non-Maxwellian plasma. Previous studies have just retained the so called "resonant term" in the Bessel function expansion which appears in the ion contribution to the plasma dielectric function.

4.2. DISPERSION RELATION

From the Poisson and Vlasov equations we obtain the dispersion relation for electrostatic wave modes (ω, $\mathbf{k}$) in an external magnetic field,

$$\varepsilon = 1 + \varepsilon_e + \varepsilon_i + \varepsilon_i' = 0, \tag{4.1}$$

where the electron and ion contributions to the dielectric function ε are given by the well-known expression (e.g. St.-Maurice, 1978)

$$\varepsilon_\alpha = -\frac{\omega_{p\alpha}^2}{k^2} \sum_{n=-\infty}^{\infty} \int \left(k_{||} \frac{\partial f_\alpha}{\partial v_{||}} + \frac{n\Omega_\alpha}{v_\perp} \frac{\partial f_\alpha}{\partial v_\perp} \right) \frac{J_n^2\left(\frac{k_\perp v_\perp}{\Omega_\alpha}\right)}{\omega - k_{||} v_{||} - n\Omega_\alpha} d v_{||}\, 2\pi v_\perp\, d v_\perp . \tag{4.2}$$

The subscript α denotes the species (α = e, i for the electrons and for the ions respectively), f_α is the normalized velocity distribution function, assumed to be gyrotropic around the magnetic field in velocity space, and J_n is the ordinary Bessel function of order n. The symbols || and $\perp$ denote the directions parallel and perpendicular to the geomagnetic field respectively; $\omega_{p\alpha}$ and Ω_α are the ion/electron plasma and cyclotron frequencies respectively. In (4.1), the prime $'$ refers to the ion species nonresonant with the waves (this characterization will be discussed below), and the unprimed ion contribution is due to the resonant species. The same convention will be used throughout this chapter for all quantities associated with the ions.

The dielectric function constructed by using expressions of the form (4.2) ignores collisional damping of the fluctuations. This

approximation will be discussed in Section 4.4. It should be noted, however, that although collisional effects are neglected in the rapidly oscillating part of the kinetic equation, they are important in establishing the steady-state non-Maxwellian velocity distribution, as discussed in Section 1.1. Now, assuming a Maxwellian distribution for the electrons and using (1.14) for the ions, (4.2) becomes, after some straightforward manipulation,

$$\varepsilon_i = 2\frac{\omega_{pi}^2}{k^2 v^{*2}}\left\{1+2\sum_{n=-\infty}^{\infty}\left[\frac{\omega}{k_{\|}v^*}A_n - \frac{n\Omega_i}{k_{\|}v^*}D^*B_n\right]Z\left(\frac{\omega-n\Omega_i}{k_{\|}v^*}\right)\right\} \tag{4.3}$$

for the ions [the identities (A.8) and (A.11) were used] and

$$\varepsilon_e = 2\frac{\omega_{pe}^2}{k^2 v_e^2}\left[1+\frac{\omega}{k_{\|}v_e}\sum_{n=-\infty}^{\infty}C_n\left(\frac{k_\perp^2 v_e^2}{2\Omega_e^2}\right)Z\left(\frac{\omega-n\Omega_e}{k_{\|}v_e}\right)\right] \tag{4.4}$$

for the electrons in the **E**x**B** drift frame. Here Z is the plasma dispersion function (see Appendix A.1), $k_{\|}$ is conventionally positive, and the functions A_n, B_n and C_n are defined by

$$A_n = \int_0^\infty dx\, x\, \exp\left(-D^{*2}-x^2\right) I_0(2D^*x)\, J_n^2(\kappa x) \tag{4.5}$$

$$B_n = \int_0^\infty dx\, \exp\left(-D^{*2}-x^2\right) I_1(2D^*x)\, J_n^2(\kappa x) \tag{4.6}$$

$$C_n(x) = \exp(-x)\, I_n(x), \tag{4.7}$$

where

$$\kappa = \frac{k_\perp v^*}{\Omega_i} \tag{4.8}$$

and I_n is the modified Bessel function of order n. Equations (4.3), (4.5) and (4.6) are written explicitly for the resonant ion species; the corresponding equations for the nonresonant ions are obtained by making the obvious replacements $\omega_{pi} \rightarrow \omega_{pi}'$, $v^* \rightarrow v^{*\prime}$ etc. We are interested in the instability threshold conditions. Consequently, all the equations in this section will be written for real ω corresponding to marginally unstable modes. Most of the electrostatic wave modes associated with the above dispersion relation are stable and, consequently, of no interest. Which modes in $(\omega, \mathbf{k})$ space are most easily excited by the instability? The "resonance parameters" are defined as

$$\Delta_e = \frac{\omega}{k_{||} v_e} \tag{4.9}$$

and

$$\Delta_i = \frac{\omega - N\,\Omega_i}{k_{||}\, v^*}, \tag{4.10}$$

for which we assume that $|\Delta_e| \gtrsim 1$ and $|\Delta_i| \lesssim |\Delta_e|$ for some particular integer number N. These conditions, which are only order-of-magnitude requirements ($|\Delta_e|$ should not be too close to zero and $|\Delta_i|$ not several orders of magnitudes larger than $|\Delta_e|$) are expected to be satisfied by the most interesting wave modes for which the ion cyclotron resonance is strong and the electron Landau damping not too severe. We then find from (4.9) and (4.10) that

$$\left|\frac{\omega - N\,\Omega_i}{\omega}\right| \lesssim \frac{v^*}{v_e} \sim \left(\frac{m_e}{m_i}\right)^{1/2} << 1\,, \tag{4.11}$$

which leads to wave frequencies very close to $N\Omega_i$, the relative correction being of the order of $(m_e/m_i)^{1/2}$. This justifies our original choice of the parametric region for ion cyclotron waves. Consider then equation (4.3) for the resonant ion contribution to the dielectric function. The quantities A_n and B_n are << 1 for D^* and κ values of interest here (this assumption was checked afterwards). Noting that

$$\frac{\Omega_i}{k_{||} v^*} \sim \frac{1}{|N|} \frac{|\omega|}{k_{||} v^*} \sim \frac{1}{|N|} \left(\frac{m_i}{m_e}\right)^{1/2} |\Delta_e| >> 1 \qquad (4.12)$$

provided N is not too large, we find that the absolute value of $(\omega - n\Omega_i)/k_{||}v^*$, the argument of the plasma dispersion function, is much larger than unity for $n \neq N$. As a result, the leading term is the one with $n=N$ because real and imaginary parts of Z are here of the order of unity as opposed to $n \neq N$ terms where Z_R and Z_I are <<1. In fact, the imaginary part of (4.3) can be approximated by retaining the $n=N$ contribution only because the other terms are exponentially small. As far as the real part is concerned, the small $n \neq N$ terms can become important when summed over n; the reason is that Z_R decreases asymptotically only as the inverse of its argument. In Appendix B, a correction due to the $n \neq N$ terms is derived, and the reader is referred to it for details. Inserting (B.4) and (B.8) into (4.3) yields

$$\varepsilon_i = 2 \frac{\omega_{pi}^2}{k^2 v^{*2}} \left[\exp(-D^{*2}) - 2 \left(\frac{m_i}{m_e}\right)^{1/2} \left(\frac{T_e}{T^*}\right)^{1/2} \Delta_e Z(\Delta_i) \alpha \right] \qquad (4.13)$$

with

$$\alpha = D^* B_N - A_N \qquad (4.14)$$

for the resonant ion species and simply

$$\varepsilon_i' = 2\frac{\omega_{pi}'^2}{k^2 v^{*'2}} \exp(-D^{*'2}) \tag{4.15}$$

for the nonresonant species. In the expression for the electron function, equation (4.4), we adopt the same approximation scheme as used by St.-Maurice (1978). The contribution from the terms with $n \neq N$ is negligible because $|\omega| << \Omega_e$ and, by (4.12),

$$\frac{\Omega_e}{k_{||} v_e} = \frac{m_i}{m_e}\frac{\Omega_i}{k_{||} v_e} \sim \left(\frac{m_i}{m_e}\right)^{1/2} \frac{\Omega_i}{k_{||} v^*} >> 1. \tag{4.16}$$

Equation (4.4) is now in the form

$$\varepsilon_e = 2\frac{\omega_{pe}^2}{k^2 v_e^2}\left[1 + \Delta_e Z(\Delta_e) C_0\left(\frac{k_\perp^2 v_e^2}{2\Omega_e^2}\right)\right]. \tag{4.17}$$

Inserting (4.13), (4.15) and (4.17) into (4.1) and simplifying, we find that the dispersion relation for marginally unstable modes is given by the following pair of equations,

$$C_0 = \frac{1 + \dfrac{k^2 v_e^2}{2\omega_{pe}^2} + \dfrac{n_i}{n_e}\dfrac{T_e}{T^*}\exp(-D^{*2}) + \dfrac{n_i'}{n_e}\dfrac{T_e}{T^{*'}}\exp(-D^{*'2})}{\Delta_e \dfrac{Z_I(\Delta_e)}{Z_I(\Delta_i)} Z_R(\Delta_i) - \Delta_e Z_R(\Delta_e)} \tag{4.18}$$

$$\alpha = \frac{1}{2}\left(\frac{m_e}{m_i}\right)^{1/2}\frac{n_e}{n_i}\left(\frac{T^*}{T_e}\right)^{3/2}\frac{Z_I(\Delta_e)}{Z_I(\Delta_i)} C_0, \tag{4.19}$$

where n_i and n_i' are the resonant and non-resonant ion densities respectively. Assuming that the parameters $k_\perp^2 v_e^2/2\Omega_e^2$ and $k^2 v_e^2/2\omega_{pe}^2$ are $<<1$, (4.18) and (4.19) can be rewritten as

$$\frac{\alpha}{p} = \frac{1}{2}\left(\frac{m_e}{m_i}\right)^{1/2} \frac{Z_I(\Delta_e)}{Z_I(\Delta_i)} \tag{4.20}$$

$$1 + q = \Delta_e \frac{Z_I(\Delta_e)}{Z_I(\Delta_i)} Z_R(\Delta_i) - \Delta_e Z_R(\Delta_e) \tag{4.21}$$

with

$$p = \frac{n_e}{n_i}\left(\frac{T^*}{T_e}\right)^{3/2} \tag{4.22}$$

and

$$q = \frac{n_i}{n_e}\frac{T_e}{T^*} \exp(-D^{*2}) + \frac{n_i'}{n_e}\frac{T_e}{T^{*\prime}} \exp(-D^{*\prime 2}). \tag{4.23}$$

4.3. INSTABILITY THRESHOLD CALCULATIONS

Having tailored the general electrostatic wave dispersion relation to marginally unstable ion cyclotron waves, we now turn to the determination of the instability threshold conditions. From (4.20) one finds that a necessary condition for the plasma to be marginally unstable is $\alpha > 0$, as the RHS and the quantity p on the LHS are always positive; in the cold electron limit $|\Delta_e| \to \infty$, (4.20) takes the simple form $\alpha=0$. The integrals A_N and B_N [equations (4.5) and

(4.6)] in the expression for α, equation (4.14), were computed numerically using an adaptive integrator of the NAG library, specially suited for oscillating integrands. The numerical values obtained were in excellent agreement with analytical results in various limits. It was found that the condition $\alpha>0$ requires $D^*>1.26$; for fixed D^* above this value, α is zero at $\kappa=0$ ($N\neq0$), has a positive maximum at some value of κ and finally vanishes as $\kappa\rightarrow\infty$. The maximum value of α will be denoted by $\alpha_{max}(D^*)$. As a continuous function, α can take all the positive values less than $\alpha_{max}(D^*)$ as κ varies, of course.

Consider a plasma characterized by the parameters n_i/n_e, T^*, $T^{*\prime}$, T_e, D^* and $D^{*\prime}$. The stability of the plasma can be tested as follows. First calculate p and q using (4.22) and (4.23) and minimize the RHS of (4.20), taking the constraint (4.21) into account. Referring to the previous paragraph, if the value of α obtained in this way is less than $\alpha_{max}(D^*)$, there exists κ such that (4.20) is satisfied and the plasma is at least marginally unstable.

We first discuss the minimization of the RHS of (4.20) with respect to Δ_i and Δ_e. Only one degree of freedom is actually associated with the minimization because Δ_i is uniquely determined by (4.21) (or does not exist) once we have specified Δ_e. The uniqueness follows from the fact that the RHS of (4.21) is a monotonic function of Δ_i; this is readily demonstrated by using the properties of Z discussed in Appendix A.1 and noting that the partial derivative of the RHS with respect to Δ_i is

$$-2\Delta_e\frac{Z_I(\Delta_e)}{Z_I(\Delta_i)}, \tag{4.24}$$

which does not change sign as Δ_i varies. Furthermore, it is evident that Δ_e and Δ_i have different signs if

$$1 + \Delta_e Z(\Delta_e) + q > 0 , \tag{4.25}$$

and the same sign if the inverse is true. As far as the minimum is concerned, there are two possibilities. Either it corresponds to finite Δ_e, or the RHS of (4.20) decreases monotonically for large Δ_e values and the minimum is at $\Delta_e = \infty$. In the first case, the minimization has to be carried out numerically. The second case can be studied analytically by introducing the asymptotic expression of Z_R (see Appendix A.1) in (4.21). It is clear from (4.21) that the exponential decrease of the first term as $\Delta_e \to \infty$ can only be cancelled by letting $|\Delta_i| \to \infty$, so that we can use, without any loss of generality, the same asymptotic equation for $Z_R(\Delta_i)$. Equation (4.21) then yields

$$\Delta_i \approx -\Delta_e - \frac{\ln q}{2\Delta_e} , \tag{4.26}$$

from which (and 4.21 again) one has

$$\frac{Z_I(\Delta_e)}{Z_I(\Delta_i)} \approx q + \frac{q \ln q - q - 1}{2\Delta_e^2} . \tag{4.27}$$

It is clear from (4.27) that the RHS of (4.20) is an asymptotically decreasing function of Δ_e i.e. there is a local minimum at infinity if $q \ln q - q - 1 > 0$ or $q > 3.6$. It turns out that for q larger than about 5, this minimum is global but for smaller q the RHS of (4.20) has its minimum at some finite Δ_e and the optimization has to be completed numerically. In Table 4.1, the minimum is shown as a function of q. The resonant species was chosen to be O^+ because resonant charge exchange between O and O^+ is more effective in producing a highly non-Maxwellian velocity distribution than polarization scatter associated with interactions of molecular ions with the neutral atmosphere. This reasoning actually has some experimental verification from RPA measurements (St.-Maurice *et al.*, 1976).

The maximum α for fixed D^* was found numerically. The results are presented in Tables 4.2 and 4.3 for the N=1 and N=2 waves respectively. The normalized wave number κ corresponding to the maximum is also tabulated.

Let us first consider the case where only one ion species is present i.e. $n_i'/n_e = 0$ in (4.23); D^*_{crit}, the instability threshold, is then a function of T^*/T_e only. Let T^*/T_e= 0.2, for example. We test whether D^*=1.3 corresponds to the marginal instability of some wave mode. Now p=0.089 and q=0.923 by (4.22) and (4.23) so that the minimum of the RHS of (4.20) is $1.21 \cdot 10^{-3}$ and $\alpha = 1.07 \cdot 10^{-4}$. A glance at Tables 4.2 and 4.3 then shows that this is less than $\alpha_{max}(D^*)$ for both the first and second harmonics so that $1.26 < D^*_{crit} < 1.3$ i.e. $D^*_{crit} \approx 1.3$ to a sufficient degree of accuracy for the above value of the temperature ratio. One actually ends up with the same conclusion for all values of T^*/T_e. Formally, the reason is that D^*_{crit} increases with both p and q; now, varying T^*/T_e increases one of these quantities but decreases the other one at the same time such that the value of D^*_{crit} is practically unaffected.

How does the presence of a nonresonant ion species affect the threshold conditions? As mentioned above, the distortion of the ion velocity distribution from the Maxwellian shape is less pronounced for molecular ions than for O^+; however, values of $D^{*\prime}$ around unity seem to be possible (St.-Maurice *et al.*, 1976) so that we put $D^{*\prime}$=1.

We first choose $T^*/T_e = T^{*\prime}/T_e$=1 and determine an upper limit for the threshold. It is found that D^*_{crit} is again insensitive to variations in n_i/n_e, being close to 1.3 in most cases and increasing to 1.4 for the first harmonic only if the fractional oxygen concentration is as low as 5 %. A similar result has been presented by Suvanto (1989b). However, the contribution from the $n \neq N$ terms in (4.3) was not taken into account and, consequently, D^*_{crit} was found to start to increase considerably when the fractional oxygen concentration becomes less than about 20%.

For D^*_{crit} to be other than very close to 1.3, we have to find a case where large p *(q)* does not imply small q *(p)*. This is only possible if

Table 4.1. Minima of the RHS of equation (4.20) for O^+ ions.

q	$[\text{RHS of (4.20)}]_{\min} / 10^{-3}$	q	$[\text{RHS of (4.20)}]_{\min} / 10^{-3}$
0.1	0.00285	1.6	3.00
0.2	0.0384	1.7	3.31
0.3	0.116	1.8	3.61
0.4	0.228	1.9	3.92
0.5	0.370	2.0	4.23
0.6	0.537	2.1	4.55
0.7	0.724	2.2	4.87
0.8	0.930	2.3	5.19
0.9	1.15	2.4	5.52
1.0	1.39	2.5	5.85
1.1	1.63	2.6	6.18
1.2	1.89	2.7	6.52
1.3	2.16	2.8	6.86
1.4	2.44	2.9	7.20
1.5	2.72	3.0	7.54

Table 4.2. Maximum values of α for the case $|\omega| \approx \Omega$ (i.e. $|N|=1$). The corresponding value of the normalized wave number κ is also shown.

$\alpha_{\max}(D^*) / 10^{-3}$	D^*	κ
0.864	1.3	4.5
3.12	1.4	2.8
5.77	1.5	2.2
8.10	1.6	2.0
9.96	1.7	1.8
11.4	1.8	1.7
12.4	1.9	1.6
13.2	2.0	1.5

Table 4.3. Same as Table 4.2, but for $|\omega| \approx 2\Omega$ (i.e. $|N|=2$).

$\alpha_{max}(D^*)\,/10^{-3}$	D^*	κ
0.294	1.3	11
1.43	1.4	6.1
2.57	1.5	4.8
3.54	1.6	4.0
4.30	1.7	3.4
4.90	1.8	3.0
5.41	1.9	2.6
5.88	2.0	2.3

the assumption $T^*=T^{*\prime}$ is not made. Choosing even an unreasonably large difference between T^* and $T^{*\prime}$, such that $T^{*\prime}/T_e=1$ and $T^*/T_e=5$, we find that the fractional molecular species concentration needed to raise the threshold to 1.5 is still as large as about 80%. We thus conclude that for realistic ionospheric conditions, the instability threshold is virtually unaffected by the presence of a nonresonant species: $D^*_{crit} \approx 1.3$.

Finally, it should be remembered that in our derivation, we assumed that finite Debye length and electron Larmor radius effects are negligible. The consistency of these assumptions with the final results is easily verified by noting that typically $\omega_{pe} \sim \Omega_e$, and

$$\frac{k_\perp{}^2 v_e{}^2}{2\,\omega_{pe}{}^2} \sim \frac{k_\perp{}^2 v_e{}^2}{2\,\Omega_e{}^2} \sim \frac{1}{2}\,\kappa^2\,\frac{m_e}{m_i} \lesssim 10^{-3} \tag{4.28}$$

for typical κ values (of the order of 10 or less) considered here.

4.4. CHECK ON GROWTH RATES

In our study of the threshold conditions, the collisional damping of the fluctuations was not taken into account. It has been implicitly assumed that growth rates larger than the relevant collision frequencies are possible and occur close to the threshold conditions deduced from collisionless theory. In this section, we investigate whether sufficiently large growth rates γ exist. The cold electron approximation will be used and a single ion species assumed.

In their growth rate calculations, Lakhina and Bhatia (1984) neglected the effect of $n \neq N$ terms in the ionic contribution to the dielectric function. Furthermore, the imaginary part of the wave frequency was not taken properly into account in the ion function. As a result, their analysis was actually limited to values of the growth rate numerically less than the ion-neutral collision frequency. This is in conflict with the assumption that collisional damping of the fluctuations can be neglected, however. Instead, solutions with $\gamma/k_{\|}v^* >> 1$ should be looked for, to find growth rates exceeding the collision frequency and hence justify the collisionless treatment. The asymptotic expansion (A.6) can then be employed to approximate the plasma dispersion function in all the terms on the RHS of (4.3). As before, use is made of the fact that A_n and B_n are $<<1$; also, we restrict ourselves to cases where $\gamma^2 << \Omega_i^2$. The ionic part of the dielectric function can be written as

$$\varepsilon_i = 2 \frac{\omega_{pi}^2}{k^2 v^{*2}} \left[\exp(-D^{*2}) - 2i \frac{N \Omega_i}{\gamma} \alpha \right], \tag{4.29}$$

where the term $\exp(-D^{*2})$ arises in the same way as in the threshold calculation (Appendix B). It should be noted that to derive

(4.29), there is actually no need to assume any particular form for the *field-parallel* distribution function, as opposed to the threshold calculations presented in Sections 4.2 and 4.3. In our limit of interest, $\gamma/k_{||}v^* >> 1$, we only have to specify the distribution averaged over parallel velocity, and (4.29) follows. As a result, the generality of our results is not restricted e.g. by the assumption of a Maxwellian distribution in the magnetic field direction, which is based on the simple relaxation model. The functional form of the perpendicular distribution also originates from the use of this simplistic model but has been shown by St.-Maurice *et al.* (1976) to be a reasonable approximation for the real distribution function provided the parameters are rescaled, as discussed in Chapter 1. Recent Monte Carlo simulations by Kikuchi *et al.* (1988) also support this result.

Taking $(\omega/k_{||}v_e)^2 >> 1$, the electron part is approximated by

$$\varepsilon_e \approx \frac{\omega_{pe}^2}{\Omega_e^2} - \frac{k_{||}^2}{k^2}\frac{\omega_{pe}^2}{\omega^2}, \tag{4.30}$$

where we have used the asymptotic expansion of Z in (4.17). The first term on the RHS of (4.30) can be neglected as it is typically much smaller than the second. Inserting (4.29) and (4.30) into (4.1) and separating the real and imaginary parts we obtain

$$\left(\frac{N\Omega_i}{k_{||}v^*}\right)^2 \approx \frac{1}{2}\frac{m_i}{m_e}\exp(D^{*2}), \tag{4.31}$$

which can be used to estimate the component of the wave vector along the magnetic field, and an expression for the growth rate:

$$\left(\frac{\gamma}{N\Omega_i}\right)^2 \approx \alpha \exp(D^{*2}). \tag{4.32}$$

Taking $D^*=1.3$ and taking the ion species to be O^+, we find from (4.32) and Tables 4.2 and 4.3 that the growth rates for the first and second harmonic are 20 s^{-1} and 24 s^{-1}, respectively, increasing to 97 s^{-1} and 130 s^{-1} at $D^*=1.6$. The growth rate is thus found to be larger than the typical ion-neutral collision frequency, which is less than 10 s^{-1} in the high-latitude F-region (St.-Maurice, 1978), and it increases with D^* as one would expect.

Figure 4.1 shows the normalized wave number κ of the fastest growing mode as a function of D^*. Taking $v^*=10^3$ ms^{-1} and assuming oxygen ions, we find that wavelengths between about 1 m and 10 m are expected.

4.5. DISCUSSION

After having performed a parametric study of the threshold conditions for the ion cyclotron instability, a few comments on the implications of this work are in order. First of all, the plasma has been regarded as homogeneous and time-independent. We have concentrated on cases where the wave amplitude grows in the rest frame of the plasma (i.e. *absolute instabilities*) and not discussed *convective instabilities*. These are characterized by wave packets that propagate such that their energy is observed to grow in the moving frame but shows an asymptotic decay at any fixed point. The waves can only grow to large amplitude if the size of the unstable region is considerably larger than the ratio of the group velocity and the growth rate. In principle, a model of the spatial dependence of all the plasma parameters would be required to study these propagation effects.

It is interesting to note that the minimum value of D^* for which the ion cyclotron instability is excited, 1.26, is essentially the same as for the Post-Rosenbluth instability (Ott and Farley, 1975), even though these results have been derived using two different approaches. This is not beyond expectation since $D^*=1.26$

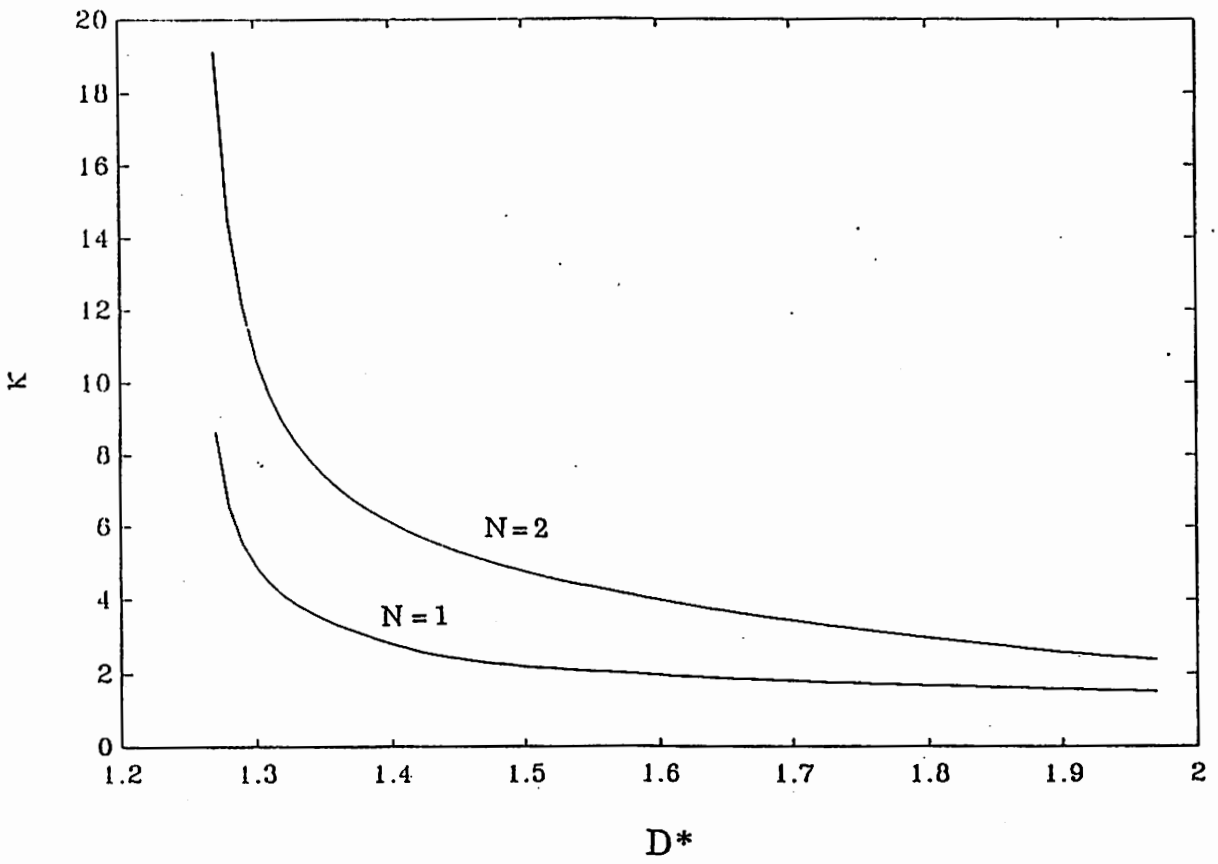

Figure 4.1. The normalized wave number κ of the fastest growing mode as a function of D^*.

corresponds to a rather flat 1-D distribution in the field-perpendicular direction. This can be qualitatitely seen from Figure 1.4 which is, however, for the aspect angle of 73.5°. Larger values of D^* indicate a positive slope, which is known to be a potential source of instabilities. We also note that the calculations presented here were for magnetized ions, while the high-frequency instability with large growth rates could be treated in the unmagnetized ion approximation.

It was found that the instability threshold is insensitive to variations in the plasma temperatures and also the fractional concentration of the non-resonant ion species for realistic F-region conditions provided $T^{*\prime}$ is not very much lower than T^*, which we do not expect to be the case because in the relaxation collision model, these quantities represent the temperatures of the neutral species colliding with the ions. It is true, of course, that the distribution function used in this work should be interpreted as an empirical extension of that model but even so, having $T^*/T^{*\prime}>5$, as in our example at the end of Section 4.3, seems unrealistic because the ion temperatures would then differ by a factor of roughly 5.

In the present investigation of the threshold conditions, the collisional damping of the fluctuations was ignored. However, instability growth rates larger than the typical ion-neutral collision frequency in the region of interest were found (using the cold electron approximation), which is consistent with the collisionless treatment. However, in cases where some of the collision frequencies involved exceeds the typical growth rate deduced from the present theory, the threshold values of D^* will be higher than discussed here.

Finally, we note that at some point of the wave growth linearized theory breaks down and the evolution of the instability is governed by nonlinear processes. This topic will be discussed in the next chapter.

CHAPTER 5

QUASILINEAR EFFECTS

5.1. NATURE OF THE PROBLEM

The linear theory calculation presented in Chapter 4 showed that the non-Maxwellian ion velocity distribution can become unstable for high enough ambient electric fields, corresponding to D^* larger than about 1.3 for realistic ionospheric parameters. The instability leads to enhanced density fluctuations above the thermal level, but only in directions almost perpendicular to the magnetic field. This is, however, not to say that the instability has no effects at smaller aspect angles, including the range used in incoherent radar research. In particular, large-amplitude waves may be observed indirectly due to their effect on macroscopic plasma properties. Ott and Farley (1975) pointed out that the turbulent, wave-induced velocity space diffusion caused by the Post-Rosenbluth instability is so strong that the ion velocity distribution will become only marginally unstable as the ambient electric field increases. However, Post-Rosenbluth waves can be considerably stabilized by the presence of a molecular ion species, whereas the threshold value of D^* for the ion cyclotron instability is insensitive to variations in the fractional concentration of the nonresonant species. As a result, diffusion due to ion cyclotron waves may well be the agent that in the first place modifies the ion velocity distribution.

To summarize the problem at hand: for a stable plasma, the ion population is driven towards a steady-state non-Maxwellian velocity distribution by ion-neutral collisions, as discussed in Chapter 1. In

the case of large-amplitude electrostatic waves, however, the velocity space diffusion acts as a competing process and must be taken into account in the kinetic equation. The steady state ion velocity distribution represents the balance of these processes [Ott and Farley (1975); St.-Maurice (1978); Suvanto (1987)]. In this chapter, a differential equation for the steady-state distribution function is derived. It turns out that in the limit where the wave spectrum is narrow and concentrated around a cyclotron harmonic, semi-quantitative predictions of the shape of the velocity distribution can be made without an involved computer simulation. In the approximation scheme to be used, the wave spectrum is represented by a single parameter, whose order of magnitude can be estimated in terms of the ratio of the electrostatic wave energy and the thermal energy i.e. the weak turbulence parameter (Suvanto, 1989b). This is an advantage because it is then possible to study the distribution shape without knowing the details of the wave spectrum. Although the saturation mechanism is not explicitly specified, the fact that the anomalous diffusion operator is written to lowest (second) order in wave amplitude, and unperturbed particle orbits are used, restricts the analysis to weak turbulence, where quasi-linear diffusion dominates over effects like mode-coupling and wave-particle resonance broadening discussed by Dupree (1966).

5.2. THEORETICAL FORMULATION

The ion kinetic equation in the plasma drift frame, with allowance for the self-consistent wave electric field, can be written as

$$\frac{\partial f}{\partial t} + \mathbf{v} \cdot \frac{\partial f}{\partial \mathbf{r}} = -\Omega \frac{\partial f}{\partial \theta} - \frac{q}{m} \mathbf{E} \cdot \frac{\partial f}{\partial \mathbf{v}} - \nu \left(f - \frac{n}{n_0} f_n \right), \tag{5.1}$$

where f is the ion velocity distribution function. We will concentrate on the case where $f(\mathbf{r},\mathbf{v},t)$ can be expressed as the sum of a spatially

homogeneous, time-independent "zeroth-order" distribution, f_0, and a rapidly oscillating part associated with the electrostatic waves. The three terms on the RHS of (5.1) respectively describe gyration effects around the magnetic field, Ω being the ion gyrofrequency and θ the gyrophase angle around the magnetic field in velocity space, the effect of the wave electric field $\mathbf{E}$, and ion-neutral collisions, which are simulated by a relaxation model for simplicity; the factor n/n_0, the ratio of the ion number density $n(\mathbf{r},t)$ and the mean ion density n_0, has been included so that collisions conserve particles locally as they should. The normalization of the velocity distributions is such that

$$\frac{\int d^3v\, f(\mathbf{r},\mathbf{v},t)}{\int d^3v\, f_n(\mathbf{v})} = \frac{n}{n_0} . \tag{5.2}$$

We consider a periodic plasma, as Chen (1987) did, the periodicity volume being L^3. The continuum limit, $L\to\infty$, will be taken later in the derivation. Time is treated in the same way; all time averages are to be taken over the (long) time period T. Averaging (5.1) over time and space yields

$$\Omega \frac{\partial \langle f \rangle_{rt}}{\partial \theta} = -\left\langle \frac{q}{m} \mathbf{E} \cdot \frac{\partial f}{\partial \mathbf{v}} \right\rangle_{rt} - \nu(\langle f \rangle_{rt} - f_n), \tag{5.3}$$

or

$$\frac{\partial \langle f \rangle_{rt}/\partial \theta}{\langle f \rangle_{rt}} = -\frac{\left\langle (q/m)\, \mathbf{E} \cdot \partial f/\partial \mathbf{v} \right\rangle_{rt}}{\Omega \langle f \rangle_{rt}} - \frac{\nu(\langle f \rangle_{rt} - f_n)}{\Omega \langle f \rangle_{rt}} . \tag{5.4}$$

Above about 130–140 km, the ion-neutral collision frequency is typically much less than the ion gyrofrequency [e.g. Ott and Farley (1975)] so that the second term on the RHS of (5.4) is $<<1$. Furthermore, the order-of-magnitude of the first term is given by

$$\frac{(q\,E\,/m\,)}{\Omega\,v_{\mathrm{th}}}, \tag{5.5}$$

where the numerator is of the order of the acceleration due to an electric field of the strength E and the denominator is essentially the centripetal acceleration provided by the magnetic field; v_{th} denotes the typical particle speed. If the electric field is low enough for this ratio to be small, which we assume to be the case, the waves will only introduce a minor perturbation to the circular motion of the ions around the magnetic field lines. As a result, the first term on the RHS is also <<1; this means that the space and time averaged velocity distribution, the quantity of major interest, is practically independent of the gyrophase angle θ and can be written as

$$f_0 \equiv \langle f \rangle_{\mathrm{r\,t}} = \langle f \rangle_{\mathrm{r\,t\,\theta}} + O\left(\frac{\nu}{\Omega}, \frac{qE\,/m}{\Omega\;v_{\mathrm{th}}}\right), \tag{5.6}$$

where the first term on the RHS is the distribution function averaged over time, space and the gyrophase angle in velocity space and the second term represents the small deviation from gyrotropy due to ion-neutral collisions and wave-particle interactions. We then average (5.3) over θ; the LHS yields exactly zero because f must be 2π-periodic in θ, i.e. single-valued. The result is thus

$$-\left\langle \frac{q}{m}\mathbf{E}\cdot\frac{\partial f}{\partial \mathbf{v}}\right\rangle_{\mathrm{r\,t\,\theta}} = \nu\,(\langle f \rangle_{\mathrm{r\,t\,\theta}} - \langle f_{\,n}\rangle_{\theta}) \approx \nu\,(f_0 - \langle f_{\,n}\rangle_{\theta}). \tag{5.7}$$

We postulate the existence of a steady fluctuation spectrum and represent the electrostatic potential by a Fourier series:

$$\mathrm{E} = -\frac{\partial \Phi}{\partial\,\mathbf{r}} = -\sum_{\mathbf{k}\omega} i\,\mathbf{k}\Phi_{\,\mathbf{k}\omega}\,\exp\left[i\,(\mathbf{k}\cdot\mathbf{r} - \omega\,t)\right]. \tag{5.8}$$

Introducing (5.8) in (5.7) and carrying out the averaging over $\mathbf{r}$ and t yields

$$-i\frac{q}{m}\sum_{\mathbf{k}\omega}\left\langle \Phi_{\mathbf{k}\omega}{}^{*}\mathbf{k}\cdot\frac{\partial f_{\mathbf{k}\omega}}{\partial \mathbf{v}}\right\rangle_{\theta}=\nu\,(f_0-\langle f_n\rangle_{\theta}), \tag{5.9}$$

where * denotes the complex conjugate. Here $\Phi_{\mathbf{k}\omega}{}^{*}$ has been written instead of $\Phi_{-\mathbf{k},-\omega}$; these are, of course, equal by the reality of (5.8). The LHS of (5.9) is to be written to lowest (second) order in terms of the electrostatic potential. It is thus sufficient to express $f_{\mathbf{k}\omega}$ as a linear response to the electric field. The linearization of (5.1) yields

$$i(\mathbf{k}\cdot\mathbf{v}-\omega)f_{\mathbf{k}\omega}+\Omega\frac{\partial f_{\mathbf{k}\omega}}{\partial\theta}-i\frac{q}{m}\Phi_{\mathbf{k}\omega}\,\mathbf{k}\cdot\frac{\partial f_0}{\partial \mathbf{v}}=-\nu\,(f_{\mathbf{k}\omega}-\frac{n_{\mathbf{k}\omega}}{n_0}f_n). \tag{5.10}$$

Provided the collision frequency is small enough, we may ignore the term on the RHS of (5.10), associated with wave-particle resonance broadening due to collisions. After replacing the RHS by zero, (5.10) becomes

$$\frac{\partial f_{\mathbf{k}\omega}}{\partial\theta}+i\frac{\mathbf{k}\cdot\mathbf{v}-\omega}{\Omega}f_{\mathbf{k}\omega}=\frac{i}{\Omega}\frac{q}{m}\Phi_{\mathbf{k}\omega}\,\mathbf{k}\cdot\frac{\partial f_0}{\partial \mathbf{v}}. \tag{5.11}$$

This is a differential equation for $f_{\mathbf{k}\omega}$, and its single-valued[1] solution is

$$f_{\mathbf{k}\omega}=-\frac{q}{m}\Phi_{\mathbf{k}\omega}\times$$

$$\times\sum_{m,n=-\infty}^{\infty}\left(k_{\parallel}\frac{\partial f_0}{\partial v_{\parallel}}+\frac{n\Omega}{v_{\perp}}\frac{\partial f_0}{\partial v_{\perp}}\right)\frac{J_m\left(\frac{k_{\perp}v_{\perp}}{\Omega}\right)J_n\left(\frac{k_{\perp}v_{\perp}}{\Omega}\right)}{\omega-k_{\parallel}v_{\parallel}-n\Omega}exp\left[i(n-m)(\theta-\theta_{\mathbf{k}})\right], \tag{5.12}$$

where $\theta_{\mathbf{k}}$ is the gyrophase angle in $\mathbf{k}$ space. Mathematically, the steps leading from (5.11) to (5.12) are very similar to those Raman

[1] The fundamental requirement is, of course, that the distribution function must be single-valued. However, it follows from the orthogonality of the Fourier series that each coefficient $f_{\mathbf{k}\omega}$ must separately satisfy this condition.

(1980) was faced with in his study of the linear electronic contribution to the incoherent scatter spectrum, and will not be discussed here. The LHS of (5.9) becomes, after the introduction of (5.12),

$$i\frac{q^2}{m^2}\sum_{\mathbf{k},\omega}\left|\Phi_{\mathbf{k}\omega}\right|^2 \times$$

$$\times\sum_{m,n=-\infty}^{\infty}\left\langle \mathbf{k}_\perp\cdot\frac{\partial}{\partial \mathbf{v}_\perp}\left\{\left(k_{\parallel}\frac{\partial f_0}{\partial v_{\parallel}}+\frac{n\Omega}{v_\perp}\frac{\partial f_0}{\partial v_\perp}\right)\frac{J_m J_n}{\omega-k_{\parallel}v_{\parallel}-n\Omega}exp\left[i(n-m)\theta'\right]\right\}\right\rangle_{\theta'} \tag{5.13}$$

Here we have introduced $\theta' = \theta - \theta_{\mathbf{k}}$ and made use of the facts

$$\mathbf{k}\cdot\frac{\partial}{\partial \mathbf{v}} \approx \mathbf{k}_\perp\cdot\frac{\partial}{\partial \mathbf{v}_\perp} \tag{5.14}$$

$$\langle\ \rangle_\theta = \langle\ \rangle_{\theta'}. \tag{5.15}$$

The arguments of the Bessel functions in (5.13) are the same as in (5.12) and have not been written down explicitly. Noting that

$$\mathbf{k}_\perp\cdot\frac{\partial}{\partial \mathbf{v}_\perp} = k_\perp\cos\theta'\frac{\partial}{\partial v_\perp} - k_\perp\frac{\sin\theta'}{v_\perp}\frac{\partial}{\partial\theta'} \tag{5.16}$$

we find that for an arbitrary function F

$$\left\langle \mathbf{k}_\perp\cdot\frac{\partial}{\partial \mathbf{v}_\perp}F(v_\perp,\theta')\right\rangle_{\theta'} = k_\perp\left\langle\cos\theta'\frac{\partial(v_\perp F)}{v_\perp\partial v_\perp}\right\rangle_{\theta'}. \tag{5.17}$$

Using this rule to perform an average over θ', (5.13) becomes

$$i\frac{q^2}{m^2}\sum_{\mathbf{k},\omega}\left|\Phi_{\mathbf{k}\omega}\right|^2\sum_{n=-\infty}^{\infty}\frac{\partial}{v_\perp\partial v_\perp}n\Omega J_n{}^2\frac{k_{||}\dfrac{\partial f_0}{\partial v_{||}}+\dfrac{n\Omega}{v_\perp}\dfrac{\partial f_0}{\partial v_\perp}}{\omega-k_{||}v_{||}-n\Omega}. \quad (5.18)$$

The Bessel function identity (A.9) has been used to obtain (5.18). In the summation, the $n=0$ term vanishes. For $n\neq 0$, we estimate, in the spirit of linearized theory and equation (4.12),

$$\left|\frac{k_{||}\,\partial f_0/\partial v_{||}}{(n\Omega/v_\perp)\,\partial f_0/\partial v_\perp}\right| \sim \left|\frac{k_{||}v_{th}}{n\Omega}\right| << 1\,, \quad (5.19)$$

so that (5.9) can be written as

$$\nu\,(f_0-\langle f_n\rangle)=i\frac{q^2}{m^2}\sum_{\mathbf{k},\omega}\left|\Phi_{\mathbf{k}\omega}\right|^2\sum_{n=-\infty}^{\infty}(n\Omega)^2\frac{\dfrac{\partial}{v_\perp\partial v_\perp}J_n{}^2\dfrac{\partial f_0}{v_\perp\partial v_\perp}}{\omega-k_{||}v_{||}-n\Omega+i0}, \quad (5.20)$$

where the angular brackets on the LHS denote the average over θ (the subscript has been depressed). The symbolic term $+i0$ has been added to the denominator on the RHS to be consistent with the principle of causality; it does not arise from the analysis itself as in the Laplace transform approach to linear theory [Sagdeev and Galeev (1969), p. 90]. Using the symbolic relation

$$\frac{1}{\omega-k_{||}v_{||}-n\Omega+i0}=P\left(\frac{1}{\omega-k_{||}v_{||}-n\Omega}\right)-i\pi\,\delta(\omega-k_{||}v_{||}-n\Omega)\,, \quad (5.21)$$

where P denotes the Cauchy Principal Value and δ is the usual Dirac delta function, we find that the RHS of (5.20) is real as it should be, and

$$\nu\,(f_0-\langle f_n\rangle)=\pi\,\frac{q^2}{m^2}\sum_{\mathbf{k},\omega}\left|\,\Phi_{\mathbf{k}\omega}\,\right|^2 \times$$

$$\times\sum_{n=-\infty}^{\infty}(n\Omega)^2\,\delta\,(\omega-k_{\|}v_{\|}-n\Omega)\,\frac{\partial}{v_\perp\partial v_\perp}\,J_n{}^2\frac{\partial f_0}{v_\perp\partial v_\perp}\,. \qquad (5.22)$$

In the light of the delta function prescription, it is appropriate to replace the summation over $\mathbf{k}$ and ω by an integral. To do that, we first note that according to our periodicity assumptions discussed after equation (5.2), only a discrete set of $\mathbf{k}$ and ω values are possible. In a Cartesian coordinate system (say), each component of $\mathbf{k}$ can have the values $p\Delta k_j \equiv p\ 2\pi/L$, where p is an integer and $j = x$, y or z. Similarly, the possible values of ω are multiples of $\Delta\omega \equiv 2\pi/T$. Consequently,

$$\sum_{\mathbf{k},\omega}=\frac{L^3T}{(2\pi)^4}\sum_{\mathbf{k},\omega}\Delta k_x\,\Delta k_y\,\Delta k_z\,\Delta\omega\ , \qquad (5.23)$$

from which we obtain the rule

$$\sum_{\mathbf{k},\omega}\rightarrow\frac{L^3T}{(2\pi)^4}\int \mathrm{d}^3\mathbf{k}\,\mathrm{d}\omega, \qquad (5.24)$$

as L and $T\rightarrow\infty$. This does not necessarily mean taking the infinite limit mathematically: the criterion is that L and T should be much larger than the typical wavelength and the wave period respectively, but much less than the length scale of any spatial large-scale inhomogeneity (gradient in the ion drift velocity etc.) and the time scale for temporal changes (in the drift, for example) respectively, so that our assumption of homogeneous and time-independent plasma would not be violated.

A direct application of (5.24) to (5.22) would make the factors L and

T appear explicitly in the diffusion operator. It would be desirable to transform to quantities which leave (5.22) independent of them, even if the integral form is used. To do this, we first note that using (5.8), the averaged electrostatic energy density can be written as

$$W_E = \frac{1}{2}\varepsilon_0 \langle \mathbf{E}^2 \rangle = \int d^3\mathbf{k}\, d\omega\; W_E(\mathbf{k},\omega), \tag{5.25}$$

with the spectral energy density

$$W_E(\mathbf{k},\omega) = \frac{1}{2}\frac{L^3 T}{(2\pi)^4}\varepsilon_0 k^2 \left| \Phi_{\mathbf{k}\omega} \right|^2. \tag{5.26}$$

The rule (5.24) was employed to replace the summation by an integral. Following Dupree (1966), we will keep the electrostatic energy density fixed as the continuous limit is taken. This means that the Fourier components of the wave spectrum must vanish as $L^{-3/2}$ $T^{-1/2}$ as L and $T \to \infty$. Applying (5.24) to (5.22) and writing the resulting expression in terms of the spectral energy density given by (5.26) leads to

$$\nu\,(f_0 - \langle f_n \rangle) = 2\pi \frac{\omega_p^2}{n_0 m} \int d^3\mathbf{k}\, d\omega\; \frac{W_E(\mathbf{k},\omega)}{k^2} \times$$

$$\times \sum_{n=-\infty}^{\infty} (n\Omega)^2 \delta(\omega - k_{\parallel} v_{\parallel} - n\Omega) \frac{\partial}{v_\perp \partial v_\perp} J_n^2 \frac{\partial f_0}{v_\perp \partial v_\perp}. \tag{5.27}$$

Here ω_p is the ion plasma frequency. Before discussing the solution of (5.27), a couple of comments on the approximations made so far are in order. Consider first the resonance condition imposed by the δ function,

$$\omega - k_{\parallel} v_{\parallel} - n\Omega = 0, \tag{5.28}$$

which means that only particles with field-parallel velocity *exactly* equal to $(\omega - n\Omega)/k_{||}$ can resonate with a particular wave mode. In quasilinear theory, the positive imaginary part (γ) of ω, responsible for linear wave growth, broadens the resonance region associated with a linear normal mode of the plasma, and one has expressions of the type

$$\frac{\gamma}{(\omega - k_{||}v_{||} - n\Omega)^2 + \gamma^2} \tag{5.29}$$

instead of the δ function factor. In fact, our diffusion operator is identical to the one in quasilinear theory in the limit $\gamma \to +0$, corresponding to the case where the plasma is only marginally unstable.

However, it would be incorrect to say that the wave saturation takes place in a purely quasilinear fashion, which would eventually result in a linearly stable steady-state velocity distribution. The reason is that the waves would then be damped and the form of the distribution thus determined by ion-neutral collisions alone, which would drive it towards a highly unstable configuration. This is in conflict with our steady-state assumption. The linear instability must thus be driven, though possibly at a low level, to maintain the waves which balance the effect of collisions. For all that, the level of turbulence is assumed to be sufficiently low so that the resonance condition of quasilinear theory in the limit of a vanishingly small positive growth rate can be used.

It follows from the work of Chapter 4 that the various cyclotron harmonics are excited almost simultaneously. For simplicity, we study the effect of a *single* harmonic on the distribution function and assume that the wave spectrum is concentrated around the first gyroharmonic (i.e. $|N|=1$). The resonance condition (5.28) can be written as

$$k_{\|} v_{th}\left(\frac{\omega - n\Omega}{k_{\|} v_{th}} - \frac{v_{\|}}{v_{th}}\right) = 0, \tag{5.30}$$

where the first term in brackets is the familiar ion resonance parameter discussed in Chapter 4 except that a general velocity scale v_{th} is used instead of the semi-empirical parameter v^*. There is, however, no need to make any distinction between these two if we just consider orders of magnitude. Noting that the velocities $v_{\|}$ of interest are of the order of v_{th} or less, it follows that we must have $|n|=1$; for other values of n the absolute value of the resonance parameter is much larger than unity by (4.12) and, consequently, (5.30) cannot be satisfied in the velocity range of interest. Using this simplification in the steady-state kinetic equation leads to

$$\nu\,(f_0 - \langle f_n \rangle) = 4\pi \frac{\omega_p^2}{n_0 m} \int d^3\mathbf{k}\, d\omega\, \frac{W_E(\mathbf{k},\omega)}{k^2} \times$$
$$\times\, \Omega^2\, \delta\,(\omega - k_{\|} v_{\|} - \Omega) \frac{\partial}{v_{\perp} \partial v_{\perp}} J_1^2 \frac{\partial f_0}{v_{\perp} \partial v_{\perp}}, \tag{5.31}$$

where the extra factor of 2 on the RHS comes from the fact that the terms in (5.27) with n=–1 and n=+1 have been retained. Performing the ω integration yields

$$f_0 - \langle f_n \rangle = A \frac{\partial}{v\, \partial v} J_1^2 \frac{\partial f_0}{v\, \partial v}, \tag{5.32}$$

where $v = v_{\perp}/v_{th}$ is the normalized field-perpendicular speed and the parameter A is given by

$$A = 2\pi \frac{\Omega}{\nu} \frac{\omega_p^2}{v_{th}^2} \frac{\Omega}{W_{TH}} \int d^3\mathbf{k}\, \frac{W_E(\mathbf{k}, \omega = \Omega + k_{\|} v_{\|})}{k^2}. \tag{5.33}$$

Here $W_{TH} = n_0 m v_{th}^2 / 2$ is the particle thermal energy density. To obtain (5.32–33), the wave spectrum has been assumed to be narrow in the field-perpendicular wavenumber, $\Delta k_\perp / k_\perp << 1$, and the argument of the Bessel function factor, which has been taken out of the integral, is to be evaluated at the value of $k_\perp$ around which the spectrum is concentrated. This probably corresponds to the wave mode which first becomes unstable if the ion drift is only slightly above its threshold value. The order of magnitude of A, which is related to the relative importance of ion-neutral collisions and wave-induced diffusion, can be estimated by

$$A \sim 2\pi \frac{\omega_p^2}{k^2 v_{th}^2} \frac{\Omega}{\nu} \frac{\Omega}{\Delta\omega} \frac{W_E}{W_{TH}}, \tag{5.34}$$

where $\Delta\omega$ characterizes the width of the wave spectrum in ω. It follows from the resonance condition imposed by the δ function in (5.31) that $\Delta\omega \sim k_{||} \Delta v_{||}$, where $\Delta v_{||}$ is the range of parallel velocities of the resonant particles and the magnitude of $k_{||}$ in the linear approximation is found from (4.31). It is clear that A can be made large simply by decreasing $\Delta\omega$. In this case, however, $\Delta v_{||}$ is also small so that only a very small fraction of particles can participate in the diffusion process. For the anomalous distortion of the distribution function to be important on average, $\Delta v_{||} \sim v_{th}$ is required. Taking $\nu = 1\ s^{-1}$, it follows that velocity space diffusion is expected to be important ($A \sim 1$) at surprisingly low levels of turbulence, $W_E/W_{TH} \sim 10^{-10}$.

However, this conclusion is only valid in the limit $\gamma \to +0$ (corresponding to the δ function description of the wave-particle resonance) i.e. the distribution should be very close to marginal stability. This is a rather restrictive assumption. We therefore estimate the diffusion parameter A using an alternative approach. In particular, the expression (5.29) is employed to describe the

resonance, with γ taken from linear instability theory. Referring to Chapter 4, the first term in the denominator of (5.29) is then negligible compared with γ^2, and (5.29) is essentially given by $1/\gamma$ so that

$$A \sim 2 \frac{\omega_p^2}{k^2 v_{th}^2} \frac{\Omega}{\nu} \frac{\Omega}{\gamma} \frac{W_E}{W_{TH}} . \tag{5.35}$$

The growth rate is expected to decrease during the diffusion process. As a result, a lower bound of A can be obtained by using the values of γ derived in Chapter 4 for the initial ion configuration. Taking $A \sim 1$ in (5.35) leads to values of W_E/W_{TH} less than about 10^{-8} for $\gamma \sim 20$ s^{-1}. Although it is difficult to estimate the wave amplitude accurately, we conclude from the above considerations that fluctuations with $W_E/W_{TH} \sim 10^{-8}$ are certainly enough to cause a significiant modification of the distribution function. We note in passing that the force on an ion due to the wave electric field is then only a fraction of the centripetal force provided by the magnetic field so that the assumption about gyrotropy, discussed after equation (5.5), is justified.

To get some idea about the diffusion process, we turn to equation (5.32), which is an ordinary second-order differential equation for f as a function of $v_\perp$. The general solution involves two parameters to be determined by the boundary conditions. A physically reasonable solution should be well-behaving together with its derivative at $v_\perp = 0$; also, f must vanish as $v_\perp \to \infty$. In fact, the solution of (5.32) at $v_\perp \to 0$ can be expressed in terms of the modified Bessel functions I_0 and K_0, and the first of the above requirements fixes one of the two free parameters in the general solution. It is also possible to construct a "physically reasonable" (the width of the spectrum in wavelength is treated as small though nonzero) asymptotic solution in terms of modified Bessel functions of order 3/5 and find that one of the free parameters is again fixed, this time by the requirement $f \to 0$ as $v_\perp \to \infty$. The details will not be discussed here but these results

suggest that a global, physically reasonable solution always exists and is unique; it has to be found numerically, however. To solve the equation by a shooting method, the initial conditions at $v_\perp = 0$ have to be specified. By introducing $f(v_\perp) = f(0) + f'(0)v_\perp + f''(0)v_\perp^2/2 + \ldots$ in (5.32), we find that the RHS is finite only if $f'(0)=0$. (If this was not true, the plasma would certainly be dominated by the Post-Rosenbluth instability!) This is one of the initial conditions; it also guarantees that the solution is well-behaved at the origin. By varying $f(0)$, we found the solution satisfying the boundary condition at infinity.

Figure 5.1 shows perpendicular ion velocity distributions for different values of the turbulence parameter A. The ion drift Mach number (or D^*, if the "semi-empirical" notation is used) has been chosen to be 1.5, and κ=2.2, motivated by Table 4.2 of Chapter 4, has been used. For A=0 we recover the familiar distribution function (1.13); increasing A tends to flatten the distribution and bring it closer to marginal stability as expected.

The flattening of the velocity distribution with the increase of A can be qualitatively seen from (5.32) by dividing it by A and taking the formal limit $A \to \infty$, which implies that $(J_1^2 / v)\, \partial f_0 / \partial v \approx$ constant. The LHS vanishes at v=0 so that this constant is equal to zero. We thus find that either $J_1^2 \approx 0$ or $\partial f_0/\partial v \approx 0$. This means that in the limit of large A, f_0 would be piecewise constant and decrease abruptly at the zeros of J_1 (except v=0) to conserve the particle density. In reality, this is not the case. First, a complete stabilization of the distribution function will not occur, as discussed earlier. Secondly, the behaviour is partially a reflection of our assumption of a vanishingly small width of the wavelength spectrum. We have only plotted the low-energy part of the velocity distribution to illustrate the evolution of the positive slope in perpendicular velocity, which drives the instability. Particles in the high-energy tail of any velocity distribution take part in ionospheric chemical reactions which further modify the distribution. It follows that as far as the high-energy part of the distribution is concerned, any calculation which

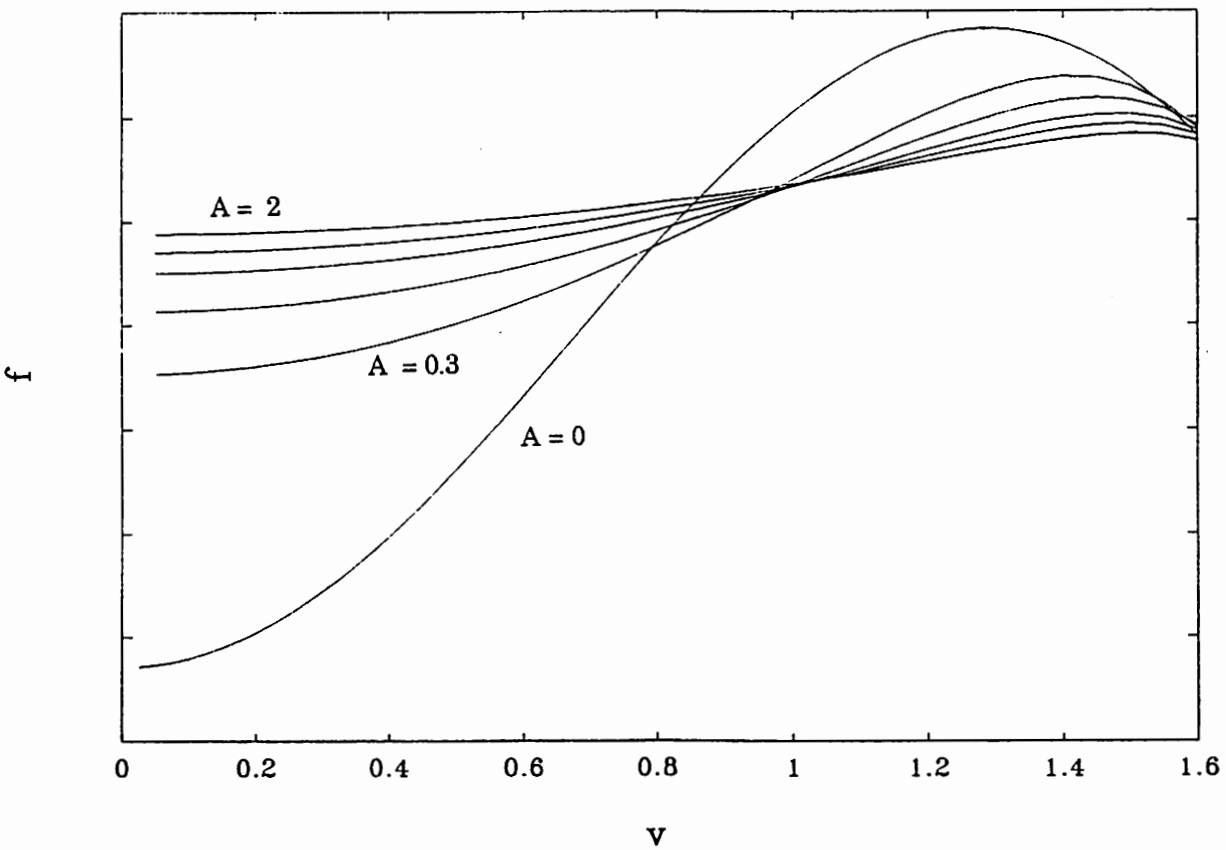

Figure 5.1. The effect of quasi-linear diffusion on the positive slope of the perpendicular distribution function for different levels of turbulence. The ion drift Mach number is 1.5 and the normalized wave number κ=2.2. Here $A=0$ corresponds to the distribution (1.13). Note that only the low-energy parts are shown.

neglects chemical reactions (like all the previous work reviewed in Chapter 1) may lead to inaccurate results.

5.3. DISCUSSION

The effect of linearly unstable ion cyclotron waves on the ion velocity distribution has been investigated. We assumed a steady fluctuation spectrum and wrote the kinetic equation in the case where the effect of ion-neutral collisions driving the non-thermal distribution is balanced by wave-induced velocity space diffusion. A simple relaxation model was used to simulate particle collisions, and the diffusion operator was written to the lowest (second) order in wave amplitude, neglecting mode coupling and resonance broadening effects (i.e. unperturbed particle trajectories were used). The approach is thus restricted to weak turbulence, where quasilinear effects dominate. We specialized in the simple case where the wave spectrum is concentrated around the first cyclotron harmonic; this is probably the most stringent restriction on the validity of the analysis. The spectrum was assumed to be narrow in wavelength, and it was shown that the velocity distribution is distorted from the shape given by (1.14) at very low fluctuation levels, $W_E/W_{TH} \lesssim 10^{-8}$. The low-energy part, which is characterized by a positive slope in non-turbulent theory, becomes flatter, and this process may stabilize the distribution against the Post-Rosenbluth instability.

In the present chapter, particular attention has been paid to the formulation of the problem. We have used an analytical approach and explored the quasilinear limit, which is the lowest-order description of the diffusion process. This work is therefore to be considered as an initial investigation, which should be followed by computer simulations that make use of more realistic collisional models and are able to follow the time evolution of the wave spectrum self-consistently with the particle velocity distribution as opposed to treating the fluctuation level as a free parameter, as we did here.

Also, the effect of the waves on individual particle orbits (e.g. trapping) should be studied. It would be of particular interest to see whether simulations would show the flattening of the velocity distribution at the very low levels of turbulence discussed in this work.

CHAPTER 6

CONCLUSIONS

In this thesis, we have investigated consequences of non-Maxwellian ion velocity distributions in the high-latitude F-region ionosphere at altitudes where the drifting ions collide mostly with the background neutrals. The distortion of the distribution function from the Maxwellian shape is due to the joint effect of a large flow perpendicular to the geomagnetic field and ion-neutral collisions. Collisions tend to establish a steady state, while the role of a strong magnetic field ($\nu << \Omega$) is to maintain gyrotropy in velocity space. Distributions of this kind are expected to exist above 130–140 km and below about 250 km.

For large ion drifts, the observed incoherent scatter spectrum takes the "exotic" form predicted theoretically by Raman (1980) and Raman *et al.* (1981), as pointed out by Lockwood *et al.* (1987). The empirical description of the ion distribution function based on the simple relaxation collision model, analysis of RPA data (St.-Maurice *et al.*, 1976) and Monte Carlo simulations has been used to approximate the field-perpendicular distribution function in our data analysis. The fact that a Maxwellian was used for the field-parallel part does not restrict the validity of the results obtained by 1-D analysis, as discussed in Sections 2.5 and 3.1. Allowance for the extra fit parameter D^* in the spectral analysis program at the Rutherford Appleton Laboratory has considerably improved the quality of fits, the fit variance being often decreased to about 50% of its value for the standard Maxwellian analysis. The parameter D^* was

found to increase with the ion drift speed, which is consistent with the theoretical expectations the analysis procedure is based on, but does not usually exceed the value of about 1.3. This kind of behaviour has also been reported by St.-Maurice *et al.* (1976) who found that D^* corresponding to the best fit to the real perpendicular 1-D distribution increases rapidly with ion temperature for D^* less than about unity but tends to remain below about 1.4 even for very large relative ion-neutral drifts. At least two explanations for these experimental results should be considered. First, the nature of ion-neutral collisions may become different for very large drift velocities. Secondly, the plasma is linearly unstable if $D^*>1.3$, and velocity space diffusion may prevent a further increase of the positive slope of the distribution function.

It is clear from the discussions of Chapter 5 that the excitation of microinstabilities is *not* a separate problem to be studied in its own right only. Large-amplitude waves affect the shape of the ion velocity distribution function and may have to be taken into account in the analysis of incoherent scatter radar data for very large drifts. For a pure oxygen plasma, the Post-Rosenbluth and ion cyclotron instabilities are excited almost simultaneously as the drift increases i.e. for roughly the same value of D^* ($\approx$1.3). Above this value, theoretical 1-D distribution functions at sufficiently large aspect angles are characterized by a positive slope, and energy can be fed to both high- and low-frequency waves. It is stressed that our analytical estimates of the instability growth rate in Section 4.4 do not rely on any assumed form of the field-parallel distribution. The critical D^* for the Post-Rosenbluth instability can be considerably increased by the presence of a molecular ion population which is only slightly non-thermal, while the threshold for ion cyclotron waves is practically independent of the ion composition (as well as the plasma temperatures), as found in Chapter 4. This means that if the fractional concentration of molecular ions is large enough, the ion cyclotron instability is excited first, leading to velocity space diffusion of the kind discussed in Chapter 5. The distribution function is

expected to be modified at very low levels of turbulence, the ratio of the electrostatic wave energy density to the thermal energy density being of the order of 10^{-8} or less. In our study of quasilinear effects, we specified in the case where the weakly turbulent wave spectrum is concentrated around the first cyclotron harmonic and narrow in wavelength. Furthermore, the pure relaxation model was used to simulate ion-neutral collisions.

As far as future incoherent scatter research is concerned, further investigations are needed to either confirm or invalidate the model (1.14) of the 3-D distribution function and to study the spectral shape above the instability threshold. Multi-receiver radar facilities like EISCAT could be used to probe the same volume of plasma at different angles. This point was discussed in Section 3.5. If (1.14) turns out to be a reasonable approximation in the case of a non-turbulent plasma, the analysis procedure discussed in this thesis can be routinely employed to deduce the average ion temperature, which is needed in energy balance considerations. If not, the Monte Carlo results by Kikuchi *et al.* could be used to relate the line-of-sight ion temperature and the degree of shape distortion obtained by 1-D analysis to the average ion temperature.

As our final point we note that increasing the number of free plasma parameters naturally makes the analysis of incoherent scatter data more difficult and possibly ambiguous. In what circumstances is it possible to fit for the non-Maxwellian parameters and the ion composition simultaneously? To what extent can small D^* values be resolved? In Chapter 3, these and other questions were studied using a limited number of examples. Recently, Lehtinen (1986) has established a mathematical formalism, based on statistical inversion theory, which can be used to analyse problems of this kind more generally and, what is more, used to find the relevant questions related to the statistical inversion procedure. For example, one can consider the experimental accuracy required to be able to fit for a given combination of parameters. This work has already been applied to the analysis of Maxwellian plasma. Its extension to non-

thermal effects will be of importance to data analysis and also the design of new experiments on non-thermal plasma.

APPENDIX

A. MATHEMATICAL FORMULAE

A.1. The plasma dispersion function

In the perturbation analysis of small-amplitude waves in a thermal plasma, one is faced with a certain analytic function, called the *plasma dispersion function* (Fried and Conte, 1961), which is defined by

$$Z(\xi) = \pi^{-1/2} \int_C dz \, \frac{\exp(-z^2)}{z - \xi}, \tag{A.1}$$

where C denotes the Landau contour: C is the real axis if Im $\xi > 0$ and the real axis indented below $z = \xi$ if Im $\xi \leq 0$. Using (A.1), it is easy to show that Z satisfies the differential equation

$$Z' + 2\xi Z + 2 = 0 \tag{A.2}$$

with the initial condition

$$Z(0) = i\pi^{1/2}. \tag{A.3}$$

Equations (A.2–3) can be solved by standard methods to yield

$$Z(\xi) = \exp(-\xi^2)\left[i\pi^{1/2} - 2\int_0^{\xi} dz\ \exp(z^2) \right]. \qquad \text{(A.4)}$$

Expressing the integrand by its Taylor series and performing the integration term by term yields the small argument series expansion of Z,

$$Z(\xi) = i\pi^{1/2} \exp(-\xi^2) - 2\xi\ (1 - 2\xi^2/3 + \ldots). \qquad \text{(A.5)}$$

The asymptotic expansion has been discussed in detail by Stix (1962). Different expansions are required for different portions of the ξ plane. These are given by

$$Z(\xi) = i\pi^{1/2}\ \varepsilon\ \exp(-\xi^2) - \frac{1}{\xi}(1 + 1/2\xi^2 + \ldots), \qquad \text{(A.6)}$$

where

$$\varepsilon = \begin{array}{l} 0 \text{ if } \operatorname{Im}\xi > |\operatorname{Re}\xi| \\ 1 \text{ if } |\operatorname{Im}\xi| < |\operatorname{Re}\xi| \\ 2 \text{ if } \operatorname{Im}\xi < -|\operatorname{Re}\xi| \end{array} . \qquad \text{(A.7)}$$

A.2. Bessel functions and related integrals

Bessel functions of the first kind (J_n), and modified Bessel functions (I_n) are defined as in Abramowitz and Stegun (1972). The identity

$$\sum_{n=-\infty}^{\infty} J_n^2(x) = 1 \tag{A.8}$$

and the recurrence relation

$$J_{n-1}(x) + J_{n+1}(x) = \frac{2n}{x} J_n(x) \tag{A.9}$$

are needed in Chapters 4 and 5. In Chapter 2, use is made of the series expansion

$$I_0(x) = \sum_{k=0}^{\infty} \frac{(x^2/4)^k}{k!^2} . \tag{A.10}$$

Finally, we note that

$$\int_0^{\infty} dx\, x \exp(-x^2) I_0(\alpha x) = \frac{1}{2} \exp(\alpha^2/4) \tag{A.11}$$

as a special case of integral 6.633:4 of Gradshteyn and Ryzhik (1980), and

$$\int_0^{\infty} dx\, \exp(-x^2) I_1(\alpha x) = \frac{1}{\alpha}\left[\exp(\alpha^2/4) - 1\right] \tag{A.12}$$

by equations 11.4.31 and 10.2.13 of Abramowitz and Stegun (1972). These are used in Chapter 4 and Appendix B respectively.

B. ION CONTRIBUTION TO THE DIELECTRIC FUNCTION: APPROXIMATION SCHEME

Using the asymptotic expansion of Z_R in terms with $n \neq N$, the real part of the summation over the A_n terms in (4.3) becomes

$$\sum_{n=-\infty}^{\infty} \frac{\omega}{k_{\parallel} v^*} A_n Z_R\left(\frac{\omega - n\Omega_i}{k_{\parallel} v^*}\right) = \frac{\omega}{k_{\parallel} v^*} A_N Z_R(\Delta_i) - \sum_{n \neq N} A_n \frac{\omega}{\omega - n\Omega_i}. \tag{B.1}$$

To keep the notation simple, we consider $N=1$ corresponding to the first cyclotron harmonic; the general case can be treated in a similar fashion with obvious modifications. Noting that $\omega \approx \Omega_i$, the second term on the RHS of (B.1) becomes

$$-A_0 - \frac{1}{2} A_1 - 2 \sum_{n \geq 2} \frac{A_n}{1 - n^2}. \tag{B.2}$$

The first two terms are <<1. The order-of-magnitude of the third term can be estimated by replacing the summation by an integral:

$$-2 \sum_{n \geq 2} \frac{A_n}{1 - n^2} \sim -2 \langle A \rangle \int_2^{\infty} \frac{dx}{1 - x^2} = \langle A \rangle \ln 3, \tag{B.3}$$

where <A> denotes the order-of-magnitude of the quantities A_n. This is also small compared with unity. We thus find that to a good approximation (the generalization to any value of N being straightforward) that

$$\sum_{n=-\infty}^{\infty} \frac{\omega}{k_{\parallel} v^*} A_n Z_R\left(\frac{\omega - n\Omega_i}{k_{\parallel} v^*}\right) \approx \frac{\omega}{k_{\parallel} v^*} A_N Z_R(\Delta_i). \tag{B.4}$$

Consider then the real contribution from the B_n terms, which is given by

$$\sum_{n=-\infty}^{\infty} \frac{n\,\Omega_i}{k_{||}v^*} B_n Z_R\left(\frac{\omega - n\Omega_i}{k_{||}v^*}\right) = \frac{N\,\Omega_i}{k_{||}v^*} B_N Z_R(\Delta_i) - \sum_{n \neq N} B_n \frac{n\Omega_i}{\omega - n\Omega_i},$$

(B.5)

where the second term on the RHS can be written as (N=1)

$$-B_0 - \frac{3}{2}B_1 + \sum_{n=-\infty}^{\infty} B_n - 2\sum_{n \geq 2} \frac{B_n}{1-n^2}. \qquad \text{(B.6)}$$

Here the first two terms are negligible and so is the last term, whose magnitude is again estimated by an integral as in (B.3). The third term can be calculated exactly using equations (A.8) and (A.12):

$$\sum_{n=-\infty}^{\infty} B_n = \int_0^{\infty} dx\, \exp\left(-D^{*2} - x^2\right) I_1(2D^* x) = \frac{1}{2D^*}\left[1 - \exp\left(-D^{*2}\right)\right].$$

(B.7)

We thus find, again generalizing the result to arbitrary N, that

$$\sum_{n=-\infty}^{\infty} \frac{n\,\Omega_i}{k_{||}v^*} B_n Z_R\left(\frac{\omega - n\Omega_i}{k_{||}v^*}\right) \approx \frac{N\,\Omega_i}{k_{||}v^*} B_N Z_R(\Delta_i) + \frac{1 - \exp\left(-D^{*2}\right)}{2D^*}.$$

(B.8)

Here the second term on the RHS represents the correction due to the $n \neq N$ terms.

REFERENCES

Abramowitz, M., and I.A. Stegun, *Handbook of mathematical functions,* Dover, New York, 1972.

Banks, P.M., Collision frequencies and energy transfer, ions, *Planet. Space Sci.* **14,** 1105, 1966.

Barakat, A.R., R.W. Schunk and J.-P. St.-Maurice, Monte Carlo calculations of the O^+ velocity distribution in the auroral ionosphere, *J. Geophys. Res.* **88,** 3237, 1983.

Bowles, K.L., Observation of vertical incidence scatter from the ionosphere at 41 Mc/sec, *Phys. Rev. Lett.* **1,** 454, 1958.

Chen, L., *Waves and instabilities in plasmas,* World Scientific, 1987.

Clemmow, P.C., and J.P. Dougherty, *Electrodynamics of particles and plasmas,* Addison-Wesley, 1969.

Cowley, S.W.H., Interpretation of observed relations between solar wind characteristics and effects at ionospheric altitudes, in *High latitude space plasma physics,* edited by B. Hultqvist and T. Hagfors, Plenum Press, New York, 1983.

Dougherty, J.P., The conductivity of a partly ionized gas in alternating electric fields, *J. Fluid Mech.* **16,** 126, 1963.

Dougherty, J.P., and D.T. Farley, A theory of incoherent scattering of radio waves by a plasma, *Proc. Roy. Soc.* (London) **A259,** 79, 1960.

Dungey, J.W., Interplanetary magnetic field and the auroral zones, *Phys. Rev. Lett.* **6,** 47, 1961.

Dupree, T.H., A perturbation theory for strong plasma turbulence, *Phys. Fluids* **9,** 1773, 1966.

Evans, J.V., Theory and practice of ionosphere study by Thomson scatter radar, *Proc. of IEEE* **57,** 496, 1969.

van Eyken, A.P., H. Rishbeth, D.M. Willis and S.W.H. Cowley, Initial EISCAT observations of plasma convection at invariant latitudes 70–77°, *J. Atm. Terr. Phys.* **46,** 635, 1984.

Farley, D.T., The ionospheric plasma, in *Solar System Plasma Physics,* vol. III, 271, edited by L.J. Lanzerotti, C.F. Kennel and E.N. Parker, North Holland Publishing Company, 1979.

Farmer, A.D., M. Lockwood, T.J. Fuller-Rowell, K. Suvanto and U.-P. Løvhaug, Model predictions of the occurrence of non-Maxwellian plasmas and analysis of their effect on EISCAT data, *J. Atmos. Terr. Phys.* **50,** 487, 1988.

Fejer, J.A., Scattering of radio waves by an ionized gas in thermal equilibrium, *Can. J. Phys.* **38,** 1114, 1960.

Fried, B.D., and S.D. Conte, *The Plasma Dispersion Function,* Academic Press 1961.

Gordon, W.E., Incoherent scattering of radio waves by free electrons with application to space exploration by radar, *Proc. IRE* **46,** 1824, 1958.

Grad, H., Principles of the kinetic theory of gases, *Handbuch der Physik,* XII, 205, 1958.

Gradshteyn, I.S., and I.M. Ryzhik, *Table of integrals, series and products,* Academic Press, New York, 1980.

Hagfors, T., Density fluctuation in a plasma in a magnetic field with applications to the ionosphere, *J. Geophys. Res.* **66,** 1699, 1961.

Harris, E.G., Unstable plasma oscillations in a magnetic field, *Phys. Rev. Lett.* **2(2),** 34, 1959.

Holzer, T.E., J.A. Fedder and P.M. Banks, A comparison of kinetic and hydrodynamic models of an expanding ion exosphere, *J. Geophys. Res.* **76,** 2453, 1971.

Hubert, D., Non-Maxwellian distribution functions and incoherent scattering of radar waves in the auroral ionosphere, *J. Atm. Terr. Phys.* **46,** 601, 1984.

Kikuchi, K., J.-P. St.-Maurice and A. Barakat, Monte Carlo computations of F-region incoherent radar spectra at high latitudes and the use of a simple method for non-Maxwellian spectral calculations, *Ann. Geophys.*, in press, 1988.

Lakhina, G.S., and K.G. Bhatia, Ion cyclotron instability in the auroral F-region, *J. Geophys. Res.* **89**, 9845, 1984.

Landau, L.D., On the vibrations of the electronic plasma, *J. Phys. USSR* **10**, 25, 1946.

Lehtinen, M.S., *Statistical theory of incoherent scatter radar measurements*, Ph.D. thesis, University of Helsinki, 1986.

Lejeune, G., EISCAT Technical Note **18**, 1979.

Lockwood, M., and T.J. Fuller-Rowell, The modelled occurence of non-thermal plasma in the ionospheric F-region and the possible consequences for ion outflows into the magnetosphere, *Geophys. Res. Lett.* **14**, 371 and 581, 1987.

Lockwood, M., and K.J. Winser, On the determination of ion temperature in the auroral F-region ionosphere, *Planet. Space Sci.*, in press, 1989.

Lockwood, M., B.J.I. Bromage, R.B. Horne, J.-P. St.-Maurice, D.M. Willis and S.W.H. Cowley, Non-Maxwellian ion velocity distributions observed using EISCAT, *Geophys. Res. Lett.* **14**, 111, 1987.

Lockwood, M., K. Suvanto, J.-P. St.-Maurice, K. Kikuchi, B.J.I. Bromage, D.M. Willis, S.R. Crothers, H. Todd and S.W.H. Cowley, Scattered power from non-thermal F-region plasma observed by EISCAT – evidence for coherent echoes?, *J. Atmos. Terr. Phys.* **50**, 467, 1988.

Lockwood, M., K. Suvanto, K.J. Winser, S.W.H. Cowley and D.M. Willis, Incoherent scatter radar observations of non-Maxwellian ion velocity distributions in the auroral F-region, *Adv. Space Res. (COSPAR Proceedings)*, in press, 1989a.

Lockwood, M., K. Suvanto, S.W.H. Cowley, R.B. Horne, T.J. Fuller-Rowell, B.J.I. Bromage, D.M. Willis and J.-P. St.-Maurice, Incoherent scatter observations of non-Maxwellian ion velocity distributions in the auroral F-

region of the ionosphere, *Space Sci. Rev.*, to be submitted, 1989b.

Lockwood, M., P.E. Sandholt and S.W.H. Cowley, Dayside auroral activity and momentum transfer from the solar wind, *Geophys. Res. Lett.*, in press, 1989c.

Løvhaug, U.P., and T. Flå, Ion temperature anisotropy in the auroral F-region as measured with EISCAT, *J. Atmos. Terr. Phys.* **48,** 959, 1986.

Mintzer, D., Generalized orthogonal polynomial solutions of the Boltzmann equation, *Phys. Fluids* **8,** 1076, 1965.

Moorcroft, D.R., On the determination of temperature and ionic composition by electron backscattering from the ionosphere and magnetosphere, *J. Geophys. Res.* **69,** 955, 1964.

Moorcroft, D.R., and K. Schlegel, Evidence for non-Maxwellian ion velocity distributions in the F-region, *J. Atmos. Terr. Phys.* **50,** 455, 1988.

Ott, E., and D.T. Farley, Microinstabilities and the production of short-wavelength irregularities in the auroral F-region, *J. Geophys. Res.* **80,** 4599, 1975.

Perraut, S., A. Brekke, M. Baron and D. Hubert, EISCAT measurements of ion temperatures which indicate non-isotropic ion velocity distributions, *J. Atm. Terr. Phys.* **46,** 531, 1984.

Post, R.F., and M.N. Rosenbluth, Electrostatic instabilities in finite mirror confined plasmas, *Phys. Fluids* **9,** 730, 1966.

Raman, R.S.V., *Incoherent scattering of radar waves in the auroral ionosphere,* Ph.D. thesis, University of Michigan, 1980.

Raman, R.S.V., J.-P. St.-Maurice and R.S.B. Ong, Incoherent scattering of radar waves in the auroral ionosphere, *J. Geophys. Res.* **86,** 4751, 1981.

Rosenbluth, M.N., and R.F. Post, High-frequency electrostatic plasma instability inherent to "loss-cone" particle distributions, *Phys. Fluids* **8,** 547, 1965.

Sagdeev, R.Z., and A.A. Galeev, *Nonlinear Plasma Theory,* W.A. Benjamin, New York, 1969.

Salpeter, E.E., Electron density fluctuations in a plasma, *Phys. Rev.* **120,** 1528, 1960.

Sanderson, J.J., Kinetic theory, in *Plasma Physics and Nuclear Fusion Research,* 119, edited by R.D. Gill, Academic Press, 1981.

Schunk, R.W., Mathematical structure of transport equations for multispecies flows, *Rev. Geophys. Space Phys.* **15,** 429, 1977.

Schunk, R.W., and J.C.G. Walker, Ion velocity distributions in the auroral ionosphere, *Planet. Space Sci.* **20,** 2175, 1972.

Spitzer, L., *Physics of Fully Ionized Gases,* Interscience, New York, 1956.

St.-Maurice, J.-P., On a mechanism for the formation of VLF electrostatic emissions in the high-latitude F-region, *Planet. Space Sci.* **26,** 801, 1978.

St.-Maurice, J.-P. and R.W. Schunk, Auroral ion velocity distributions using a relaxation model, *Planet. Space Sci.* **21,** 1115, 1973.

St.-Maurice, J.-P., and R.W. Schunk, Behaviour of ion velocity distributions for a simple collision model, *Planet. Space Sci.* **22,** 1, 1974.

St.-Maurice, J.-P., and R.W. Schunk, Use of generalized orthogonal polynomial solutions of Boltzmann's equation in certain aeronomy problems: Auroral ion velocity distributions, *J. Geophys. Res.* **81,** 2145, 1976.

St.-Maurice, J.-P., and R.W. Schunk, Auroral ion velocity distributions for a polarization collision model, *Planet Space Sci.* **25,** 243, 1977.

St.-Maurice, J.-P., and R.W. Schunk, Ion velocity distributions in the high-latitude ionosphere, *Rev. Geophys. Space Phys.***17,** 99, 1979.

St.-Maurice, J.-P., W.B. Hanson and J.C.G. Walker, Retarding Potential Analyzer measurement of the effect of ion-neutral collisions on the ion velocity distribution in the auroral ionosphere, *J. Geophys. Res.* **81,** 5438, 1976.

Stix, T.H., *The theory of plasma waves,* McGraw-Hill, New York 1962.

Suvanto, K., Auroral F-region ion velocity distributions in the presence of large

flows and electrostatic waves, *Planet. Space Sci.* **35,** 1429, 1987.

Suvanto, K., Incoherent scattering of radar waves from non-thermal F-region plasma: analytical methods of spectral synthesis, *Radio Sci.* **23,** 989, 1988.

Suvanto, K., Ion cyclotron microinstability driven by non-thermal F-region plasma, *Planet. Space Sci.* **37,** 1, 1989a.

Suvanto, K., Microinstabilities driven by non-thermal plasma in the high-latitude F-region, *Adv. Space Res.* (*COSPAR Proceedings*), in press, 1989b.

Suvanto, K., M. Lockwood and T.J. Fuller-Rowell, The influence of anisotropic ion velocity distributions on ion upflows into the magnetosphere, *J. Geophys. Res.* **94,** 1347, 1989a.

Suvanto, K., M. Lockwood, K.J. Winser, A.D. Farmer and B.J.I. Bromage, Analysis of incoherent scatter radar data from non-thermal F-region plasma, submitted to *J. Atmos. Terr. Phys.*, 1989b.

Suvanto, K., M. Lockwood, K.J. Winser, A.D. Farmer and B.J.I. Bromage, Analysis of incoherent scatter spectra from non-Maxwellian plasma, *Adv. Space Res.* (*COSPAR Proceedings*), in press, 1989c.

Swift, D.W., The effect of electric fields and ion-neutral collisions on Thomson scatter spectra, *J. Geophys. Res.* **80,** 4380, 1975.

Todd, H., B.J.I. Bromage, S.W.H. Cowley, M. Lockwood, A.P. van Eyken and D.M. Willis, EISCAT observations of bursts of rapid flow in the high-latitude dayside ionosphere, *Geophys. Res. Lett.* **13,** 909, 1986.

Vallinkoski, M., Incoherent scatter spectrum, *Proceedings of the 3rd EISCAT research seminar in Finland,* 1987 (in Finnish).

Willis, D.M., M. Lockwood, S.W.H. Cowley, A.P. van Eyken, B.J.I. Bromage, H. Rishbeth, P.R. Smith and S.R. Crothers, A survey of simultaneous observations of the high-latitude ionosphere and interplanetary magnetic field with EISCAT and AMPTE-UKS, *J. Atmos. Terr. Phys.* **48,** 987, 1986.

Winser, K.J., M. Lockwood and G.O.L. Jones, Non-thermal plasma observations using EISCAT: aspect angle dependence, *Geophys. Res. Lett.* **14,** 957, 1987.

Winser, K.J., M. Lockwood, G.O.L. Jones and K. Suvanto, Observations of non-thermal plasmas at different aspect angles, *J. Geophys. Res.* **94**, 1439, 1989a.

Winser, K.J., M. Lockwood, G.O.L. Jones and K. Suvanto, Radar observations of non-thermal plasmas at different aspect angles, *Adv. Space Res. (COSPAR Proceedings)*, in press, 1989b.